THE
PHYSICAL REVIEW
A journal of experimental and theoretical physics established by E. L. Nichols in 1893

SECOND SERIES, VOL. 71, NO. 1 JANUARY 1, 1947

A Method for Measuring Half-Lives

A. C. GRAVES* AND R. L. WALKER**
University of California, Los Alamos Scientific Laboratory, Santa Fe, New Mexico
(Received August 29, 1946)

A method for measuring half-lives with Geiger counters which is independent of counting losses is described. Foils which have been irradiated for various times are counted after a lapse of time adjusted to make the counting rates of the foils the same. Saturated activities of the foils will be different if an incorrect value of the decay constant has been assumed. Equations are given for obtaining a more correct value of the decay constant. The method is illustrated by data on the 54-minute period of indium.

INTRODUCTION

MEASUREMENT of the half-life of an artificial activity with a counter has usually required a correction for counting losses.[1] This correction is time-consuming and is not easy to make with precision.[2] In the following a method of making such measurements which does not require this correction is reported.

THEORY

If the total number of counts N obtained by counting the emission of a sample for t_2 minutes is measured, the saturated activity A_s (the initial counting rate of a sample irradiated for an infinite time) is given by the formula,

$$A_s=\lambda N \exp(\lambda t_3)/(1-\exp(-\lambda t_1))\times(1-\exp(-\lambda t_2)), \quad (1)$$

where t_1 is the time the sample was irradiated, t_3 is the time between the irradiation and the start of the counting period, $\lambda=\ln 2/T$, and T is the half-life in minutes. If the derivative of A_s with respect to λ is calculated and counting times selected to make this derivative zero, the value of A_s will not depend strongly on a small error in λ. Then if other counting schedules are selected with which the derivative is not zero, the calculated value of A_s will differ from the above value if an incorrect value of λ has been assumed. Differentiation of Eq. (1) yields the formula,

$$dA_s/d\lambda=KA_s, \quad (2)$$

where

$$K=1/\lambda+t_3-\frac{t_1\exp(-\lambda t_1)}{1-\exp(-\lambda t_1)}-\frac{t_2\exp(-\lambda t_2)}{1-\exp(-\lambda t_2)}. \quad (3)$$

If one assumes that A_s is approximately a linear function of λ one can write

$$\lambda=\lambda'+(A_s-A_s')/K'A_s', \quad (4)$$

* Now on leave from University of Texas.
** Now at Cornell University.
[1] See for example: H. Volz, Zeits. f. Physik **93**, 539 (1935); L. I. Schiff, Phys. Rev. **50**, 88 (1936); W. B. Lewis, Proc. Camb. Phil. Soc. **33**, 549 (1937); A. E. Ruark and F. E. Brammer, Phys. Rev. **52**, 322 (1937); L. Alaoglu and N. Smith, Jr., Phys. Rev. **53**, 832 (1938); J. Kurbatov and H. B. Mann, Phys. Rev. **68**, 40 (1945).
[2] H. Lifschutz and O. Duffendack, Phys. Rev. **54**, 714 (1938); J. Cork and J. Lawson, Phys. Rev. **56**, 291 (1939); D. E. Hull and H. Seelig, Phys. Rev. **60**, 553 (1941).

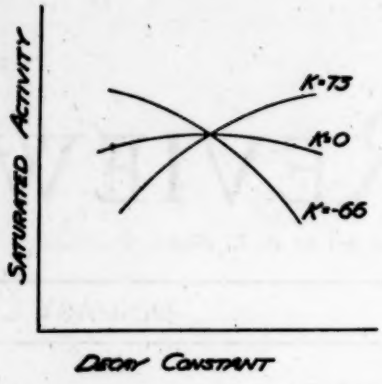

FIG. 1. Schematic representation of calculated saturated activity *vs.* decay constant.

where λ' is the assumed decay constant, A_s is the correct saturated activity, A_s' is the saturated activity calculated from Eq. (1) with the assumed value of decay constant, and λ is a more nearly correct value of the decay constant.

In order for this method to be useful enough counts must be recorded to make statistical errors small, K must have predetermined values, and counting rates with the various schedules must be nearly the same. Since there are three conditions to be fulfilled and three parameters, t_1 and t_2 and t_3 to adjust, appropriate schedules can always be obtained.

Since all foils have the same activity when counted, the counting loss correction will be the same for all foils and will not affect the value of λ as given by Eq. (4). From Eq. (2) it can be seen that the sensitivity of the method (the percent difference in A_s divided by the percent error in λ) is equal to $K\lambda$. Hence, for example, for indium where $\lambda=0.0128$ a value of about 80 for K is required to give a sensitivity of one. If one is attempting to detect an error in λ of one percent with a counting schedule adjusted to make $K=80$, one must measure activities to one percent. Figure 1 shows a schematic representation of A_s as a function of λ for three different counting schedules. Since A_s cannot vary with the counting schedule if the correct value of λ is used in calculating saturated activities, all such curves must intersect at one point as shown. In practice, because of experimental errors, the three curves will not be concurrent but will give three points of intersection and three values of λ. If Eq. (4) is applied to any two such curves and A_s eliminated from the resulting equations one obtains,

$$\lambda=\lambda'+(A_s''-A_s')/(K'A_s'-K''A_s''). \quad (5)$$

A_s'' and A_s' are saturated activities calculated with the assumed decay constant λ' for counting schedules corresponding to K'' and K'.

HALF-LIFE OF INDIUM

A test of this method was made with indium.[3] Data were taken on two Geiger counters with three different counting schedules. The three different schedules and corresponding values of K are given in Table I. K is calculated from Eq. (3) with $\lambda=0.012836$. The times t_1, t_2, and t_3 have the same significance as in Eq. (1). Table II gives the calculated activities corresponding to the three values of K. N_1 and A_{s1} are the number of foils measured with counter 1 and the calculated activities. N_2 and A_{s2} are the corresponding quantities measured on counter 2. A_s gives the average activity. A_{s1} and A_{s2} have been multiplied by appropriate factors to make the sensitivities of the two counters the same. Using the

TABLE I. Calculated values of K for three counting schedules.

K min.	t_1 min.	t_2 min.	t_3 min.
−66	9	10	3
0	20	10	63
+73	52	10	123

TABLE II. Activities calculated for three values of K.

K min.	N_1	A_{s1} counts/min.	N_2	A_{s2} counts/min.	A_s counts/min.
−66	13	34882±31	13	34867± 97	34875±50
0	9	35002±75	7	34973±136	34988±77
73	6	34904±90	7	34948±136	34926±90

TABLE III. Half-life of indium.

K'; K'' min.	min.	Half-life T min.
−66; 0	0.012787±0.000040	54.21±0.17
0; 73	0.012860±0.000047	53.90±0.20
−66; 73	0.012825±0.000021	54.05±0.09
	mean	54.05±0.16

[3] See also; E. Amaldi, O. d'Agostino, and E. Segrè, Ricerca Scient. 5, 2 (1934); E. Amaldi, O. d'Agostino, E. Fermi, B. Pontecorvo, F. Rasetti, and E. Segrè, Proc. Roy. Soc. 149, 522 (1935).

three saturated activities in pairs one obtains from Eq. (5) values for the half-life of indium shown in Table III. In this table errors given are probable errors calculated from the root mean square deviations of the data.

CONCLUSION

These measurements were undertaken with the primary purpose of determining whether or not the half-life of indium was sufficiently different from 54 minutes to produce a significant systematic error in experiments being performed with indium as a neutron detector. An error of a percent or more in T was considered sufficient to affect these experiments. Since the authors were not looking for errors of the order of a few tenths of a percent the measurement suffers from two uncertainties. First, while the indium used was known to be quite pure, no check of the purity was made. Hence, it is possible that an impurity with a large cross section may have been present and affected the result. Second, no attempt was made to time operations with the precision necessary to obtain an accuracy of a few tenths of a percent. It is believed that the result should be correct to one percent or better and that the half-life of indium is 54.05 ± 0.5. However, it is felt that the method is useful and it is hoped the measurements reported give an indication of the accuracy which may be obtained by this method of determining the half-life of an artificially induced activity.

This work was carried out under contract between the University of California and the Manhattan District, Corps of Engineers, War Department.

PHYSICAL REVIEW VOLUME 71, NUMBER 1 JANUARY 1, 1947

Photo-Fission in Heavy Elements*

G. C. BALDWIN AND G. S. KLAIBER
Research Laboratory, General Electric Company, Schenectady, New York

(Received October 4, 1946)

Measurements have been made of the yields of photo-fission in uranium and thorium together with a search for photo-fission in other heavy elements, using continuous x-rays from a 100-Mev betatron. Fission was detected in the presence of an intense background of x-rays by a differential ionization chamber and linear amplifier, the substance investigated being coated on an electrode of one chamber. A Victoreen r-thimble, surrounded by $\frac{1}{4}$-inch lead walls, was used to monitor the radiation. Curves were obtained of the number of fissions per roentgen unit for uranium and thorium. These are of similar shape, the uranium curve showing a rapid rise with increasing x-ray energy up to 18 Mev, followed by a gradual decrease as the maximum energy of the x-rays is further increased; the yield of fissions per roentgen at 100 Mev is about half that at 18 Mev. The ratio of uranium and thorium yields is very nearly two at all x-ray energies. No fissions were observed in intense 100-Mev irradiations of Bi, Pb, Tl Au, W, and Sm. Determination of cross sections from the yield curves is complicated by the continuous spectrum of the x-rays which has not been measured experimentally. A rough analysis of the data has been made in which a spectrum is assumed for which the intensity is constant in each unit energy interval and the r-meter efficiency calculated roughly from a simplified picture of the generation of secondaries in the lead walls. The resulting analysis of the yield curves shows that the cross section for photo-fission as a function of quantum energy passes through a maximum and then decreases and is extremely small above 30 Mev. The maximum cross section is of the order of 5×10^{-26} cm² for uranium and half that for thorium. In the other elements studied, the cross section must be below 10^{-29} cm².

INTRODUCTION

ACCORDING to Bohr and Wheeler's theory of the fission process,[1] fission should be possible for all heavy nuclei which lie well beyond the minimum of the packing fraction curve, provided sufficient excitation is provided to produce the necessary deformation of nuclear fluid which precedes division of the nucleus. Such excitation can be provided by particle

* A preliminary report of this work was presented in an invited paper at the January, 1946 meeting of the American Physical Society.

[1] N. Bohr and J. A. Wheeler, Phys. Rev. 56, 426 (1939).

capture or by absorption of a γ-ray into the nucleus.

Shortly after the discovery of fission, Roberts, Meyer, and Hafstad[2] attempted, without success, to induce fission in uranium by bombardment with the 6.3-Mev γ-rays from the $F^{19}(p, \gamma)$ reaction. The negative result of this experiment was explained by Bohr and Wheeler,[1] who calculated that the cross section should be of the order of 10^{-27} cm^2. Using higher intensities, Haxby, Shoupp, Stephens, and Wells[3] later succeeded in observing photo-fission of uranium and thorium with 6.3-Mev γ-rays from fluorine. The measured cross sections at 6.3 Mev were $(3.5\pm1.0)\times10^{-27}$ cm^2 for uranium, $(1.7\pm0.5)\times10^{-27}$ cm^2 for thorium. The ratio of uranium and thorium cross sections was practically two. These results were confirmed by a group of Japanese investigators.[4]

While natural γ-rays have the advantage that only simple line spectra of radiation are involved, sources of γ-rays of sufficient energy and intensity for accurate photo-fission measurements are practically non-existent. Using continuous x-rays with maximum energies up to 20 Mev, Koch[5] has measured the yields of photo-fission in uranium and thorium and sought unsuccessfully for photo-fission in other elements. The failure to observe fission in lead and other heavy elements is somewhat surprising, since the critical energies for fission calculated according to the theory of Bohr and Wheeler[1] are well below the 20 Mev accessible to Koch. We have accordingly undertaken a search for photo-fission at still higher energies in a number of heavy elements, and have investigated the energy dependence of fission in uranium and thorium.

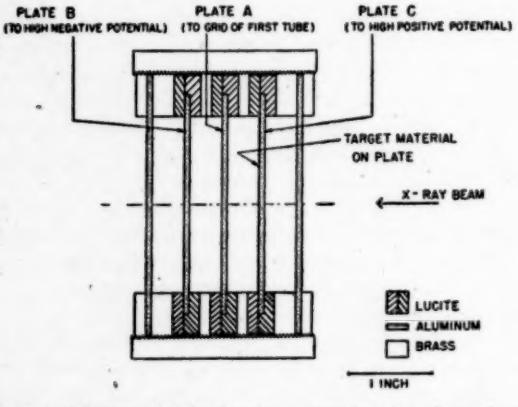

FIG. 1. Differential ionization chamber for detection of fission in the presence of intense x-radiation. The material investigated for fission is coated on plate *C*.

APPARATUS

The source of radiation employed in the present experiments was the 100-Mev betatron of the General Electric Research Laboratory.[6] This generates a continuous spectrum of quanta of any desired maximum energy up to 100 Mev, the radiation appearing in pulses of short duration with a 60-cycle repetition rate.

Fission processes were detected by observing the ionization produced by fission fragments originating in a thin layer of material deposited on the inner wall of an ionization chamber. Because individual x-ray pulses from the betatron are very intense, it was necessary to use a balanced differential chamber. It was possible by balancing a double chamber to reduce the x-ray ionization pulses to the same level as the natural background noise of the amplifier; ionization produced by particles from material coated on the wall of one chamber could then readily be detected in the presence of intense x-radiation.

Figure 1 shows details of the ionization chamber. The aluminum plates *A*, *B*, and *C* defined the two chambers, each 1 cm deep. The center plate, *A*, was connected to the grid of the first stage of a linear amplifier. Plates *B* and *C*

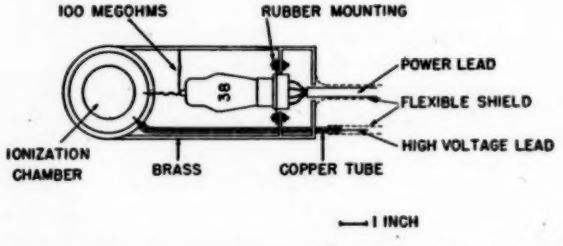

FIG. 2. Housing arrangement of ionization chamber and first stage of the linear amplifier.

[2] R. B. Roberts, R. C. Meyer, and L. R. Hafstad, Phys. Rev. **55**, 417 (1939).
[3] Haxby, Shoupp, Stephens, and Wells, Phys. Rev. **59**, 57 (1941).
[4] Arakatu, Vemura, Sonada, Shimizu, Kimura, and Kuraoka, Proc. Phys.-Math. Soc. Japan **23**, 440 (1941).
[5] H. W. Koch, Ph.D. Thesis, University of Illinois, 1944 (unpublished).
[6] W. F. Westendorp and E. E. Charlton, J. App. Phys. **16**, 581 (1945).

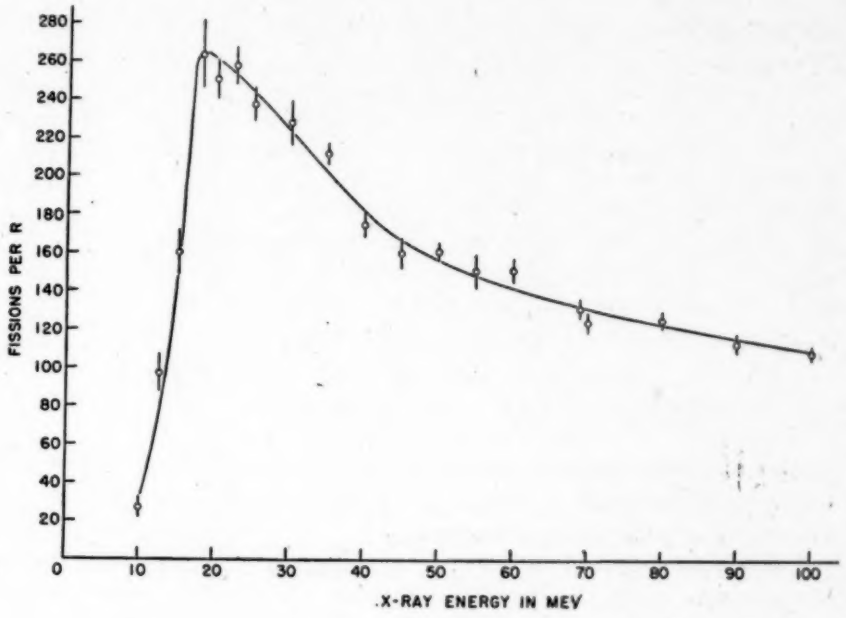

FIG. 3. X-ray fission yield for uranium. The ordinate is the number of fission pulses per roentgen unit recorded by the monitor.

were connected to individually adjustable 1000-volt stabilized sources of negative and positive potential, respectively; balancing of the chambers was greatly facilitated by having these potentials variable. Plate *C* was readily interchangeable with other plates on which various substances to be investigated were coated.[7] The chamber was filled with air at atmospheric pressure.

Figure 2 shows the housing arrangement of the ionization chamber and the first stage of the amplifier. The entire structure was made very rugged to eliminate microphonic disturbances, as it was necessary to operate the chamber close to the betatron where the sound level was about 100 decibels. The chamber housing was mounted on pads of sponge rubber two inches thick to eliminate mechanical vibration.

Pulses from the ionization chamber were amplified by a five-stage linear amplifier similar to that described by Waddell.[8] The output was fed to a vacuum-tube discriminating and thyratron-recording circuit. The output of the third stage of the amplifier was observed visually with an oscilloscope throughout each run to insure that pulses which were registered by the discriminating circuit occurred only at the phase at which x-rays were produced; to facilitate this, the chamber was always operated slightly unbalanced. A slight 60-cycle pick-up from stray magnetic fields of the betatron did not interfere with operation of the amplifier.

The radiation incident on the chamber was monitored by means of a standard Victoreen *r*-thimble and condenser *r*-meter. The thimble was placed in a lead cap of $\frac{1}{8}''$ wall thickness directly behind the chamber.

EXPERIMENTS

Preliminary tests were made with a layer of thorium oxide on Plate *C* (Fig. 1) to determine the proper value of the discriminator setting in order that the recording circuit would register only pulses larger than those due to alpha-particles. The discriminator setting was carefully maintained throughout all subsequent measurements at such a value that no pulse less than four times the maximum height of the alpha-particle pulses was recorded as owing to a fission fragment.

The ionization chamber was then placed in the center of the x-ray beam 11 feet from the target of the betatron; at this point, the diameter of the x-ray beam is comparable with the dimensions of the chamber. With uncoated plates in the chamber, an intense irradiation at 100 Mev

[7] Remarkably uniform coatings were deposited for us by Messrs. Dunbar, Huthsteiner, and Young of this laboratory under the supervision of Dr. Dushman.

[8] Waddell, R. C., Rev. Sci. Inst. **10**, 311 (1939).

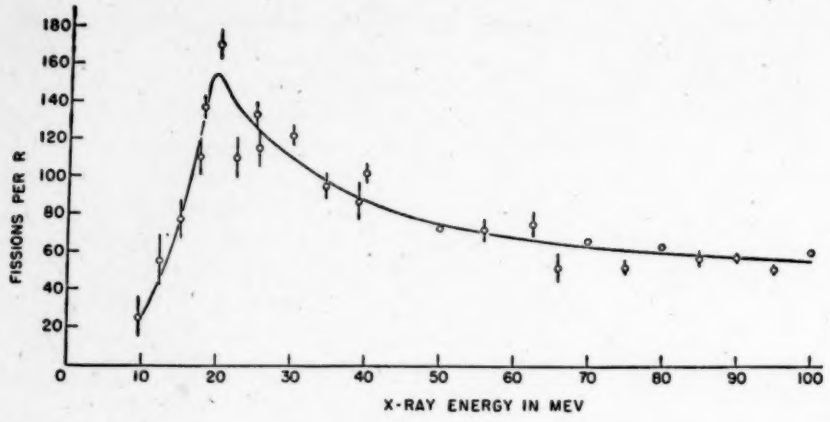

FIG. 4. X-ray fission yield for thorium.

was given. No pulses were observed; hence, any pulses observed with a coated plate must be attributed to the coating substance.

Using a plate coated with a layer of 4 mg/cm² of uranium oxide, measurements were then made of the x-ray fission yield (i.e., the number of fission pulses observed per roentgen unit of radiation as recorded by the *r*-meter) for x-radiation of various maximum energies from 10 to 100 Mev. For these measurements, the x-ray intensity was maintained at a sufficiently low value so that the chance of two fission pulses occurring in the same cycle was below one percent. The results are plotted in Fig. 3, in which the observed number of fissions per roentgen unit is given as a function of the maximum x-ray energy. The x-ray fission yield rises rapidly with increasing x-ray energy up to about 18 Mev. As the maximum x-ray energy is increased above 18 Mev, however, the yield decreases and continues to fall until, at 100 Mev, the yield is less than half that obtained at 18 Mev. The significance of this feature of the curve will be explained in the following section.

After a thorough cleaning, the ionization chamber was checked by a run with an uncoated target for any possible uranium contamination, and a target plate was installed with a coating of 9 mg/cm² of thorium oxide. The x-ray fission yield for thorium was then determined; it is plotted in Fig. 4. This curve closely resembles the curve for uranium except that its maximum occurs at 20 Mev, slightly higher than for uranium. It will be noted that for x-ray energies above 25 Mev the yield from uranium is 2.0±0.1 times the yield from thorium. Below 25 Mev, the ratio of the yields decreases slightly, the lowest value of 1.75 being reached at the maximum of the thorium yield curve, because the two maxima are slightly displaced with respect to each other. Below 18 Mev, the steepness of the curves is such that it is difficult to determine the ratio of the yields with precision; however even near 10 Mev it appears to be approximately two.

Upon completion of the work with thorium the chamber was again cleaned and checked for contamination. A target plate coated with 3 mg/cm² of lead oxide was then installed and given an irradiation of 21 *r* with 100-Mev x-radiation. No fission pulses were observed. Another target plate coated with 7.3 mg/cm² of metallic lead deposited by evaporation was irradiated with 14 *r* of 100-Mev x-rays and with 10 *r* of 50-Mev x-rays; no fission pulses were observed in either irradiation.

Similar experiments were carried out using other target materials. Substances investigated are listed in Table I; except for uranium and thorium, none gave any indication of fission.

Upon the conclusion of these experiments, the

TABLE I. Substances investigated for photo-fission.

Substance irradiated	Thickness of coating, mg/cm²	Irradiation at 100 Mev	Fissions observed
Uranium oxide	4.0	13.5 *r*	1460
Thorium oxide	9.0	23.4	1286
Tungsten metal, powdered	4.0	12.1	0
Lead oxide	3.0	21.0	0
Lead metal	7.3	14.0	0
Bismuth metal	6.5	9.5	0
Gold metal	4.7	9.0	0
Thallium metal	11.4	11.9	0
Samarium oxide	3.0	11.0	0

thorium target was reinstalled and the excitation curve of Fig. 4 was rechecked, indicating that the negative results with other substances were not owing to failure of the apparatus.

ANALYSIS OF RESULTS

In attempting to interpret the excitation curves of Figs. 3 and 4, one must remember that these curves were obtained with *continuous* x-rays. The fission processes observed at some maximum x-ray energy E are caused by quanta of all energies between the fission threshold and E. It must also be remembered that the ordinates are the number of fissions per roentgen unit as recorded by the r-meter under the conditions of the experiment. This "x-ray fission yield" is thus a ratio of the yields of two entirely different processes. Before the photo-fission cross section as a function of quantum energy can be determined, it is necessary to know the spectral distribution of the radiation in the x-ray beam from the betatron and to calculate the reading in roentgen units of the monitor when it has been irradiated with a given intensity of radiation having this spectral distribution. Experimental knowledge of the spectrum is not yet available and the efficiency of the ionization monitor can be calculated only approximately. A provisional approximate analysis of the yield curves will be attempted, however.

Let a target of area A containing N atoms per cm² be irradiated normally with x-rays of maximum energy E of intensity such that $n(\epsilon, E)d\epsilon$ quanta per cm² of energy between ϵ and $\epsilon+d\epsilon$ are incident on the target. Let $\sigma(\epsilon)$ be the cross section for photo-fission by a quantum of energy ϵ. Then the number of fission processes which occur in the target will be

$$F(E)=NA\int_0^E \sigma(\epsilon)n(\epsilon, E)d\epsilon. \qquad (1)$$

The number of fissions per atom of target material produced when the target is irradiated with continuous x-rays whose quanta have a maximum energy E is thus given by the area lying under a curve which is the product of the cross section for photo-fission by the spectral distribution of the quanta. The number of fissions observed is divided by the reading of the ionization monitor in r-units and the quotient plotted as the x-ray fission yield corresponding to "x-rays of energy E."

X-Ray Spectrum

Since the target of the betatron is thin, the x-ray spectrum can be expected to be practically the same as the spectrum calculated by Bethe and Heitler in their theoretical treatment of bremsstrahlung.[9] According to their result, the

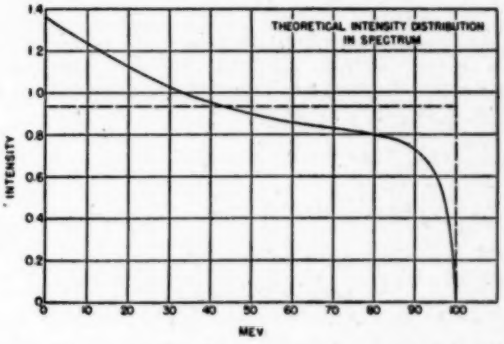

FIG. 5. Bremsstrahlung spectrum as calculated by Bethe and Heitler. The dotted curve is the simplified spectrum assumed for analysis of the fission data.

intensity per unit energy interval is approximately constant except near the high and low energy ends of the spectrum. Since the decrease in fission yield for $E>20$ Mev indicates a relatively small fission cross section above this energy, little error will be introduced by "squaring off" the upper end of the spectrum by the assumption of a rectangular intensity distribution. The spectral distortion introduced by absorption of the x-rays in their passage through the glass walls of the betatron doughnut and other intervening material will also be neglected in the following analysis, since this distortion is slight except for quanta of very low energy, for which it tends to act as a filter. In Fig. 5, the theoretical intensity spectrum of Bethe and Heitler is given by the solid curve, and the approximate intensity spectrum employed in this treatment is shown as the dotted curve.

The number of quanta per square centimeter with energy between ϵ and $\epsilon+d\epsilon$ can thus be

[9] H. A. Bethe and W. Heitler, Proc. Roy. Soc. 146A, 83 (1934). W. Heitler, *The Quantum Theory of Radiation* (Oxford University Press, New York, 1944), second edition. B. Rossi and K. Greisen, Rev. Mod. Phys. 13, 240 (1941).

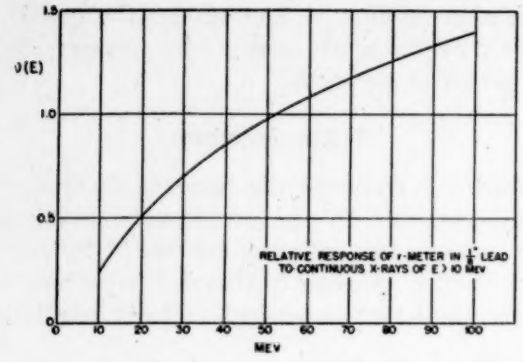

FIG. 6. Relative response of the monitor (Victoreen γ-thimble surrounded by $\frac{1}{8}$-inch lead walls) to continuous x-rays of the spectrum assumed with maximum energy given by the abscissa, the intensity being such that the constant K in Eq. (2) is unity.

written

$$n(\epsilon, E)d\epsilon = Kd\epsilon/\epsilon \quad \epsilon < E, \qquad = 0 \quad \epsilon > E. \tag{2}$$

γ-Meter Sensitivity

The ionization recorded by the γ-meter is the result of the passage through the thimble of negative and positive electron secondaries produced by absorption or scattering of x-ray quanta in the walls of the 3-mm lead cap. To calculate this exactly would require taking account of the detailed energy and angular distribution of the secondaries, of specific ionization as a function of electron energy, of scattering of the electrons, of tertiary processes, of the complicated geometry, and of the exact spectrum of the radiation.

An approximate calculation has been made which it is believed describes the relative dependence of γ-meter efficiency on the maximum x-ray energy, in which an extremely simplified set of assumptions has been used.

Consider a beam of x-ray quanta with the spectral distribution assumed above incident upon an absorbing slab of thickness t. At a depth x in the slab, the number of quanta per square centimeter with energies between ϵ and $\epsilon+d\epsilon$ is given by

$$n(\epsilon, E, x)d\epsilon = K\exp(-\tau x)d\epsilon/\epsilon \quad \epsilon < E, \qquad = 0 \quad \epsilon > E, \tag{3}$$

where the absorption coefficient τ is the sum of three partial coefficients τ_π, τ_c, and τ_φ representing, respectively, pair production, Compton scattering, and photoelectric effect. Each absorption act is assumed to produce two electrons of average energy $\epsilon/2$ if by pair production, one electron of average energy $\epsilon/2$ if by Compton effect, and one electron of average energy ϵ if by photoelectric absorption. These electrons are assumed to proceed in the forward direction.

The wall thickness, t, employed in these measurements is a fraction of a radiation length and is equal to the range of a 5-Mev electron. Tertiary processes in the wall can accordingly be neglected without introducing significant error.

The number of electrons emerging into the space beyond the wall is then

$$\nu(E) = \int_0^E [(2\tau_\pi f_\pi + \tau_c f_c + \tau_\varphi f_\varphi)/\epsilon]d\epsilon. \tag{4}$$

The factors f take account of absorption of quanta in the wall together with the fact that an electron of low energy can emerge from the wall only if its point of production lies within its range of the second surface:

$$f = \int_{t-R}^{t} \exp(-\tau x)dx,$$

or

$$f = \int_0^t \exp(-\tau x)dx,$$

according to whether or not the range R of a given secondary is less or greater than t. In

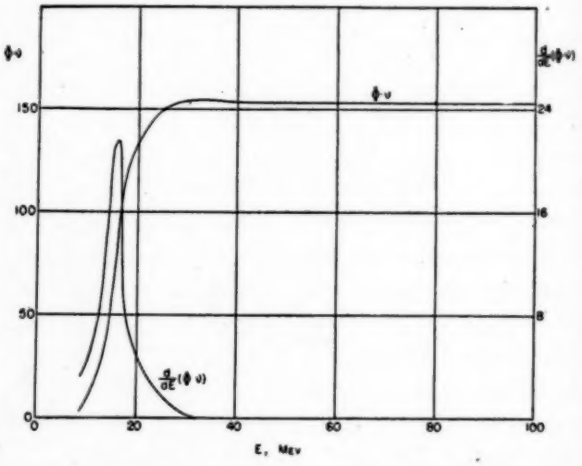

FIG. 7. Analysis of the uranium yield curve of Fig. 4.

evaluating f, the range of an electron has been taken proportional to its energy.

We now assume that all electrons from the wall which enter the thimble produce an equal average ionization, δ, of 60 ion pairs per centimeter. The specific ionization of electrons is nearly independent of energy for electron energies above 300 kev, amounting for air to 76 ion pairs per centimeter at 300 kev, decreasing to 53 at 2 Mev, then rising slowly to 70 ion pairs per centimeter at 100 Mev. Low energy electrons which ionize appreciably higher than this are also highly scattered and are contributed from very thin layers of the wall; therefore, the error introduced by neglecting their higher ionizing power is not serious. The effect of multiple scattering and of the initial angular distribution of produced secondaries is somewhat reduced by having the thimble surrounded by the lead on all sides.

The integration of (4) was carried out graphically. For $E=10$ Mev, the number of secondaries contributed from all three absorption processes was calculated. To this were added the pairs and recoils resulting from absorption of quanta above 10 Mev for a sequence of values of E up to 100 Mev, the x-ray spectrum in each case having the form assumed above and with the constant K adjusted to unity. The result of this calculation is given in Fig. 6. Absolute accuracy cannot be claimed for it, but it is believed that its trend with energy closely parallels the actual variation of sensitivity of the r-thimble.

The reading of the r-meter can then be written

$$r(E)=e\cdot\delta\cdot\nu(E)\cdot K \\ =2.9\times10^{-8}\cdot\nu(E)\cdot K \text{ e.s.u.} \qquad (5)$$

It follows that to produce a reading of 1 roentgen unit (i.e., one e.s.u. of charge per cubic centimeter) in the r-meter when the thimble is irradiated with 100-Mev x-rays and surrounded with $\frac{1}{8}''$ of lead, there must be approximately $2.5\times10^{7}/\epsilon$ quanta of energy ϵ per unit energy interval per square centimeter.

Analysis of the Excitation Curves

The "x-ray fission yield" is the quotient

$$\Phi(E)=F(E)/r(E), \qquad (6)$$

where $F(E)$ and $r(E)$ are given by (1) and (5). From them it follows that the fission cross section is

$$\sigma(E)=\frac{2.9\times10^{-8}E}{NA}\frac{d(\Phi\nu)}{dE}. \qquad (7)$$

Figure 7 shows the analysis of the data for uranium. It is evident that the cross section for photo-fission must be extremely small for quantum energies above 30 Mev. The resulting curve of $\sigma(E)$ *vs.* E is given in Fig. 8 for uranium.

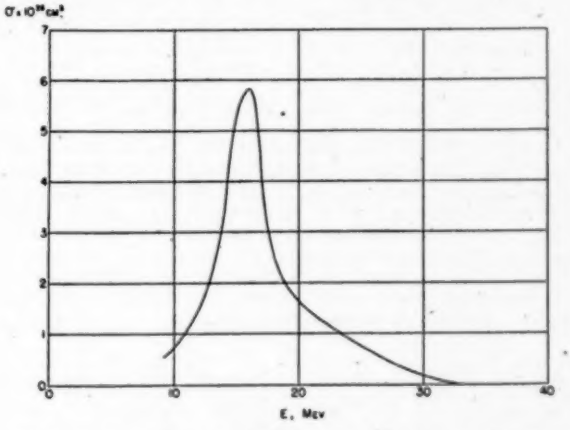

FIG. 8. Cross section for photo-fission of uranium. Because of approximations made in the analysis and uncertainty of the experimental data for low x-ray energies, this curve must be considered of only qualitative significance.

The determination of the cross section involves first drawing a smooth curve through the experimental points, multiplying the ordinates of this curve by a function known only roughly, and then differentiating the product. It is evident that the given data are not sufficiently precise to determine the cross section as a function of energy, even if the calculation of $r(E)$ were exact, since in this case the portion of the yield curve which is most significant to the determination of the cross section is that below 30 Mev. The experimental points in this region are subject to considerable fluctuation, and the true yield curve may be appreciably different from that shown in Fig. 3. It is also true that the effects of the approximations made in calculating $r(E)$ are more serious at low energies. Therefore, it must be stressed that no significance can be attributed to the shape of the curve of σ *vs.* E nor to the absolute values of the cross section given on the scale of ordinates. The curve of

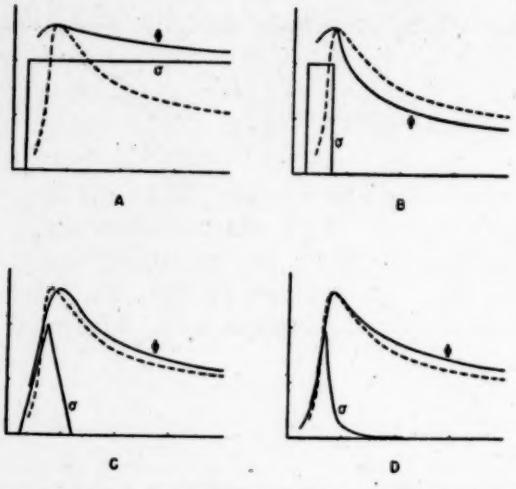

FIG. 9. Four attempts to fit the experimental yield curve by assuming simple functions for the photo-fission cross section, identified by "σ" in each figure. In each case, the curve denoted by "Φ" is the yield curve which should result from the assumed cross section with x-rays of the simple spectrum assumed in the text. The experimental curve is shown dotted. In "*D*" the cross section assumed is a resonance curve with 16-Mev resonance energy and 3-Mev half-width at half-maximum.

Fig. 8 is given for purposes of illustration and to emphasize the fact that the cross section must be very small above 30 Mev.

The thorium data can be analyzed in the same manner. Owing to large fluctuation in the points below 40 Mev, it is not possible to compare the cross sections for uranium and thorium in detail. However, the data indicate similar variation with energy, the curve for thorium being displaced by 1 or 2 Mev owing to its higher threshold energy for fission. If it is permissible to assume that both targets were thick and that the average range of a fission fragment from thorium is equal to that of a fragment from uranium, then it can be concluded that the ratio of the photo-fission cross sections for uranium and for thorium at corresponding energies is 2.0 ± 0.1

The problem of interpretation of the yield curves can also be approached in another way. One can assume several possible functions for $\sigma(E)$ and for each construct the corresponding yield curve which would result with an x-ray spectrum of the simple form assumed and with the r-meter sensitivity varying with maximum x-ray energy in the manner calculated above. One can then see how sensitive the result obtained by direct analysis is to the exact shape of the yield curve.

Figure 9 shows several simple functions representing possible approximate cross sections and the corresponding yield curves. In each figure, the experimentally obtained yield curve is shown dotted. It will be evident that only an extremely small photo-fission cross section can be possible if the decrease in yield above 30 Mev is to be accounted for on the basis of the assumptions made above.

According to the theory of Bohr and Wheeler,[1] photo-fission should be energetically possible and the fission fragments should have sufficient kinetic energy to be readily observable for all of the elements listed in Table I with the exception of samarium. However, of all the elements which were investigated, only uranium and thorium gave a positive result. The photo-fission cross sections of all other elements tested can hardly exceed 10^{-3} times the cross section for uranium; i.e., they are of the order of 10^{-29} cm^2 or less.

The decrease in the photo-fission cross section at high energies exhibited by uranium and thorium together with the absence of fission in the other heavy nuclei investigated is probably to be attributed to the competition of other types of photo-disintegration.[10]

[10] G. C. Baldwin and G. S. Klaiber, Phys. Rev. **70**, 259 (1946).

The Disintegration of Li^7 by Deuterons

W. E. BENNETT,* T. W. BONNER, H. T. RICHARDS,‡ AND B. E. WATT§
The Rice Institute, Houston, Texas

(Received October 14, 1946)

The yield function for the disintegration of lithium bombarded by deuterons has been measured with detectors sensitive to neutrons, gamma-rays, and beta-rays. A gamma-ray of 4.9-Mev energy was found in the course of this investigation. Resonances were found at 0.65, 1.02, and 1.35 Mev corresponding to excited states of the intermediate nucleus (Be^9) at 17.14, 17.43, and 17.69 Mev. The resonance at 1.35 Mev was found only for the formation of radioactive Li^8 accompanied by the emission of a proton. Apparently proton emission is permitted and neutron emission forbidden from the 17.69-Mev state.

THE yield of Li^8, neutrons and alpha-particles from lithium bombarded by deuterons of energies up to 1 Mev has been measured by Rumbaugh, Roberts, and Hafstad.[1] Their excitation curves showed a smooth increase in yield with energy until energies of about 700 kev were reached. From 700 to 1000 kev their yield curves continued to increase but less rapidly than at lower energies. Later experiments[2] which were carried out at Rice Institute on the excitation curves of carbon bombarded by deuterons of energies up to 2.0 Mev showed a number of resonances with half-widths of from 10 kev to 100 kev. These experiments with carbon suggest that similar resonances might be found in the disintegration of lithium by deuterons and so a similar study was undertaken for lithium bombarded by deuterons; preliminary results of these experiments were reported at a meeting of the American Physical Society.[3,4]

APPARATUS

The Rice Institute pressure Van de Graaff machine was used to produce bombarding particles of homogeneous and variable energy. Thin targets of LiCl, LiOH, and metallic lithium were used. They were produced by evaporation from a tungsten filament onto a polished disk of pure silver or copper. The LiCl targets blackened rapidly during bombardment and the yield of neutrons increased with time as a result of the deposition of carbon. These targets were made thicker (50–100 kev) than the metallic lithium targets which were used later so that the carbon would have a relatively small effect. They were also moved frequently to bombard a new spot. The thickness of the targets was estimated from the amount of material evaporated, and also, somewhat more precisely, by comparing the yield from the thin target with that of a thick target of the same material. The latter calculation was possible after the yield function for the reaction was known. It also involved suitable correction for the range-energy relationship of the bombarding particles in the thick target. The thickness of the target was expressed in kev, meaning the average energy lost by a bombarding particle in passing through it.

The yields of beta- and gamma-rays were measured with Geiger counters filled with a self-quenching mixture of argon and alcohol. A scale of eight was used in the recording circuit. Coincidence counting was sometimes used, a bias being set to cut out pulses from one counter and record only the pulses of double size produced by simultaneous discharge of the two counters. To count gamma-rays, carbon blocks were used to absorb out the beta-radiation.

THE GAMMA-RAYS FROM Li^7+H^2

Only one gamma-ray (of 450-kev energy) has been reported[5] from the deuteron bombardment

* Now at Illinois Institute of Technology, Chicago, Illinois.
‡ Now at University of Wisconsin, Madison, Wisconsin.
§ Now at Texas Company, Houston, Texas.
[1] L. H. Rumbaugh, R. B. Roberts, and L. R. Hafstad, Phys. Rev. **54**, 657 (1938).
[2] W. E. Bennett, T. W. Bonner, E. Hudspeth, H. T. Richards, and B. E. Watt, Phys. Rev. **59**, 781 (1941).
[3] W. E. Bennett and B. E. Watt, Phys. Rev. **60**, 167 (1941).
[4] T. W. Bonner and H. T. Richards, Phys. Rev. **60**, 167 (1941).
[5] J. H. Williams, W. G. Shepherd, and R. O. Haxby, Phys. Rev. **52**, 390 (1937).

of lithium. In the course of these experiments, a gamma-ray of higher energy was found.[6] Its energy was determined by inserting aluminum sheets between two coincidence counters and recording the coincidence counting rate as a function of the thickness of aluminum. The curve is given in Fig. 1. The maximum range of Compton electrons as estimated from this curve is 8.7±0.4 mm of aluminum. This corresponds to an energy of 4.9±0.3 Mev. The relation between

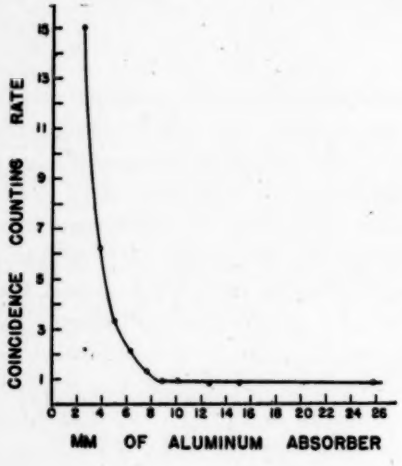

FIG. 1. The rate of coincidence counting as a function of the thickness of aluminum between counters. The end point at 8.7±0.4 mm implies an energy of 4.9±0.3 Mev for the gamma-rays from Li^7+H^2.

range and energy had previously been determined by measurements on gamma-rays of known energy with the same apparatus.[7]

It is very probable that the high energy gamma-ray is associated with a neutron group as indicated by the following equation:

$$_3Li^7+{}_1H^2\rightarrow {}^*_4Be^8+{}_0n^1+10.1 \text{ Mev},$$
$$^*_4Be^8\rightarrow {}_4Be^8+\gamma+4.9 \text{ Mev}.$$

The spectrum of neutrons from this reaction shows evidence of the associated neutron group. Both Stephens[8] and Richards[9] found a wide group of neutrons at about 10.5 Mev. This group is too wide and of too low energy to be entirely accounted for by the 2.8-Mev level in Be^8 which breaks up into two alpha-particles, but it may be regarded as consisting of two unresolved groups, one associated with the 2.8-Mev level and the other with a level at 4 or 5 Mev which emits gamma-rays because of a selection rule which forbids the break-up into alpha-particles. A similar level in Be^8 at 17.5 Mev is responsible for the high energy gamma-rays from Li^7 bombarded by protons.

To detect 4.9-Mev gamma-rays in the presence of 450-kev gamma-rays, coincidence counters were used, the wall thickness being sufficient to prevent detection of gamma-rays of less than 2-Mev energy. However, this procedure was found unnecessary and a single Geiger counter was used for the final data. The single counter was used to take a lead absorption curve under good geometrical conditions and the radiation seemed to be homogeneous. The 450-kev radiation was too feeble to give a noticeable effect under our conditions. The single Geiger counter did not respond appreciably to neutrons. A block of paraffin which reduced the neutron intensity to half, did not affect the counting rate in the Geiger counter. The neutrons produced radioactivity in the counter walls, but this was subtracted as part of the natural effect.

THE YIELD CURVE FOR GAMMA-RAYS AND NEUTRONS

The yield of gamma-rays and neutrons as a function of energy from 0.5 to 1.9 Mev is given in Fig. 2. The neutrons were observed in the forward direction. The scale of ordinates is arbitrary and different for the two curves. The absolute yield of gamma-quanta was roughly 3 percent of the yield of neutrons. This figure was arrived at by assuming that the Geiger counter was 2 percent efficient for counting gamma-rays and by using the data of Amaldi, Hafstad, and Tuve[10] for the yield of neutrons from a thick target.

The similarity of the gamma-ray and neutron curves shows that the same intermediate nucleus is involved. Since most of the neutrons are from bombardment of the Li^7 isotope, it is out of the

[6] W. E. Bennett, T. W. Bonner, H. T. Richards, and B. E. Watt, Phys. Rev. **59**, 904 (1941).
[7] W. E. Bennett, T. W. Bonner, and Bob E. Watt, Phys. Rev. **59**, 793 (1941).
[8] W. E. Stephens, Phys. Rev. **53**, 223 (1938).
[9] H. T. Richards, Phys. Rev. **59**, 796 (1941).
[10] E. Amaldi, L. R. Hafstad, and M. A. Tuve, Phys. Rev. **51**, 896 (1937).

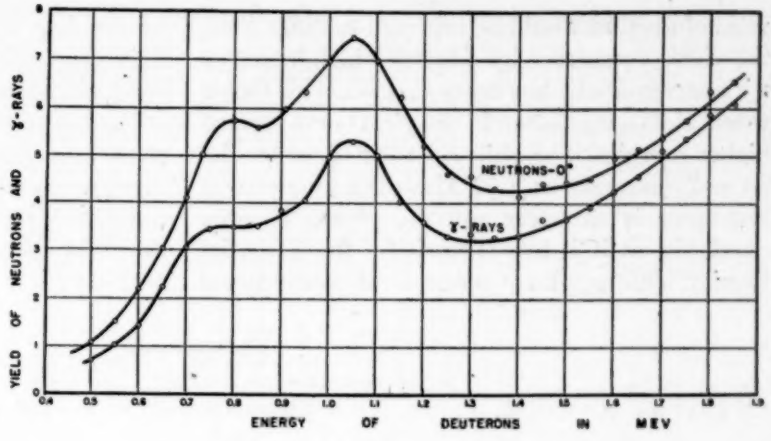

FIG. 2. Yields of neutrons and gamma-rays from "partially thin" targets of lithium bombarded by deuterons. The thickness of the targets was 55 kev for the gamma-ray curve and 90 kev for the neutron curve. The scale of ordinates is arbitrary and different for the two curves.

question that the gamma-rays might have been produced by bombardment of the Li^8 isotope.

THE YIELD CURVE FOR BETA-RAYS AND NEUTRONS

Coincidence Geiger counters were used to detect the beta-rays. The wall thickness discriminated against beta-rays of less than 2 Mev energy. The arrangement counted some gamma-rays. To see how many gamma-rays were counted, carbon absorbers were placed between the target and the counters to absorb out the beta-rays. Less than one percent of the counts remained after absorption of all the beta-rays from the target.

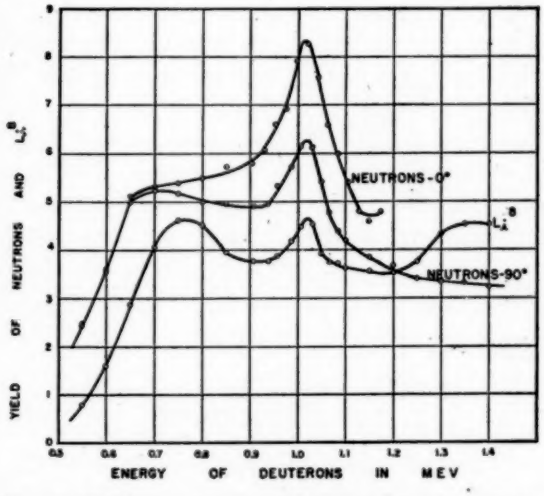

FIG. 3. Yields of neutrons and gamma-rays from "thin" lithium targets bombarded by deuterons. The yield is in arbitrary units, different for each curve. The neutron curves have been fitted at 0.55 Mev. The angular distribution of neutrons changes with bombarding energy.

The yield curves for beta-rays and neutrons were taken simultaneously. The methane-filled electroscope used to detect neutrons was placed at 90° to the bombarding beam. The beta-rays were detected in the forward direction. The target was made by evaporating lithium metal in vacuum, and its thickness was estimated from the yield to be 14 kev.

The excitation curves for beta-rays and for neutrons at 90° were run from 0.55 Mev to 1.4 Mev. They are shown in Fig. 3. Another curve was run with the neutron detector in the forward direction. This was normalized to agree with the 90° curve at 0.55 Mev and plotted in Fig. 3.

The neutron curve shows resonances at 0.65 and 1.02 Mev. The neutrons show a departure from a spherical symmetry which is different for the two resonances. If there is spherical symmetry for the first resonance, then the second resonance shows a marked maximum of neutron intensity in the forward direction. Further studies of the angular distribution of the neutrons from the reaction would be desirable.

For beta-rays, the first resonance appears to be at 0.75 Mev, about 0.1 Mev higher than the corresponding neutron resonance. It may, however, correspond to the same state of the intermediate nucleus. The beta-rays are produced in the reaction:

$$_3Li^7 + {}_1H^2 \rightarrow {}_3Li^8 + {}_1H^1 - 0.26 \text{ Mev},$$

$$_3Li^8 \rightarrow {}_4Be^8 + \beta.$$

The yield of beta-rays is equal to the yield of low energy protons. The protons must penetrate a potential barrier to escape and, therefore, the

yield of protons would be expected to differ from the yield of neutrons by a factor which increases with energy in the low energy region. This factor would shift a maximum in the yield curve toward higher energies. This shift does not occur for the second resonance at 1.02 Mev; but this second resonance is narrower and the proton is more energetic, so it is less affected by the potential barrier. This argument seems to be contradicted by the fact that the first resonance is stronger than the second for proton emission; however, other differences in the states of the intermediate nucleus may affect the strength of a resonance. A third resonance at 1.35 Mev in the beta-ray curve corresponds to a state of Be^9 for which neutron emission is forbidden or at least is much weaker than for the other resonances at 0.65 and 1.02 Mev.

PHYSICAL REVIEW VOLUME 71, NUMBER 1 JANUARY 1, 1947

The Self-Diffusion Coefficient of Uranium Hexafluoride*

EDWARD P. NEY AND FONTAINE C. ARMISTEAD**
Rouss Physical Laboratory, University of Virginia, Charlottesville, Virginia
(Received October 9, 1946)

A method is reported for measuring the self-diffusion coefficient of a vapor by observing with a mass spectrometer the rate at which material enriched in one isotope diffuses into normal material in an apparatus of known geometry. A value of ρD (where ρ is the density and D the diffusion constant) was obtained for uranium hexafluoride at 30°C. Knowledge of the viscosity together with the constants reported here allow calculation of the molecular force law.

IN the kinetic theory of transport phenomena ρD is a prominent factor whose value must be known. Heretofore its value has been determined from the coefficient of viscosity, η, on the basis of the equation $\rho D = \epsilon\eta$ where ϵ is at best an uncertain quantity. The following is a report of the measurement of ρD in which D is understood to be the diffusion coefficient for one gas diffusing into another where the only difference between the gases is their isotopic ratios.

This measurement represents an excellent approximation to the self-diffusion coefficient, which strictly speaking cannot be measured.[1] If one may speak of the self-diffusion of a gas whose molecules are composed of more than one isotope, one should probably define it as the diffusion of one gas in which the isotopes are in their normal ratio into another with normal ratio. The ideal experiment to measure this would consist of tagging one group of molecules differently from the other group in such a way that the tagging would not affect the phenomenon of diffusion. If uranium hexafluoride slightly enriched in U^{238} and uranium hexafluoride slightly enriched in U^{235} diffuse into each other exactly as normal uranium hexafluoride diffuses into normal then isotopic concentration is just such an ideal tag. As can easily be seen the measurement of the changing concentration of one isotope as the diffusion takes place gives directly the changing concentration of one group in the mixture of both groups of molecules.

I. DESCRIPTION OF APPARATUS AND PROCEDURE

The apparatus is shown schematically in Fig. 1. The diffusion bulbs F and B were two coaxial copper cylinders of volumes 925 and 259 cubic centimeters, respectively. They were connected by the copper pipes C (length 6.80 cm; area

* This paper is based on work performed under Contract No. OEMsr-398 with the Office of Research and Development at the University of Virginia, in 1942 and 1943. "The information presented in this paper will appear in Division X of the Manhattan Project Technical Series as part of the contribution of the Physics Department, University of Virginia."
** Now at Clinton Laboratories, Oak Ridge, Tennessee.
[1] Rigorously the self-diffusion coefficient can be defined only for a gas composed of identical molecules, e.g., all $U^{235}F_6$ or all $U^{238}F_6$.

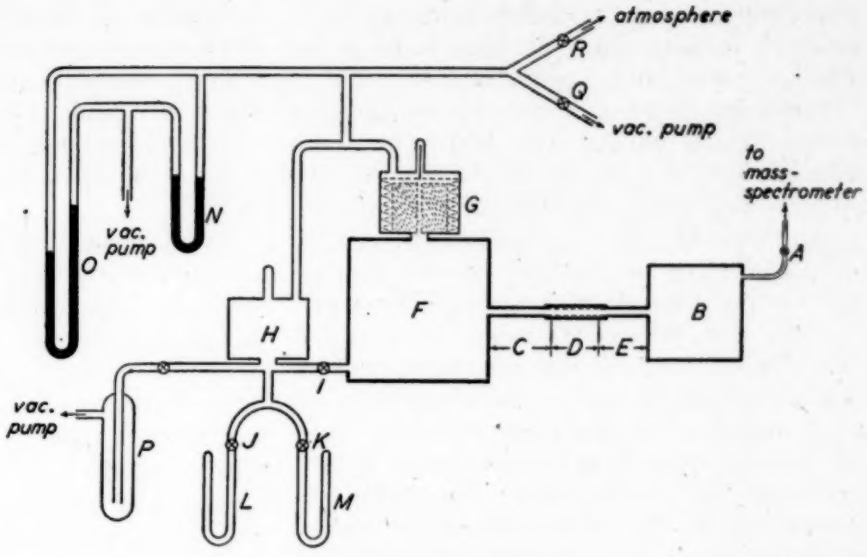

FIG. 1. Schematic drawing of the diffusion apparatus (not to scale).

0.3215 cm²) and E (length 6.78 cm; area 0.3238 cm²) and by the Neoprene tubing, D, of area 0.2714 cm². In order to obtain different relaxation times, the length of the Neoprene was made 2.08 cm in six of the runs and 6.10 in two of them. Connected to bulb F is a null type sylphon pressure gauge G. The pressure above the sylphon could be made equal to the pressure in the bulbs by operating valves R and Q to obtain a null reading of the indicator needle which was observed in a microscope field. The neutralizing pressure was read on the mercury manometer N and the oil manometer O, the latter being capable of showing a pressure change of 0.06 mm Hg.

Material from bulb B was drawn through the adjustable capillary leak A into the ion source of the mass spectrometer. The leak A and the valve I add negligible volumes to the diffusion bulbs.

The system used for purifying the samples and filling the bulbs was connected to them through the valve I. This system consisted of a pressure gauge H and a manifold to which samples could be connected at L and M. The diffusion system was submerged in a 12-gallon water bath which was equipped with a vigorous stirrer and with a cover to minimize evaporation. A Beckman thermometer was placed beside each bulb.

Measurements of the dimensions of the apparatus were straightforward with the exception of the cross section of the Neoprene tube (D). This cross section was decreased by the pressure on the outside and by the thin uranium hexafluoride reaction coating on the inside. Both of these effects were measured. The Neoprene used did not undergo any continuous reaction with uranium hexafluoride.

In order to establish that the samples were pure after admission to the diffusion bulbs, and that they remained pure throughout the course of an experiment, the impurity peaks were examined in the mass spectrometer. Samples with impurities less than one percent by volume were obtained for the experiment.

A certain amount of material was drawn by the mass spectrometer. This withdrawal causes some mass flow from F to B. An upper limit to this effect was determined by the following test. A sample of uranium hexafluoride was admitted to the diffusion bulbs. The pressure in the bulbs and the intensity of the ion peaks in the spectrometer were made the same as those used in the diffusion runs. After a careful reading on the the gauge (G) had been obtained, the Neoprene (D) was pinched and left closed for 15 hours. If there had been a rate of withdrawal of such magnitude as to affect the measurement of the diffusion constant by as much as one percent there would have been an instantaneous and observable change at the gauge (G) upon unpinching D. No change was noted.

Before making any diffusion runs, the entire apparatus was pretreated. When it was necessary to replace some part of the apparatus, the pre-

treatment was repeated before more runs were made. A vacuum was maintained in the bulbs when runs were not being made.

In making the runs, samples were attached at L and M and purified. One sample had been enriched in $U^{238}F_6$, the other in $U^{235}F_6$. The first sample was then admitted to the diffusion system (through valve I) to a pressure of 1 cm of mercury. The Neoprene (D) was then pinched bulb F was pumped out and filled to 1 cm with material from the second sample. The character of the first sample was then the character of the material in bulb B at the start of the diffusion. Only moderate care was taken to remove traces of the first sample from F and from the walls of the purifying system before introducing the second sample. The presence of a slight amount of the first sample in F would not affect the calculation of ρD, but would merely reduce the over-all concentration change measured. Before starting the diffusion the Neoprene tube was unpinched for 10 seconds in order to assure equal pressures in F and B. (A) was opened and peaks were brought into the mass spectrometer; the Neoprene was unpinched, and the diffusion started. Continuous measurement of the 235/238 ratio was made in the mass spectrometer by the null method.[2] This consists essentially of balancing a fraction of the 238 current against the 235 current, and reading this fraction on a voltage divider. Readings were taken every ten minutes for a period of two to three hours, the relaxation time of the system. The resolution of the mass spectrometer remained good throughout the runs. The Beckmann thermometers showed temperature agreement to better than 0.01°C rise of one bulb over the other per hour. A variation of the order of ten times this could have been tolerated without affecting the accuracy of the measurement.

At the end of the relaxation time the leak A was closed and the peaks in the mass spectrometer dropped to their residual value. A standard sample was measured before and after the diffusion run. This permitted correction of the diffusion points for apparatus drift. This correction was, on the average, about 4 percent of the total change measured in the diffusion run. Careful measurements of the pressure in the bulbs were made before and after the runs.

Several methods were used to obtain the value of the concentration after complete mixing (C^∞).

In five of the runs C^∞ was measured 20 hours after the start of the experiment by making an analysis of the material in the diffusion bulbs (i.e., comparing the 235/238 ratio with that of standard material); in two of the runs C^∞ was obtained by pumping the material out of the bulbs into a copper trap and making a routine analysis of this; and in one of the runs C^∞ was obtained by calculation from the known initial values of the concentration in bulbs F and B. Of course, in all cases C^∞ could be thus calculated, and this was done as an added check. The agreement was found to be within the accuracy of measurement.

In six of the runs the diaphragm in the sylphon gauge (G) was pressed against the inside plug of the gauge by admitting air above it. The diaphragm thus acted as a valve closing off the main volume of the sylphon gauge from bulb F. In these instances the calculations were made on the basis of the two-bulb problem. In two of the runs the diaphragm of the sylphon gauge was forced against the upper stop of the gauge by pumping a vacuum through the valve Q. The volume of the sylphon gauge then communicated with the bulb F throughout the experiment. The calculations for this case was made on the basis of the three-bulb problem (described later).

II. THEORY

The following is a list of symbols to be used in developing the theory:

C_2' = concentration in grams/cc of $U^{235}F_6$ in bulb B at time "t"
C_1' = concentration in grams/cc of $U^{235}F_6$ in bulb F at time "t"
D = coefficient of diffusion in cm²/sec.
V_2 = volume of bulb B in cc
V_1 = volume of bulb F in cc
l = effective length of connecting tube
A = effective area of connecting tube
C^∞ = equilibrium value of the concentration after complete mixing

[2] A. O. Nier, E. P. Ney, and M. G. Inghram, "Null method for the comparison of two ion currents in a mass spectrometer," Chicago Meeting of the American Physical Society, June 22, 1946.

$$V_0=V_1+V_2$$
$$\gamma=\frac{DA}{l}\left[\frac{V_0}{V_1V_2}\right]$$
$$\beta=\frac{DA}{l}\left[\frac{V_0C^\infty}{V_1V_2}\right]$$
$$\alpha=\frac{D}{\Sigma_j(l_j/A_j)}\left[\frac{(V_0+Al)}{(V_1+Al/2)(V_2+Al/2)}\right].$$

The simplest case of the diffusion problem will be worked out first and the necessary corrections will be calculated later.

The assumptions made in the simple theory are:

(A) The concentration gradient in the connecting tube is linear.

(B) The concentration gradient is all in the connecting tube.

(C) The volume of the connecting tube is negligible compared with the volume of the bulbs.

Under these conditions we can write the equation for Q, the rate of transfer of $U^{235}F_6$ by diffusion:

$$Q=-DA\ \text{grad}C. \tag{1a}$$

Because of assumptions A and B above:

$$Q=-(DA/l)(C_2^t-C_1^t). \tag{1b}$$

The rate of transfer in terms of the time is given by:

$$Q=V_2\delta C_2^t/\delta t. \tag{2}$$

Equating (1) and (2), we obtain the differential equation

$$\delta C_2^t/\delta t=-(DA/lV_2)(C_2^t-C_1^t). \tag{3}$$

In view of the relation (4) between C_1^t and C_2^t, we can write Eq. (5) using β and γ as previously defined.

$$V_2C_2^t+V_1C_1^t=V_0C^\infty, \tag{4}$$

$$\delta C_2^t/\delta t=-\gamma C_2^t+\beta. \tag{5}$$

We also have the boundary condition:

$$C_2^t=C_2^0 \text{ at } t=0. \tag{5a}$$

The solution of (5) subject to the boundary condition is:

$$C_2^t=C^\infty+(C_2^0-C^\infty)e^{-\gamma t}. \tag{6}$$

Equation (6) is the solution of the diffusion equation for the simple case. In order to apply it to our experiment it is necessary to modify it by making proper corrections for assumptions A, B, and C.

The assumption of a linear concentration gradient enters in the above as a substitution of $A(C_2-C_1)/l$ for $A\cdot\text{grad}C$. Since the concentration gradient is linear in each element of length l_j with cross section A_j; l/A must be taken to mean $\sum_j l_j/A_j$ which is the equivalent single l/A for the connecting tube.

Since in our experiment, the l/A for the bulbs was one-half of one percent of the l/A for the connecting tube the assumption that the gradient is all in the connecting tube is justified providing a small end correction is made. For the purpose of making this correction, we assume that the conditions at the ends of the connecting tube are the same as they would be if the bulbs had infinite volumes. The magnitude of the correction for the analogous electrical case has been shown by Rayleigh[3] to be an effective increase in the length of the tube at each end by about 0.82 times the radius. This additional length is considered only in $\sum_j l_j/A_j$. It can also be shown by a method similar to that of Loschmidt[4] that the concentration gradient in the connecting tube is set up in a time of the order of $\frac{1}{2}$ minute, with our geometry.

The connecting tube has a volume that can not be neglected. Because of the symmetry of the connecting tube about the point of pinching the Neoprene connector, the average concentration in the connecting tube ($\bar{C}_L$) is at any time the mean of the concentrations at the ends of the connecting tube.

$$\bar{C}_L=\tfrac{1}{2}(C_1^t+C_2^t). \tag{7}$$

Equation (4) must then be replaced by:

$$V_2C_2^t+V_1C_1^t+\bar{C}_LAl=(V_0+Al)C^\infty. \tag{8a}$$

And using (7) and grouping terms, (8a) becomes:

$$(V_2+Al/2)C_2^t+(V_1+Al/2)C_1^t=(V_0+Al)C^\infty. \tag{8b}$$

Equation (6) can be made consistent with this condition if one replaces in γ, V_1 by $(V_1+Al/2)$, V_2 by $(V_2+Al/2)$, and V_0 by (V_0+Al).

[3] See Maxwell, *Electricity and Magnetism* (Oxford, 1892), p. 434; Lord Rayleigh, *Theory of Sound* (The MacMillan Company, 1878), Vol. II, pp. 291–295.

[4] Loeb, *Kinetic Theory of Gases* (McGraw-Hill Book Company, Inc., New York, 1934), pp. 268–272.

The quantity which embodies all of the above corrections, and which will replace γ, will be called α.

$$\alpha=\frac{D}{\sum_j(l_j/A_j)}\left[\frac{(V_0+Al)}{(V_1+Al/2)(V_2+Al/2)}\right]. \quad (9)$$

The equation which describes the diffusion is then:

$$\frac{C^\infty-C_2^t}{C^\infty-C_2^0}=e^{-\alpha t}. \quad (10)$$

The constant $1/\alpha$ is the relaxation time of the system.

As was mentioned earlier, in some cases the diffusion was allowed to proceed with the sylphon gauge open to the adjacent bulb. The solution for the three-bulb problem will be indicated here. We use the same notation which we used previously with the addition of:

l_2/A_2 = effective l/A between sylphon gauge and bulb F.

V_3 = volume of sylphon gauge (G).

C_3^t = concentration of $U^{235}F_6$ in (G) at time "t."

The equations which must be satisfied are:

$$V_2\frac{\delta C_2^t}{\delta t}=\frac{DA}{l}(C_1^t-C_2^t), \quad (11a)$$

$$V_1\frac{\delta C_1^t}{\delta t}=\frac{DA_2}{l_2}(C_3^t-C_1^t)+\frac{DA}{l}(C_2^t-C_1^t), \quad (11b)$$

$$C_3^t=\frac{(V_1+V_2+V_3)C^\infty-V_1C_1^t-V_2C_2^t}{V_3}. \quad (11c)$$

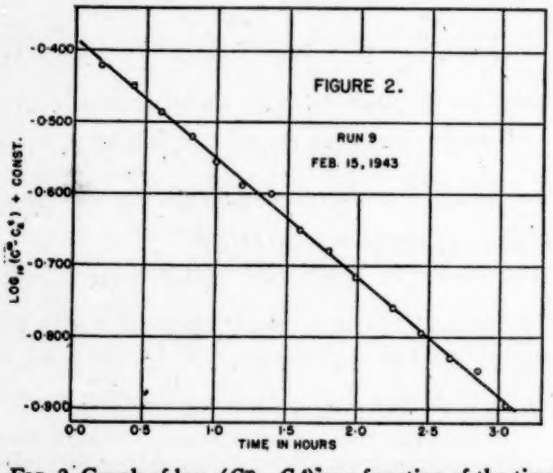

FIG. 2. Graph of $\log_{10}(C^\infty-C_2^t)$ as a function of the time. The slope of the least squares solution, together with the geometrical constants gives the diffusion coefficient.

With the boundary conditions:

$$C_2=C_2^0; \quad (12a)$$

$$C_1=C_3=C_1^0=C_3^0; \quad \text{when } t=0. \quad (12b)$$

The solution of Eqs. (11) and (12) has for one of our numerical cases the form:

$$\frac{C_2^t-C^\infty}{C_2^0-C^\infty}=0.966\exp(-9.49Dt\times10^{-5})+0.034\exp(-16.45Dt\times10^{-5}).$$

If in Eqs. (11) $C_3^t=C_1^t$, the equations reduce to the two-bulb case, for which the corresponding numerical solution is:

$$\frac{C_2^t-C^\infty}{C_2^0-C^\infty}=\exp(-9.72\times10^{-5}Dt).$$

The value of D as calculated assuming a two-bulb problem, when the diffusion actually follows the three-bulb equations can be shown to be too small by approximately 0.8 percent.

III. CALCULATIONS AND RESULTS

The time derivative of the logarithm of $|C^\infty-C_2^t|$ gives (from (10)):

$$\frac{\delta}{\delta t}\log_e|C^\infty-C_2^t|=-\alpha.$$

The slope of the plot of $\log_e|C_2^t-C^\infty|$ against time thus gives $-\alpha$. A graph of $\log_{10}(C^\infty-C_2^t)$ against time is shown in Fig. 2. The line indicated was obtained by the method of least squares. The C_2^t of the theory was obtained from the 235/238 ratio measured in the mass spectrograph.

The quantity D/α was calculated from the measured geometric constants (9). The diffusion constant was then obtained by multiplying this D/α by the experimental α obtained from the least-squares solution.

In order to know ρD (where ρ is the density), ρ was calculated assuming the ideal gas law to hold. This assumption has been shown to be justified at one centimeter pressure and room temperature.

The results obtained are presented in Table I. As is indicated, half of the runs were made with C_2^t decreasing, and half with C_2^t increasing. Calling Δ the concentration difference between

TABLE I. Observational results.

Run	Date made	Cm Hg pressure	Temp.	Two-bulb or three-bulb	C_3^4 increasing or decreasing	Concentration difference	Geometry	$(\rho D)_{t°}$* micropoises
5	Nov. 10, 1942	1.08 cm	27.6°C	III bulb	decreasing	Δ	*A*	235
6	Nov. 16, 1942	0.94	23.9°	III	increasing	Δ	*A*	215
7	Nov. 25, 1942	1.08	27.4°	II	increasing	Δ	*A*	254
8	Feb. 12, 1943	1.09	26.4°	II	decreasing	4Δ	*A*	238
9	Feb. 15, 1943	1.10	26.2°	II	increasing	4Δ	*A*	234
10	Feb. 18, 1943	1.11	26.2°	II	decreasing	4Δ	*A*	237
11	Feb. 25, 1943	1.07	27.2°	II	decreasing	4Δ	*B*	244
12	March 1, 1943	1.08	26.9°	II	increasing	4Δ	*B*	215

Average $(\rho D)_{30°}=234$ micropoises

* The value of $(\rho D)_{t°}$ was calculated from ρD at the temperature measured (for example from $(\rho D)_{27.4°}$) by utilizing the known temperatur e dependence of viscosity. This was justified because of the smallness of the correction.

the bulbs at the start of runs 5, 6, and 7, the concentration difference between the bulbs at the start of runs 8, 9, 10, 11, and 12 was about 4Δ. The average ρD was the same for both of these conditions. This indicates that there is no memory effect in the mass spectrograph which would keep it from following the changes in concentration at the proper rate. Geometry *A* indicates that the Neoprene (D) was 2.08 centimeters long, geometry *B* means that the Neoprene was 6.10 centimeters. The values of ρD corrected to 30°C are shown in the last column of Table I. The average value for $(\rho D)_{30°}$ was 234 ± 3 micropoises. The cumulative error in the measurement of the geometrical constants is about 3 percent. The error in measuring the pressure is less than one percent. In view of this:

$$(\rho D)_{30°}=234\pm9 \text{ micropoises.}$$

Knowledge of ρD makes it possible to determine ϵ in the theoretical relation $\rho D=\epsilon\eta$, where η is the viscosity coefficient. This ϵ is of peculiar interest in that a value for the force field exponent of the molecule may be deduced from it. According to classical theory ϵ should range from 1.200 for hard sphere molecules to 1.54 for molecules interacting as the inverse fifth power of their separation.

The value of the ratio of ρD to η at 30°C is 1.31. This gives for the molecular force law $F=\text{const.}/r^{20}$.

The writers wish to thank Professors A. O. Nier at the University of Minnesota and J. W. Beams at the University of Virginia for suggesting the problem and for giving a great many helpful suggestions. We wish to thank Professor L. B. Snoddy for invaluable aid given in frequent consultations.

We wish to express our sincere appreciation to Dr. P. H. Abelson, Dr. Ross Gunn, and Mr. John Hoover of the Naval Research Laboratory for supplying many of the enriched samples. The remainder of the samples were furnished by Professors Beams and Snoddy, Dr. J. W. Moore, and the Virginia group to whom we are also indebted.

On the Scattering of Fast Neutrons by Protons and Deuterons

M. AGENO,* E. AMALDI,* D. BOCCIARELLI,† AND G. C. TRABACCHI†
Instituto Superiore di Sanità, Roma, Italia

(Received August 4, 1945)

The scattering cross sections of the proton, deuteron, and the carbon nucleus have been determined for 4.1-, 12.5-, and 13.5-Mev neutrons by detecting the corresponding recoil protons. A coincidence set of three proportional counters was used. Similar measurements were made with 14-Mev neutrons from the reactions D+Li. These were detected by the 9.9-min. activity arising from the reaction ${}_{29}Cu^{63}+{}_0n^1\rightarrow{}_{29}Cu^{62}+2{}_0n^1$. The $n-2n$ disintegration of the deuteron has been investigated for 14-Mev neutrons and cross section found to be of the order of 9–4 $\times10^{-26}$ cm². The scattering cross sections at 4.1, 12.5, and 13.5 Mev are, respectively, for H 1.73, 0.69, 0.694×10^{-24} cm²; for D 1.79, 0.78, 0.864×10^{-24} cm²; for C 1.99, 1.40, 1.23×10^{-24} cm². The experimental results are compared with those of other experimenters and with theoretical predictions.

1. INTRODUCTION

INFORMATION about the nuclear forces can be deduced by comparing the experimentally determined energy-dependence of the neutron-proton scattering cross section with the corresponding theoretical predictions. The more valuable experiments for such a purpose are those carried on with mono-energetic neutrons. Such neutrons are produced according to reaction

$${}_1D^2+{}_1D^2\rightarrow{}_2He^3+{}_0n^1, \qquad (1)$$

whose spectrum energy is variable with both the observation angle and the voltage used to accelerate the impinging deuterons.

Of the numerous experiments performed with reaction (1) we shall mention that of Aoki[1] who, by changing the observation angle, was able to determine the proton-neutron cross section for five different values of the energy of the impinging neutrons ranging between 2.14 and 2.76 Mev. Other experiments performed with reaction (1) refer to neutron energies varying, from case to case, between 2.4 and 3 Mev.[2] Besides these measurements and those performed with slow neutrons,[3] there have been others carried on with neutrons of about 0.2–0.3 Mev produced by nuclear photo-effect[4] or by the reaction[5]

$${}_1D^2+{}_6C^{12}\rightarrow{}_7N^{13}+{}_0n^1. \qquad (2)$$

For energies larger than 3 Mev there is a lack of published experimental data. As far as we know only Salant, Roberts, and Wang[6] and Salant and Ramsay[7] have performed measurements with the neutrons from the reaction

$${}_1D^2+{}_3Li^7\rightarrow{}_4Be^8+{}_0n^1 \qquad (3)$$

detected by means of the activity of 9.9-min. period, produced in copper according to the reaction

$${}_{29}Cu^{63}+{}_0n^1\rightarrow{}_{29}Cu^{62}+2{}_0n^1, \qquad (4)$$

$${}_{29}Cu^{62}\rightarrow{}_{28}Ni^{62}+e^+. \qquad (5)$$

It is to be noticed that reaction (4) has an appreciable yield only for energies of the impinging neutron larger than 11 Mev,[8] so that the results of these authors refer to neutrons of about 14 Mev.

Finally, considering all the measurements performed up to the present, it is to be noticed that the experimental methods are different for different energy, excepting the measurements of

* Instituto di Fisica dell' Università, Centro di Fisica Nucleare del C.N.R.

† Instituto Superiore di Sanità.

[1] H. Aoki, Phys. Rev. **55**, 795 (1939).

[2] E. T. Booth and C. Hurst, Proc. Roy. Soc. **A161**, 248 (1937); R. Ladenburg and M. H. Kanner, Phys. Rev. **52**, 911 (1937); W. H. Zinn, S. Seely, and V. W. Cohen, Phys. Rev. **56**, 260 (1939).

[3] E. Amaldi and E. Fermi, Ricerca Scient. 7–1, 223, 393 (1936); Phys. Rev. **50**, 899 (1936); L. Simons, Phys. Rev. **55**, 792 (1939); Kgl. Danske Vid. Sels. Math.-Fys. Medd. 16 (1940); V. W. Cohen, H. H. Goldsmith, and J. Schwinger, Phys. Rev. **55**, 106 (1938); H. B. Hanstein, Phys. Rev. **57**, 1045 (1940).

[4] A. Leipunski, L. Rosenkewitsch, and D. Timoschuk, Phys. Sov. **10**, 625 (1936); W. E. Good and G. Scharff-Goldhaber, Phys. Rev. **58**, 89 (1940).

[5] E. Amaldi, D. Bocciarelli, and G. C. Trabacchi, Ricerca Scient. **11**, 121 (1940).

[6] E. O. Salant, R. B. Roberts, and P. Wang, Phys. Rev. **55**, 984 (1939).

[7] E. O. Salant and N. F. Ramsay, Phys. Rev. **57**, 1075 (1940).

[8] R. Sagane, Phys. Rev. **53**, 492 (1938).

Aoki, which cover a rather narrow energy interval.

For a strict comparison with theory it would be very convenient to have measurements performed with mono-energetic neutrons whose energy could be varied within wide limits.

In Section 2 we shall explain a method which satisfies rather well such a condition; it has been applied to the determination of the scattering cross sections of hydrogen, deuterium, and carbon for 4.1-, 12.5-, and 13.5-Mev neutrons.

In other sections we attempt to clarify some interesting points about the neutron-proton and neutron-deuteron collisions.[9]

2. THE METHOD

Our experimental arrangement is shown in Fig. 1. Neutrons emitted by the source S impinge on the paraffin layer P whose thickness (2 mm) is negligible with respect to the absorption of neutrons and large with respect to the range of recoil protons. Protons projected in the forward direction and fast enough to go through the Al-absorber A, are registered by a coincidence-set of three proportional counters, $c_1c_2c_3$.

The triple coincidences are caused only in part by protons recoiling from P; in part they are caused by random coincidences whose number, depending on the type of neutron source and on the geometry of the arrangement can be determined by inserting in position O' an absorber thick enough to stop all recoil protons. Therefore, all measurements were performed by counting the triple coincidences with this last absorber in position O (obturator opened) and then in position O' (obturator closed) and taking the difference between the two numbers so obtained.

The absorber A determines the minimum energy E_0 of the registered recoil protons. All the measurements were performed with protons scattered in the forward direction; hence, the energy of recoil protons is equal to the energy of the impinging neutrons. If E_{max} is the maximum energy of the neutrons emitted by the source S, the difference between the numbers of triple coincidences counted with obturator open and closed is caused only by recoil protons from neutrons whose energy lies in the interval E_0-E_{max}. That is, our apparatus is a detector sensitive only to neutrons lying in a narrow energy interval close to the end of the spectrum of the neutrons from the source. This last limitation can be eliminated by replacing the thick obturator with another one chosen in such a way that only protons of energy equal or larger than E' can be registered when both the absorber A and the new obturator are in the path of the particles recoiling from P.

Under these last conditions the difference between the numbers of triple coincidences counted with this new obturator open and closed is caused only by recoil protons from neutrons whose energy lies between the two arbitrarily fixed values E_0 and E'.

As we shall see in Section 4, our measurements of the cross sections have been performed, by means of the first of these methods, for neutrons of energy equal to 4.1, 12.5, and 13.5 Mev.

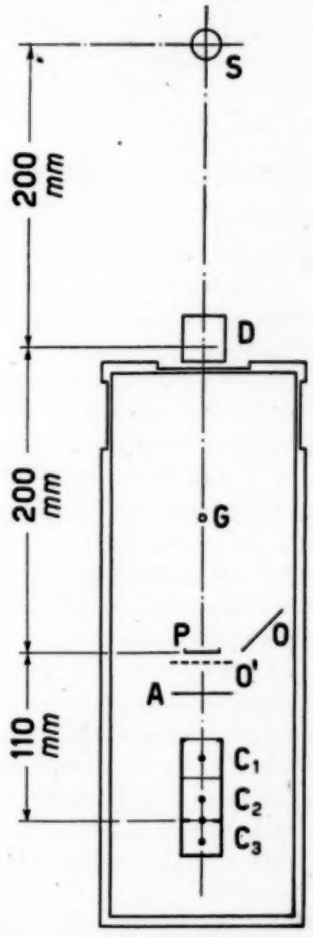

FIG. 1. Arrangement of source and scattering chamber.

[9] M. Ageno, E. Amaldi, D. Bocciarelli, and G. C. Trabacchi, Naturwiss. 31, 231 (1943); Nuovo Cimento 1, 253 (1943).

With the second method a measurement at 8 Mev was attempted; however, the result was rather uncertain on account of the large statistical error affecting a rather small difference between large numbers.

In order to determine the total (transmission) cross section of a given element for neutrons of the chosen energy interval, it is sufficient to insert, at about half-way between S and P, a scatterer D containing that element. The ratio of the numbers of recoil protons observed with and without such a scatterer in the position shown in Fig. 1, gives the transmitted fraction of impinging neutrons which is connected by a simple well known relation to the desired total cross section.

In conclusion for every value of both the energy E_0 (and E_{max}) and the thickness of the scatterer, we must perform four measurements under the following conditions: with obturator open and without scatterer: OO; with obturator open and with scatterer: OS; with obturator closed and without scatterer: CO; and with obturator closed and with scatterer: CS.

TABLE I. Data on scattering as determined by recoil proton. Each transmission determination is the result of 200 measurements except as indicated.

Scatterer	Thickness (cm)	Thickness (g/cm^2)	Number of recoil protons OO	OS	CO	CS	Transmission T
D+Be; E_0=3.2 Mev; E_{max}=4.6 Mev; $\bar{E}$=4.1 Mev							
$C_{22}H_{46}$	1.6	1.4	6601	4802	732	659	0.706±0.016
	2.95	2.6	6055	3381	727	538	0.534±0.014
	6.0	5.2	6403	2235	791	454	0.317±0.011
$C_{22}D_{72}$	3.0	2.94	5836	3329	698	475	0.555±0.015
	4.85	4.74	6305	2602	743	545	0.370±0.012
C	4.0	6.34	6010	3336	702	526	0.529±0.014
	6.0	9.51	6345	2808	720	541	0.403±0.012
	8.0	12.68	6208	2191	753	515	0.307±0.011
D+B; E_0=9.4 Mev; E_{max}=13.2 Mev; $\bar{E}$=12.5 Mev							
$C_{22}H_{46}$	6.0	5.2	2815	1683	923	655	0.543±0.022
$C_{22}D_{72}$	4.85	4.74	2647	1795	889	692	0.627±0.024
C	4.0	6.35	2843	2036	853	753	0.644±0.024
D+Li; E_0=11.5 Mev; E_{max}=14.5 Mev; $\bar{E}$=13.5 Mev							
$C_{22}H_{46}$	2.95	2.6	13706	10382	5343	4128	0.748±0.019
	6.0	5.2	13094	7322	5369	3318	0.518±0.016[1]
	8.95	7.8	9462	4354	3664	1773	0.445±0.016[3]
$C_{22}D_{72}$	3.0	2.94	14063	10269	5096	3970	0.702±0.017
	4.85	4.74	13027	8054	5462	3512	0.600±0.018
C	2.0	3.17	12211	10183	4248	3680	0.817±0.020[2]
	6.0	9.5	13560	8366	5136	3469	0.581±0.016
	10.0	15.9	8461	3350	3018	1456	0.385±0.015[4]

[1] Result of 160 measurements.
[2] Result of 150 measurements.
[3] Result of 210 measurements.
[4] Result of 130 measurements.

3. THE EXPERIMENTAL ARRANGEMENT

The experimental arrangement was about the same as that used in an earlier research[10]; therefore, details of the construction and the voltage (2140 v) applied to the counters and on the registering set will not be given here.

The scattering chamber was changed as shown in Fig. 1. The paraffin arc used in our preceding research was taken away from its support G and replaced by a 2-mm thick paraffin layer P of 25×40 mm^2 area, supported by a brass plate 1 mm thick.

The distance between the paraffin surface and the first wall of the third counter was 110 mm. The walls of the counters were of Al 1.93 mg/cm^2 thick. The scattering chamber was filled with commercial argon at atmospheric pressure. As shown in Fig. 1 the distances between the source S and scatterer $D(d_1)$ and between scatterer D and paraffin $P(d_2)$ were both 200 mm.

The neutron source S was a target of Be, B, or Li bombarded with deuterons of 0.8 Mev produced by the one million-volt equipment of the Istituto Superiore di Sanità. The target was reduced to a disk of 20-mm diameter by means of an iron screen. The neutrons were observed at 90° with respect to the direction of the impinging deuterons.

The scatterers had an area equal to 30×30 mm^2 and thicknesses varying between 20 and 90 mm.

In order to count the triple coincidences alternatively in the four conditions OO, OS, CO, CS, we have used the same automatic device used in our preceding research, conveniently modified[10]: the scattering chamber containing the paraffin P and the counters remained in a fixed position while the scatterer D, supported by a long 2 mm thick aluminum arm, was periodically inserted and taken away from the path of the neutrons coming from S and impinging on P.

The triple coincidences were registered for 28 sec. in each of the four above-mentioned arrangements; then the arrangement was changed automatically in 2 sec. By alternating so frequently the four measurements, the effect of slow varia-

[10] E. Amaldi, D. Bocciarelli, B. Ferretti, and G. C. Trabacchi, Naturwiss. 30, 582 (1942); Ricerca Scient. 13, 502 (1942).

tions of the neutron emission or detection sensitivity was made as small as possible. By means of a convenient caliper the distances and the alignment were frequently checked during the measurements.

4. THE MEASUREMENTS

The measurements were performed with neutrons from the three reactions Be(D, n), B(D, n), Li(D, n). The more critical point in all measurements of the transmitted fraction of neutrons is to ascertain that the number of neutrons scattered by the surrounding materials and room-walls is negligible with respect to the number of neutrons impinging on the detector directly from the neutron source.

Although the experiments described in subsection (6a3) and (6a4) of our earlier paper[10] had given very satisfactory results on this point, we performed two more checks with D+Li neutrons at $E_0=11.15$ Mev.

(a) We have verified that the number of registered protons varies proportionally to the square of the distance $r=d_1+d_2$ of the paraffin P from the source S. By increasing this distance from $r'=16.6$ cm to $r''=29.6$ cm, the number of registered protons decreased by a factor 3.12 ± 0.15, in satisfactory agreement with $(r''/r')^2=3.18$.

(b) In our apparatus the target was cooled by means of a water layer about 2 mm thick which could give rise to a few scattered neutrons. In order to check this point we substituted for the scattered D a 6-cm thick paraffin ring whose inner and outer diameter were, respectively, 4.5 and 9.0 cm. We found that the paraffin ring increased the number of registered protons by a factor 1.109 ± 0.031. Considering the thickness and the geometrical disposition of the water-cooling, we can conclude that it gives rise to a negligible number of neutrons scattered to the detector with energy high enough to be registered.

We measured the fraction of neutrons transmitted by scatterers of light paraffin, heavy paraffin, and graphite. The melting point of the light paraffin was between 68° and 70°C so that we can assume the formula $C_{32}H_{66}$. The melting point of heavy paraffin was higher than 77°C so that we can assume the formula $C_{35}D_{72}$; the graphite used was "Acheson."

In the measurements with neutrons from Be, B, and Li the Al absorber A was, respectively, 0 mg/cm², 124 mg/cm², and 175.5 mg/cm² thick. Taking into account the thickness of the five counter-walls ($5\times1.93=9.6$ mg/cm² Al), the distance (11 cm of argon) between the paraffin P and the first wall of the third counter, and the stopping-power of aluminum,[11] we found that the minimum ranges of recoil protons, in the three above-mentioned conditions, were, respectively, 17.5, 103, 140 air cm, corresponding to $E_0=3.2$, 9.4, 11.15 Mev.

The results of our measurements are given in Table I; in addition to the minimum energy E_0, the maximum energy E_{max}, and the mean energy $\bar{E}$ are also given. For the neutrons from B and Li E_{max} was deduced from the absorption curves of recoil protons given in our earlier paper.[10] A similar curve was measured in the case of the neutrons from Be which turned out to agree very well with the results of other authors.[12]

The mean energy $\bar{E}$ was calculated by formula (11) of our earlier paper from the above-mentioned absorption curves for B and Li neutrons, and the spectrum of Bonner and Brubaker for Be neutrons. In Table I, besides the thickness of the scatterers, we give the numbers of recoil protons registered in the 4 dispositions *OO OS CO CS*, and the transmitted fraction

$$T=(OS-CS)/(OO-CO). \qquad (6)$$

The errors are calculated from the square root of the number of counted pulses, by means of the usual propagation rule. In some cases we have calculated the standard deviation which turned out to be about 1.3 times the error calculated from the square root of the number of pulses.

In the case of the neutrons produced by means of reaction

$$_1D^2+{}_5B^{10,11}\rightarrow{}_6C^{11,12}+{}_0n^1, \qquad (7)$$

the measurements were performed for a single value of the thickness of the scatterer because the mean energy of these neutrons does not differ very much from that of neutrons produced in reaction (3) which has the advantage of a much higher intensity.

We have also attempted to measure the transmitted fraction of the neutrons of the second group of reaction (7) which extends between 7.3 and 9.1 Mev. For such a purpose the obturator was replaced by an Al absorber 60.6 mg/cm²

[11] M. S. Livingstone and H. A. Bethe, Rev. Mod. Phys. 9, 276 (1937).
[12] T. W. Bonner and W. M. Brubaker, Phys. Rev. 50, 308 (1936).

thick; the Al absorber A was 54.8 mg/cm² thick; and the paraffin P 43 mg/cm², corresponding to 43 cm air. Under these conditions with obturator open and closed we counted only recoil protons whose range was equal or larger than, respectively, 66 cm of air (7.3 Mev) and 97 cm of air (9.1 Mev); the calculated mean energy $\bar{E}$ was 8 Mev.

From these measurements we found, for each scatterer studied, a result intermediate to that obtained at $\bar{E}=4.1$ Mev (D+Be) and at $\bar{E}=13.5$ Mev (D+Li). However, the statistical errors were appreciably higher than that reported in Table I, as we must expect, taking into account that in this case we deal with relatively small differences between rather large numbers. Therefore we do not report in detail these results which, although in agreement with all other measurements, are not usable for a strict comparison with theory.

In order to check our results by a different method we repeated the measurements of the transmitted fraction of the D+Li neutrons, using, as detector, the activity induced in copper according to reaction (4). This method [6,7] is very simple; it is, however, to be noticed that the value of the threshold of reaction (4) is rather uncertain and the dependence of its cross section on the energy of the impinging neutrons is practically unknown. For this reason the agreement between the results obtained by detecting fast neutrons by means of recoil protons and by means of the copper activity, must be considered as a reciprocal check of the two methods.

In order to have geometrical conditions similar to those used in the preceding measurements, the copper detectors were plates, 1 mm thick, bent in the form of cylinders 25 mm in diameter and 40 mm long so that their section (25×40 mm²) was equal to the area of the paraffin sheet of Fig. 1. The distance between source and detector was again 40 cm and the scatterer was placed at half this distance.

To reduce, as much as possible, the number of scattered neutrons, all surrounding materials were removed; the scatterer and the detector were supported by an aluminum plate, 1 mm thick and 3 cm wide, marked with convenient lines, which permitted the distances and the alignment of scatterer and detector in the successive experiments to be reproduced accurately. During irradiation the detector was screened with cadmium 0.78 g/cm² thick to eliminate the copper activity of 5-min. period produced by slow neutrons.

The influence of slow intensity-variation in the neutron emission was eliminated by irradiating at the same time two copper detectors placed at the same distance from the source, in two directions forming an angle of about 30°: the scatterer was placed in the path of the neutrons impinging on one of these two copper cylinders.

After ten minutes irradiation, the two detectors were placed around two thin-walled glass counters and the number of pulses was registered by means of a "scale-of-16" and a "scale-of-8." The counting continued for 19 minutes, starting one minute after the end of irradiation. The measurement was repeated with the same scatterer placed in the path of the neutrons impinging on the other copper cylinder and the results of the two measurements were added together. The zero effect was measured before and after each measurement.

The results are summarized in Table II; the values given are the sum of the pulses counted in four measurements. In column 8 we give the transmitted fraction T' deduced from the preceding data, while in column 9 we reproduce, for comparison, the transmitted fraction of neutrons T deduced by means of (6) from the recoil-proton measurements (Table I, D+Li).

The agreement is very satisfactory so that it seems to us reasonable to assume that the meas-

TABLE II. Scattering of neutrons from the D+Li reaction detected by use of the Cu^{62} 9.92-min. activity.

cm	g/cm²	Number of counts without scatterer	Zero effect	Number of counts with scatterer	Zero effect	Transmission T'	Transmission T
				Scatterer $C_{31}H_{64}$			
2.95	2.6	28016	4820	21696	4970	0.721±0.009	0.748±0.019
6.0	5.2	25829	4900	16848	4857	0.573±0.009	0.518±0.016
8.95	7.8	29768	5170	15648	5060	0.430±0.008	0.445±0.016
				Scatterer $C_{31}D_{72}$			
3.0	2.94	29592	5530	23190	5530	0.730±0.009	0.702±0.017
4.85	4.74	27597	5150	18640	5160	0.592±0.008	0.600±0.018
				Scatterer C			
2.00	3.17	25944	5080	22576	4980	0.843±0.011	0.817±0.020
6.0	9.5	27746	5000	17712	4870	0.564±0.008	0.581±0.016
10.0	15.9	28202	4980	13840	4910	0.384±0.007	0.385±0.015

TABLE III. Scattering cross sections from the data of Tables I and II.

Scatterer	Δ	K'	K''	$T-K$	$\sigma\times10^{24}$	Molecular $\sigma\times10^{24}$ (average)	Atomic $\sigma\times10^{24}$ (average)
				D+Be $\bar{E}=4.1$ Mev			
C	6.34	0.003	0.003	0.523	2.04± 0.08		$\sigma(C)=1.99\ \pm0.04$
Δ=6.5 cm	9.51	0.004	0.007	0.392	1.99± 0.07		
protons	12.68	0.005	0.012	0.290	1.97± 0.06		
$C_{28}D_{72}$	2.94	0.003	0.003	0.549	192± 8.7	199±5.4	$\sigma(D)=1.79\ \pm0.08$
Δ=4.9 cm	4.74	0.004	0.008	0.358	204± 7.0		
protons							
$C_{22}H_{66}$	1.4	0.003	0.000	0.703	188±12		
Δ=4.9 cm	2.6	0.006	0.001	0.527	185± 7.6	178±4	$\sigma(H)=1.73\ \pm0.06$
protons	5.2	0.008	0.006	0.303	173± 5.2		
				D+B $\bar{E}=12.5$ Mev			
C	6.35	0.003	0.001	0.640	1.40± 0.12		$\sigma(C)=1.40\ \pm0.12$
protons							
$C_{28}D_{72}$	4.74	0.003	0.002	0.622	95± 7.7		$\sigma(D)=0.78\ \pm0.12$
protons							
$C_{22}H_{66}$	5.2	0.006	0.002	0.535	90.5± 6		$\sigma(H)=0.69\ \pm0.11$
protons							
				D+Li $\bar{E}=13.5$ Mev			
$\bar{E}=13.5$ Mev	3.17	0.001	0.000	0.816	1.29± 0.16		
C	9.5	0.003	0.002	0.576	1.17± 0.06	1.22±0.037	
Δ=10.6 cm	15.9	0.004	0.008	0.373	1.25± 0.05		$\sigma(C)=1.23\ \pm0.015$
protons							
$\bar{E}=14$ Mev	3.17	0.001	0.000	0.842	1.09± 0.08		
C	9.5	0.003	0.002	0.559	1.23± 0.03	1.23±0.016	
Cu	15.9	0.004	0.008	0.372	1.24± 0.02		
$\bar{E}=13.5$ Mev							
$C_{28}D_{72}$	2.94	0.002	0.001	0.699	115±10	107±5.1	
Δ=9.2 cm	4.74	0.003	0.002	0.595	104± 6		$\sigma(D)=0.864\pm0.028$
protons							
$\bar{E}=14$ Mev	2.94	0.002	0.001	0.727	102± 4	105±2.2	
$C_{28}D_{72}$	4.74	0.003	0.002	0.587	106± 2.7		
Cu							
$\bar{E}=13.5$ Mev	2.6	0.003	0.000	0.745	84.5± 7.3		
$C_{22}H_{66}$	5.2	0.006	0.002	0.510	97.2± 4.5	86.5±2.6	
Δ=9.4 cm	7.8	0.007	0.004	0.434	80.5± 3.5		$\sigma(H)=0.694\pm0.019$
protons							
$\bar{E}=14$ Mev	2.6	0.003	0.000	0.718	95.2± 3.5		
$C_{22}H_{66}$	5.2	0.006	0.002	0.566	82.2± 2.3	85.0±1.35	
Cu	7.8	0.007	0.004	0.419	83.8± 1.9		

urements, performed with both methods, cannot be affected by serious systematical errors.

As a further check of the measurements performed with a copper detector, we have plotted, on a semilogarithmic scale, the decay curve of Cu obtained by adding the pulses counted in each minute, in all the measurements used to deduce Table II. Such a decay curve turned out to be a straight line corresponding to a half period of 8.3±0.4 min. As this value is appreciably lower than that obtained by Crittenden[13] (9.92 ±0.05), one could suspect a slight influence, in our measurements, of the 5-min. period. Although our decay curves can be analyzed only with difficulty into two exponentials of 5- and 9.9-min. periods, we have calculated under this assumption the percentage of the total number of pulses which could be attributed to slow neutrons. We found less than five percent so that we considered it unnecessary to introduce any correction for this reason.

[13] E. C. Crittenden, Phys. Rev. **56**, 709 (1939).

5. RESULTS

If the transverse dimensions of neutron-source S, detector P and scatterer D are negligible with respect to the distances d_1, d_2, the percentage

of the transmitted neutrons varies exponentially with the thickness z of the scatterer

$$e^{-z/\Lambda}. \tag{8}$$

$\Lambda=1/N\sigma$ is the mean free path, σ the total cross section, and N the number of nuclei per cm³.

If δ and M are the density and the atomic weight of the scatterer we have

$$\frac{z}{\Lambda}=\frac{z\delta\sigma}{M1.67\times10^{-24}}=\frac{\delta}{M}\frac{\sigma}{1.67\times10^{-24}} \tag{9}$$

where $\Delta=z\delta$ is the thickness of the scatterer in g/cm².

In our experimental disposition the transverse dimensions of the neutron source and detector were small but not negligible with respect to d_1 and d_2. Therefore we must introduce two corrections caused by:

(1) "scattering in," that is, neutrons which are scattered through such a small angle that they still impinge on the detector.

(2) "double scattering," that is, neutrons which impinge on the detector on account of a second collision in the scatterer.

Both these effects increase the percentage T of the transmitted neutrons with respect to the value (8) one would expect under ideal geometrical conditions. Therefore we can write

$$T(z)=e^{-z/\Lambda}+K'+K'', \tag{10}$$

where K' and K'' correspond to the above-mentioned effects.

By simple geometrical considerations we found for our experimental conditions

$$K'=0.007\frac{\sigma(0)}{\bar{\sigma}}(1-e^{-z/\Lambda}) \tag{11}$$

for scatterer of atomic weight larger than 1, and

$$K'=0.014\frac{\sigma(0)}{\bar{\sigma}}(1-e^{-z/\Lambda}) \tag{12}$$

for hydrogen. $\sigma(0)$ is the differential cross section in the forward direction and $\bar{\sigma}$ is the differential cross section averaged over all directions. If the scattering is isotropic in the center of gravity system we have $\sigma(0)/\bar{\sigma}=1$.

In practice, we have used for D and C,

$$K'=0.007(1-T); \tag{11'}$$

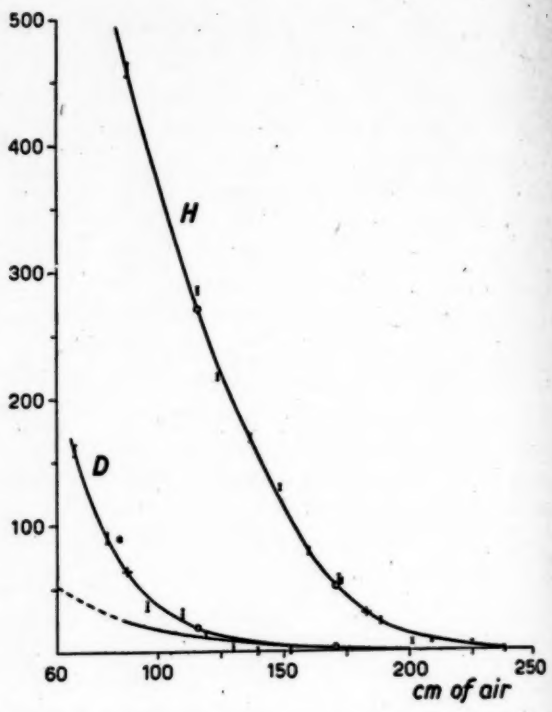

FIG. 2. Absorption curves of recoiling particles.

for H

$$K'=0.014(1-T) \tag{12'}$$

in the case of neutrons of 4 Mev, and

$$K'=0.018(1-T) \tag{12''}$$

in the case of neutrons of 12.5–13.5 Mev as suggested by our preceding results.[10]

K'' was calculated numerically in the case of a scatterer of 30×30 mm² section and $z=\Lambda=90$ mm thick. We found, for nuclei of atomic weight larger than 1,

$$K''=0.008; \tag{13}$$

for hydrogen

$$K''=0.002. \tag{14}$$

The low value of K'' in this case is caused by the energy-loss that a neutron undergoes in collisions against hydrogen. As we must expect that K'' varies roughly proportionally to $(z/\Lambda)^2$ we used

$$K''=0.008(z/\Lambda)^2 \tag{13'}$$

in the case of D and C, and

$$K''=0.002(z/\Lambda)^2 \tag{14'}$$

in the case of hydrogen.

Of course in the case of paraffin we used the

average of the corrections due to carbon and hydrogen.

Table III contains the cross sections calculated by means of (9) and (10); we give also the values of K', K'', and $T-(K'+K'')$ in order to show that the corrections represent always only a few percent of the transmitted fraction T of neutrons. The mean free path given in column 1 is obtained from a semilogarithmic graph of the uncorrected transmitted percentage of neutrons; therefore it is only an approximate value. In the first column we have also indicated the detector: recoil-protons or Cu-activity. In this last case, according to Salant and Ramsay,[7] we assume for the mean energy of the detected neutrons $\bar{E}=14$ Mev. Such a high value is justified by the presumably rapid increase of the cross section of process (4) with the energy of the impinging neutrons.

Column 6 contains the cross section per molecule whose weighted averages are given in column 7. The atomic cross sections are given in the following column. Finally for D+Li neutrons we have averaged the values obtained with two different detection methods although the corresponding mean energies are slightly different.

Such a procedure appears justified considering that the two averaged values are equal to one another within the experimental errors, and that, under all known reasonable assumptions about the proton-neutron interaction, the scattering cross section does not change appreciably in a narrow energy interval.

6. COMPARISON OF THE NEUTRON-PROTON AND NEUTRON-DEUTERON COLLISION

Although the results contained in the last column of Table III are to be discussed in Section 7, we will now compare the neutron-proton and neutron-deuteron cross sections. From Table III we see that they are equal, within the experimental errors, at 4.1 Mev, while at higher energies the deuteron cross section is slightly larger than the proton cross section. From the data of Table III we have, at 14 Mev,

$$\sigma_D/\sigma_H=1.22\pm0.05. \tag{15}$$

For such a high energy the neutron-proton cross section is caused only by the scattering, while in the case of deuterons we must consider also the $(n, 2n)$ process

$$_0n^1+{}_1D^2\rightarrow{}_1H^1+2{}_0n^1+Q, \tag{16}$$

where Q is equal to the mass-defect of the deuteron, i.e., $Q=-2.17$ Mev. Therefore we can write

$$\sigma_D=\sigma_e+\sigma_d, \tag{17}$$

where σ_e is the cross section for elastic scattering and σ_d the cross section of process (16).

To investigate reaction (16) and to evaluate the corresponding cross section, we have performed the following experiments:

(1) We replaced the light paraffin P with a heavy paraffin layer and measured the absorption curve of the recoiling particles. This curve is reproduced, as a function of the range in cm of air, in Fig. 2 (curve D); in the same figure we give also the absorption curve of protons recoiling from light-paraffin (curve H).

As we have shown in an earlier paper,[10] the ordinate $N(E_0)$ of the two curves of Fig. 2, are given by the equation

$$N(E_0)=\frac{N_0 g}{F}\int_{E_0}^{\infty}\int_{E}^{\infty}f(E)\sigma(E)dE, \tag{18}$$

where $F=dE/dR$ is the energy loss of the recoiling particles in light or heavy paraffin, N_0 the number of protons or deuterons per cm^3, $f(E)dE$ the number of neutrons emitted by the source with energy between E and $E+dE$, $\sigma(E)$ the corresponding cross section, and g a pure geometrical factor. Under the reasonable assumption that $\sigma(E)$ varies only slowly in the energy interval involved, and considering that N_0 was about the same in the light (7.44×10^{22}) and heavy paraffin (7.35×10^{22}), we can write

$$N(E_0)\cong\frac{1}{F}\bar{\sigma}\Phi(E_0), \tag{19}$$

where

$$\Phi(E_0)=\int_{E_0}^{\infty}\int_{E}^{\infty}f(E)dE \tag{20}$$

is the twice integrated spectrum of the emitted neutrons and $\bar{\sigma}$ the cross section averaged over the energy interval extending from E_0 to the maximum energy E_{max} of the neutron spectrum.

(2) The energy of a deuteron recoiling in a head-on collision with a 15-Mev neutron is

8/9 of 15 or 13.3 Mev corresponding to a range in air $R_D=112$ cm. Considering that E_{max} for the D+Li neutrons is certainly lower than 15 Mev, curve D of Fig. 2 gives evidence that the paraffin also emits a few protons. In order to settle this point, we took the paraffin layer away from its position P in Fig. 1 and arranged on the two opposite faces of a brass plate 2 mm thick two layers of light and heavy paraffin each 1 mm thick. The brass plate was secured to the pivot G so that we could change very rapidly the light and heavy paraffin and compare the numbers of recoiling particles. Using an Al absorber A so thick that the registered particles had a range equal or larger to 116 cm of air, we found

$$N_l(116)/N_w(116)=14\pm2.2, \qquad (21)$$

i.e., the heavy paraffin bombarded with D+Li neutrons emits protons of energy larger than 10 Mev whose number is equal to about 7 percent of the number of protons of the same energy recoiling from light paraffin. In Fig. 2 the two circles plotted at $R=116$ cm represent the result of this measurement.

(3) The number of protons emitted from the heavy paraffin we used is so small that it could be caused completely or in part by light hydrogen impurity. Assuming again that the maximum energy of the D+Li neutrons is 15 Mev, the maximum energy of protons emitted in the forward direction in reaction (16) is equal to 12.5 Mev corresponding to 171 cm of air. Therefore we repeated a measurement similar to that described in (2) for this higher value of the range. We found

$$N_l(171)/N_w(171)=11\pm6. \qquad (22)$$

The two circles marked in Fig. 2 at $R=171$ cm represent this result.

Although the experimental error is very high, we can conclude that the observed protons are due at least in part to hydrogen impurity.

The heavy paraffin is supposed to contain no more than five percent of light paraffin,* which is consistent with our preceding results.

In any case, from the above results it is impossible to form any conclusion about the existence of process (16) except that its cross section must be very small for neutrons of 13–14 Mev.

(4) Finally instead of comparing the numbers of particles, emitted from light and heavy paraffin, having the same range, we have compared the numbers of recoiling particles due to neutrons of the same energy. The experiment was performed for neutrons of energy equal or larger to 13 Mev which give rise to recoiling protons and deuterons of, respectively, 13 and 11.15 Mev.

The corresponding ranges in air ($R_p=183$, $R_D=88$ cm) were obtained by using two convenient Al absorbers in the two cases (223 and 87.6 mg/cm²). We remember that in this experiment the distance from paraffin to the first wall of the third counter was 20 cm (of argon). We found, in 72 measurements,

$$N_w=5765\pm134 \qquad N_l=N_H=2724\pm122$$
$$N_w/N_l=2.12\pm0.11.$$

These data, represented in Fig. 2 by two crosses, were used to adjust the two absorption curves on the same scale.

Now we must consider that the particles emitted from the heavy paraffin are of three types: recoil deuterons, disintegration protons, and recoil-protons due to light paraffin impurity. The number of these last can be deduced by curve H of Fig. 2 once we know the percentage (five or seven percent) of the impurity: for instance the lower curve of Fig. 2 was obtained by multiplying curve H by 0.05.

In the following we shall show some simple calculations in both cases of five and seven percent impurity.

We have

$$5\% \quad N_D=N_w-\frac{5}{100}N_H=3665, \qquad (23)$$

$$7\% \quad N_D=N_w-\frac{7}{100}N_H=2865. \qquad (23')$$

Neglecting a constant factor and applying (19) to our case, we have

$$N_D=\frac{1}{F_D}\sigma_s\Phi(13)+\frac{1}{F_H}\sigma_d\Phi(10.9),$$
$$N_H=\frac{1}{F_H}\sigma_H\Phi(13). \qquad (24)$$

* The Norsk Hydro-Elektrisk Kvoelstofaktieselskab, from which we bought the heavy paraffin, kindly communicated these data to us.

The energy of the neutrons which gives rise to disintegration protons in the forward direction fast enough to be registered (8.6 Mev corresponding to $R_p=88$ cm) is 10.9 Mev. From (24) we deduce

$$\frac{N_D}{N_H}=\frac{F_H}{F_D}\frac{\sigma_e(13)}{\sigma_H(13)}+\frac{\sigma_d(10.9)}{\sigma_H(13)}\frac{\Phi(10.9)}{\Phi(13)}. \quad (25)$$

From the range-energy curve[11] we have: for protons of energy between 13 and 14 Mev, $F_H=3.84\ 10^{-2}$ Mev/cm of air; for deuterons of energy between 11.55 and 12.5 Mev, $F_D=7.5\ 10^{-2}$ Mev/cm of air:

$$F_H/F_D=0.5. \quad (26)$$

The factor $\Phi(10.9)/\Phi(13)$ can be obtained from curve H of Fig. 2

$$\frac{\Phi(10.9\text{ Mev})}{\Phi(13\text{ Mev})}=\frac{\Phi(134\text{ cm})}{\Phi(183\text{ cm})}=6. \quad (27)$$

Introducing the numerical values (23), (23′), (26), and (27) in (25) we find

$$5\% \quad 1.35=0.5\frac{\sigma_e(13)}{\sigma_H(13)}+6\frac{\sigma_d(10.9)}{\sigma_H(13)}, \quad (28)$$

$$7\% \quad 1.05=0.5\frac{\sigma_e(13)}{\sigma_H(13)}+6\frac{\sigma_d(10.9)}{\sigma_H(13)}. \quad (28')$$

We remember that the cross sections appearing in these relations are averaged from the given values of the energy up to the maximum energy of the neutrons of D+Li reaction (14.5 Mev). Recalling (15) and (16) we can write

$$\sigma_e/\sigma_H=1.22x, \qquad \sigma_D/\sigma_H=1.22(1-x) \quad (29)$$

where

$$x=\sigma_e/(\sigma_e+\sigma_d) \quad (30)$$

is the percentage of neutron-deuteron collisions which gives rise to recoil deuterons.

Under the reasonable assumption that σ_d does not vary very much when the energy of the impinging neutrons changes from 11 to 14.5 Mev, we can introduce the relations (29) in (28) and (28′) and calculate the value of x. We find

$$5\% \quad x=(6-1.1)/(6-0.5)=0.89, \quad (31)$$

$$7\% \quad x=(6-0.9)/(6-0.5)=0.93. \quad (31')$$

The result is not very sensitive to errors of the ratio $\Phi(10.9)/\Phi(13)$ or to the percentage of light paraffin. In order to have $x=1$ it would be necessary to have $N_D/N_H=1.22\times0.5=0.6$, i.e., a percentage of light paraffin equal to 13–14 percent, which seems definitively too high.

7. DISCUSSION

Excepting for the results of the measurements at 12.5 Mev (D+B), which are not very accurate for the reasons explained in Section 4, all other values of the cross sections are affected by errors of the order of a few percent. As we have already pointed out in Section 5, the good agreement between the results obtained at 14 Mev using two detectors of quite different type, can be considered as a satisfactory reciprocal check of the applied methods. By averaging these two groups of results, the experimental errors were correspondingly lowered. We can now compare our results with that of other authors and with the theoretical predictions.

As far as we know the neutron-proton and the neutron-deuteron cross sections were not yet measured for neutrons of about 4 Mev. Going to the theoretical predictions, we can use, for the neutron-proton collision, the formula deduced by Kittel and Breit,[14] considering the scattering of the S wave by a square potential-well of the Heisenberg-Majorana type. It differs from preceding simpler formula only because the finite value of the radius of nuclear forces was considered and assumed equal to the electronic radius, as suggested by the proton-proton scattering experiments.

The scattering of the P wave seems to be negligible at such a low neutron energy under all usual assumptions about the nuclear forces. From that formula we find, at 4.1 Mev,

$$\sigma=1.95\times10^{-24}\text{ cm}^2,$$

i.e., a value appreciably higher than our experimental result ($1.73\pm0.06\times10^{-24}$ cm^2); we cannot, however, exclude the possibility that such a difference is mostly caused by experimental errors.

The neutron-deuteron collision was investigated theoretically by Höcker[15] who has calcu-

[14] C. Kittel and G. Breit, Phys. Rev. **56**, 744 (1939).
[15] H. Höcker, Physik. Zeits. **43**, 236 (1942).

lated the cross sections for elastic scattering, disintegration according to reaction (16), and radiative capture.

He used, for the interaction between the three particles, the Voltz-potential, i.e., a linear combination of Majorana, Heisenberg, Bartlett, and Wigner forces decreasing with the distance according to a gaussian curve.[16] The relative values of these four terms were adjusted by Voltz to obtain the well-known saturation effect of the forces and the experimental values of the deuteron constants.

At 4.1 Mev we need to consider only the elastic scattering whose cross section was, unfortunately, calculated by Höcker only up to about 3 Mev where it is equal to 1.5×10^{-24} cm². However, considering the regularly decreasing shape of the Höcker curve, we can conclude that our experimental value is appreciably higher than the theoretical one.

The same conclusion can be drawn from the experimental results of other authors: at 2.4 Mev Kikuchi and Aoki[17] found 1.98×10^{-24} cm² where the Höcker value is 1.60×10^{-24} cm²; Zinn, Seely, and Cohen[18] found $2.17\pm0.08\times10^{-24}$ cm² at 2.88 Mev; the value given by Höcker is 1.55×10^{-24} cm².

Also for thermal energy the experimental values obtained by various authors, and particularly by Dunning and Carroll,[19] are higher than the theoretical one.

Considering that in neutron transmission experiments all systematical errors tend to give cross sections lower than the right values, it seems to us reasonable to attribute the above stated discrepancy to defects of the theory. It is however to be noticed that the above mentioned experimental data differ even more from preceding calculations of other authors.[20]

The results obtained at 12.5 Mev (D+B) although in agreement with our other measurements, are not accurate enough for a strict comparison with theoretical predictions.

For neutron energies of about 14 Mev the neutron-carbon and neutron-proton cross sections have been measured by Salant and Ramsay[7] by detecting the D+Li neutrons by means of the copper activity produced according to reaction (4). These authors performed measurements both at 90° ($\bar{E}=14$ Mev) and 0° ($\bar{E}=15$ Mev) with respect to the direction of the impinging deuterons on lithium. The results obtained in the first group of measurements can be compared with our results: they found

$$\sigma_c=(1.27\pm0.04)\times10^{-24},$$
$$\sigma_H=(0.70\pm0.06)\times10^{-24}\text{ cm}^2$$

in very good agreement with our results

$$\sigma_c=(1.23\pm0.015)\times10^{-24},$$
$$\sigma_H=(0.694\pm0.019)\times10^{-24}\text{ cm}^2.$$

According to the Kittel-Briet formula the proton cross section at 14 Mev is 0.66×10^{-24} cm².

The contribution to the total cross section due to the scattering of the P wave was calculated by Kittel and Breit[14] and by Ferretti[21] for neutrons of 16 Mev, under the assumption that the nuclear forces are of the neutral type studied by Bethe.[22] According to these authors the P wave contribution represents nine percent of the cross section deduced by the scattering of the S wave. With the neutral meson forces studied by Rarita, Schwinger, and Nye[23] the P-wave contribution would represent 46 percent of the cross section deduced by the S-wave scattering.

As we have already pointed out in an earlier paper,[10] the small difference between the experimental value and the scattering cross section deduced by the Kittel-Breit formula is in better agreement with the neutral meson theory of Bethe than with the neutral meson theory of Rarita and others.

Finally we consider the neutron-deuteron collision experiments at 14 Mev. As we have shown in section 6, for neutron energy of 13–15 Mev, the cross section of the $(n, 2n)$ deuteron disintegration process is equal to about 10 percent of the total collision cross section.

In this connection it is to be noticed that,

[16] H. Voltz, Zeits. f. Physik **105**, 537 (1937).
[17] S. Kikuchi and H. Aoki, Proc. Phys. Mat. Soc. Japan **21**, 75 (1939).
[18] W. H. Zinn, S. Seely, and V. W. Cohen, Phys. Rev. **56**, 260 (1939).
[19] See L. Motz and J. Schwinger, Phys. Rev. **58**, 26 (1940).
[20] L. I. Schiff, Phys. Rev. **52**, 242 (1937); S. Flügge, Zeits. f. Physik **108**, 545 (1938).
[21] B. Ferretti, Ricerca Scient. **12**, 843, 993 (1941).
[22] H. A. Bethe, Phys. Rev. **57**, 260, 390 (1940).
[23] W. Rarita, J. Schwinger, and H. A. Nye, Phys. Rev. **49**, 209 (1941).

according to the numerical values of the coefficients appearing in (26) and (29), our method of observation is 12 times more sensitive to disintegration-protons than to recoil-deuterons. The value we found for the disintegration cross section has to be considered an upper limit because it would decrease by increasing the assumed percentage of light-paraffin impurity. For this reason we consider it impossible to state with certainty, from our experimental results, the existence of process (16) for neutrons of 14 Mev. If it takes place as one would conclude by assuming a reasonable value for the light paraffin impurity, the corresponding cross section can be calculated from the total cross section given in Table III and the values (31), (31′) of x:

$$\sigma_d=(0.1\times0.86-0.05\times0.86)\times10^{-24}$$
$$=(0.09-0.04)10^{-24}\text{ cm}^2. \quad (32)$$

Process (16) was investigated by Bagge[24] who observed in a Wilson-chamber filled with heavy hydrogen the spectrum of recoil particles of the Rn+Be neutrons. From an irregularity observed in the spectrum at about 11.0 mm of hydrogen, this author draws the conclusion that process (16) takes place for neutrons of energy higher than $E_{th}=3.45$ Mev (threshold of the process) with a cross section of about

$$\sigma_d=0.3\times10^{-24}\text{ cm}^2.$$

Such a value is between three and seven times larger than that we found at 13–15 Mev.

If we do not assume an irregular dependence of the cross section of process (16) from the energy of the impinging neutrons, we must conclude that the irregularity observed by Bagge is not due to the $(n$–$2n)$ disintegration of deuteron.

Barkas and White[25] have investigated the disintegration process of deuterons under proton bombardment. With protons of 5.1 Mev they found a cross section equal to

$$0.014\times10^{-24}\text{ cm}^2.$$

The influence of the electrostatic repulsion on the value of the cross section has been calculated by Höcker who deduced from the Barkas and White result the following value of the cross section of process (16) for neutrons of 5.1 Mev

$$\sigma_d=0.02\times10^{-24}\text{ cm}^2.$$

This value seems to be in reasonable agreement with our result as the cross section would increase by a factor 2–5 on increasing the energy of the impinging neutrons by a factor 3.

The cross section of process (16) has been calculated by Höcker who found an increase with the energy E of the impinging neutron, roughly proportional to the square of the difference $E-E_{th}$($E_{th}=3.45$ Mev threshold of the process): at 14 Mev the absolute value would be

$$\sigma_d=2.5\times10^{-24}\text{ cm}^2, \quad (33)$$

that is, at least 30 times larger than our experimental value (32).

Such a high difference between the experimental and the theoretical value can be recognized also independently from the experiments of section 6, by simple comparison of the total cross section at 14 Mev given in Table III $(0.864\pm0.028)10^{-24}$, with the theoretical value that can be deduced by adding to (33) the theoretical elastic scattering cross section: this can be roughly evaluated to about 0.5–1.0×10^{-24} cm² by extrapolation of the Höcker corresponding curve.

We can conclude that, in contradiction with theoretical predictions at 14 Mev, and probably also at lower energy, the disintegration process (16) has a cross section very small with respect to the elastic scattering cross section.

---

[24] E. Bagge, Physik. Zeits. **43**, 226 (1942).
[25] W. H. Barkas and M. G. White, Phys. Rev. **56**, 288 (1939).

Theoretical Range-Energy Values for Protons in Air and Aluminum

J. H. SMITH
Cornell University, Ithaca, New York
(Received October 18, 1946)

In this paper there are presented a discussion of the calculation of range-energy values for protons in air and aluminum and a tabulation of the results. The calculations have been done with considerable accuracy and at sufficiently small energy intervals to allow good graphical interpolation. These figures, as well as those for the rate of energy loss in both cases, have been compiled over a wide range of energies—up to 10^{10} ev.

IN view of the efforts currently being given to the production of very high energy protons and the general interest in mesons of various energies, it will be convenient to have readily available a fairly extensive tabulation of range-energy relations for such particles. Protons up to 10^{10} ev in air and aluminum have been chosen in this instance; the range of mesons up to 10^9 ev can be deduced easily from Tables I and II. Calculations have been made previously to this to obtain similar relations[1,2]; it is intended herein to provide data compiled either with more careful numerical methods, or with extension of certain energy ranges for the sake of better accuracy, or both.

The ranges proposed are those a proton would have under the circumstance that it lose energy along its path solely through ionization and excitation of the atoms of the stopping material. These processes certainly constitute the most important mechanism for slowing-down over a rather wide range of energies; for example, meson production will not take place until a proton has at least 100 Mev and probably does not become important until a much higher energy. In addition to total ranges, the rate of energy loss by ionization and excitation will be of interest; these figures are included in the tabulation.

The figures in this paper represent *mean* ranges since they are calculated from an expression which was derived to give the average energy loss per unit thickness of stopping material. For a brief review of the theoretical derivation, see references 1 and 2. The complete expression is[3]

$$\frac{dE}{dx}=-\frac{4\pi(ez)^2e^2N}{mv^2}\times\left\{Z\left[\ln\frac{2mv^2}{I}-\ln(1-\beta^2)-\beta^2\right]-C_K\right\},$$

where

ez = charge of the incident particle,
v = velocity of the incident particle,
N = number of atoms per cm³ of stopping material,
Z = atomic number of stopping material,
I = average ionization potential of stopping material,
m = electron mass,
$\beta=v/c$, c the velocity of light,
C_K is a correction term which must be applied in case v is comparable to the velocity of the K-electron of the stopping material (but large compared to that of all others). Reference 3 gives a discussion of its calculation and figures.

There are several restrictions placed on the validity of this form for dE/dx, the most important of which are (1) that the incident particle be much more massive than an electron, (2) that the incident energy be much less than M^2c^2/m where M is the mass of the incident particle and m that of an electron (less than 10^6 Mev for protons), (3) that the proton have a velocity considerably greater than that of L electrons in the stopping atoms, and (4) that the proton energy be large enough so that electron capture and loss are of no consequence. A minimum figure suggested for the last of these is 0.1 Mev. Thus, all conditions are seen to be well satisfied for a proton with an energy between 15 Mev and 10^4 Mev in air and Al.

Let us consider the ranges of protons in air. An accurate curve of E *vs.* $R(E)$ up to 15 Mev for this case is presented in Fig. 28 of the

[1] B. Rossi and K. Greisen, Rev. Mod. Phys. 13, 249 (1941).
[2] J. Wheeler and R. Ladenburg, Phys. Rev. 60, 761 (1941).
[3] M. S. Livingston and H. Bethe, Rev. Mod. Phys. 9, 263 (1937).

Livingston-Bethe article. To find ranges beyond this point, one merely evaluates

$$R(E)=R(15)+\int_{15}^{E}\frac{dE'}{-dE'/dx}.$$

Straightforward numerical integration was found to be the only satisfactory procedure. Even for the low energies considered it proved to be not sufficiently accurate and also too laborious to perform the calculation by reducing the integral to the difference of standard exponential integrals.

Values of the constants c, e, m, and N were taken from the tables of Birge,[4] the last being made to correspond to conditions of 760 mm Hg and 15°C. The proton mass, M_Pc^2, was computed from these tables to be 937.6 Mev. The average ionization potential in air, 80.5 ev, and $Z=7.22$ are the values as found in reference 3. dE/dx is rather insensitive to changes in I; for small values of E ($\approx$15 Mev), a 3 percent change in I is reflected as about 0.5 percent in dE/dx, the sensitivity decreasing with increasing energy.

A similar procedure was followed in calculating the range of protons in Al. For energies up to 13 Mev, they are obtained from the work of Livingston and Bethe; see Figs. 30 and 34 of that article and the accompanying text. Beyond this point, numerical integration was again employed. The same data for C_K as used before are here also satisfactory. This correction due to K ionization is more important initially for Al than for air since the binding energy and velocity of the innermost electrons are greater for Al by a considerable amount. Experiments by Wilson[5] on the stopping power of Al relative to air provide a value for the average ionization potential of 150 ev.

The values for the rate of energy loss and range as given in the following tables are believed to be correct (consistent with the constants cited in this paper) to a few parts in the fourth figure where this is given. There is a serious question as to the validity of the values of dE/dx in Al for very low energies. The condition

$$E\gg(M_P/m)\times(\text{ionization potential of } L \text{ electrons})$$

is not very well satisfied in the neighborhood of $E\approx 2$ Mev. This indicates that a correction "C_L" should be applied, but it is not available. However, in the range above 13 Mev, where ranges are obtained using the theoretically computed energy loss, C_L will have become completely negligible.

The author wishes to express acknowledgment to Professor H. A. Bethe for various helpful suggestions made by him in connection with these calculations.

TABLE I. Rate of energy loss and ranges for protons in air.

E (Mev)	$-dE/dx$ (Mev/cm)	R (cm)	E (Mev)	$-dE/dx$ (Mev/cm)	R (cm)
15	3.574×10^{-2}	2.385×10^{2}	400	0.3308×10^{-2}	754.4×10^{2}
17	3.230	2.975	500	0.2994	1073
19	2.951	3.623	600	0.2789	1420
21	2.721	4.329	700	0.2649	1788
23	2.529	5.092	800	0.2547	2174
25	2.364	5.910	850	0.2507	2372
30	2.040	8.194	900	0.2472	2572
35	1.801	10.81	950	0.2442	2776
40	1.617	13.74	1000	0.2416	2982
45	1.472	16.99	1250	0.2325	4038
50	1.352	20.53	1500	0.2277	5126
60	1.173	28.49	1750	0.2252	6231
70	1.040	37.56	2000	0.2240	7344
80	0.9393	47.69	2250	0.2236	8462
90	0.8594	58.83	2500	0.2237	9580
100	0.7943	70.95	2750	0.2242	10,700
120	0.6950	97.95	3000	0.2250	11,810
140	0.6227	128.5	4000	0.2290	16,220
160	0.5678	162.1	5000	0.2335	20,540
180	0.5246	198.8	6000	0.2378	24,790
200	0.4899	238.3	7000	0.2419	28,950
250	0.4265	348.2	8000	0.2457	33,060
300	0.3840	472.1	9000	0.2492	37,100
350	0.3526	608.0	10,000	0.2524	41,080

TABLE II. Rate of energy loss and ranges for protons in aluminum.

E (Mev)	$-dE/dx$ Mev/(mg-cm^{-2})	R (mg-cm^{-2})	E (Mev)	$-dE/dx$ Mev/(mg-cm^{-2})	R (mg-cm^{-2})
1		3.45	60	0.8458×10^{-2}	39.83×10^{2}
1.5		6.69	70	0.7516	52.40
2	11.5×10^{-2}	10.8	80	0.6794	66.42
2.5	9.85	15.6	90	0.6222	81.82
3	8.62	21.0	100	0.5757	98.54
3.5	7.69	27.3	120	0.5047	135.8
4	6.96	34.5	140	0.4530	177.7
4.5	6.37	42.1	160	0.4136	224.0
5	5.88	50.3	180	0.3826	274.3
5.5	5.47	59.0	200	0.3576	328.4
6	5.12	69.1	250	0.3120	478.7
6.5	4.82	79.2	300	0.2813	648.0
7	4.55	90.0	350	0.2593	833.4
7.5	4.31	101.3	400	0.2428	1033
8	4.10	113.2	500	2.201×10^{-2}	1.467×10^{3}
8.5	3.92	125.6	600	2.054	1.938
9	3.75	138.8	700	1.952	2.438
9.5	3.59	152.4	800	1.879	2.961
10	3.45	166.7	850	1.851	3.229
10.5	3.32	181.4	900	1.826	3.501
11	3.21	196.6	950	1.802	3.777
11.5	3.10	212.5	1000	1.785	4.055
12	2.99	229.0	1250	1.721	5.484
12.5	2.90	246.1	1500	1.688	6.952
13	2.816[a]	263.7	1750	1.671	8.441
13.5	2.734	281.8	2000	1.664	9.941
14	2.658	300.6	2250	1.663	11.44
15	2.518	3.393×10^{2}	2500	1.665	12.95
17	2.281	4.228	2750	1.670	14.45
19	2.089	5.146	3000	1.677	15.94
21	1.930	6.143	4000	1.710	21.85
23	1.796	7.218	5000	1.747	27.63
25	1.682	8.369	6000	1.782	33.30
30	1.456	11.57	7000	1.815	38.86
35	1.289	15.23	8000	1.845	44.32
40	1.160	19.33	9000	1.873	49.70
45	1.058	23.85	10,000	1.898	55.01
50	0.9743	28.78			

[a] For remarks on the validity of dE/dx for $E<13$ Mev, see discussion at the end of the paper.

[4] R. T. Birge, Rev. Mod. Phys. **13**, 233 (1941).
[5] R. R. Wilson, Phys. Rev. **60**, 749 (1941).

PHYSICAL REVIEW VOLUME 71, NUMBER 1 JANUARY 1, 1947

Stress Induced Preferential Orientation of Pairs of Solute Atoms in Metallic Solid Solution*

CLARENCE ZENER
Institute for the Study of Metals, The University of Chicago, Chicago, Illinois
(Received October 7, 1946)

In a non-stressed cubic crystal the axes of pairs of adjacent solute atoms are randomly orientated along the several permissible crystallographic directions. It is shown that in the presence of a stress the equilibrium orientation is no longer random, but that certain directions become preferred, and it is further shown that the continual striving of the crystal to maintain equilibrium causes it to manifest all the characteristic anelastic effects, stress relaxation, internal friction, etc. In particular, its internal friction will be anomalously high in that temperature range where the time of relaxation for the establishment of equilibrium is comparable with the period of oscillation. The theory is developed for the dependence of anelastic effects upon temperature and upon crystallographic orientation, and it is found that in b.c.c. crystals these effects vanish for a tensile stress applied along one of the ⟨100⟩ axes. The magnitude of the anelastic effects associated with this stress induced preferential orientation may be very large. Thus in alpha-brass past experiments indicate that under optimum conditions the associated internal friction is at least 20 times as large as that due to all other causes.

NO real metal is perfectly elastic in the sense that stress and strain are single-valued functions of one another. The application of a constant stress is always followed by one or more types of relaxation, such as the relaxation of temperature fluctuations, of shear stress across viscous regions, etc., and consequently by a gradual creep, which in most cases is recoverable. These relaxations are also responsible for stress relaxation when a constant strain is applied, for a variation of the elastic moduli with frequency, and for internal friction. That property of a metal in virtue of which stress and strain are not unique functions of one another in the pre-plastic range has been called anelasticity. The various sources of anelasticity have recently been reviewed by the author.[1] In the present paper an analysis is given of one source of anelasticity which has heretofore been overlooked, the relaxation of the preferential orientation of pairs of solute atoms.

The solute atoms in a solid solution usually have a different size from that of the solvent atoms, and therefore give rise to an elastic distortion of the lattice. When the solution is of the substitutional type, and when the lattice has cubic symmetry, the distortion produced by each isolated solute atom will also have cubic symmetry. When two solute atoms are adjacent to one another, the distortion of the lattice by the pair will no longer have cubic symmetry. Thus if the solute atoms are larger than the solvent atoms, the lattice will be extended more along the axis of the pair than along any other axis. When the average stress throughout the crystal is zero, the pair axes will be randomly distributed over the several permissible crystallographic directions. When, however, a stress is applied to a crystal, the equilibrium distribution of pair axes is no longer random. Thus if the solute atoms are larger than the solvent atoms, and a tensile stress is applied, the solute pairs will tend to be oriented preferentially along those permissible axes which make the least angle with the tensile axis. This preferential distribution of pair axes will, however, require some time to be established, and consequently strain lags behind stress, i.e., the crystal is anelastic.

The internal friction in an alpha-brass (solid solution of zinc in copper) crystal was observed by the author[2] in 1942 to be anomalously high with a narrow temperature band in the vicinity of 400°C. The observations are reproduced in Fig. 1. At that time no explanation was given of this anomaly. Recently an interpretation was advanced based on the assumption that the equilibrium distribution of zinc atoms was non-uniform,[1] an assumption which has no corroborative support. In view of the above considerations, it looks as though the anomaly shown

* This research was supported by ORI (Contract No. N6ori-20-IV).
[1] C. Zener, Metals Tech. (Aug. 1946).
[2] C. Zener, Trans. A.I.M.E. 152, 122 (1943).

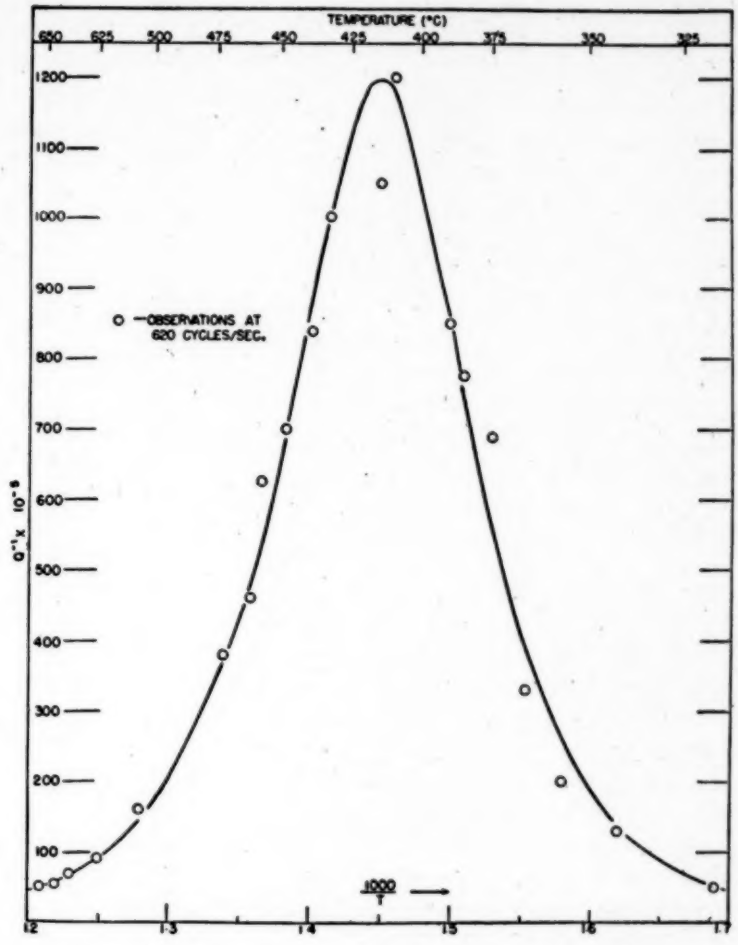

FIG. 1. Internal friction of alpha-brass crystal (After Zener, reference 2).

in Fig. 1 is a manifestation of the stress induced preferential orientation of pair axes, and that all solid solution crystals will show similar anomalies. The temperature variation of the internal friction is explained as follows. At low temperatures the time of relaxation τ for the establishment of equilibrium distribution of pair axes is very long compared with the period of vibration P. The distribution of pair axes therefore remains essentially unaltered during vibration, strain is essentially in phase with stress, and hence the internal friction is extremely low. At very high temperatures the time of relaxation τ is very short compared with the period P, and consequently the distribution of pair axes is at every instant essentially the equilibrium distribution. Strain is again essentially in phase with stress, and so the internal friction is again very small. Only in the intermediate temperature range, where

$$\tau \backsimeq P, \tag{1}$$

and hence where the pair axis distribution is neither constant nor equivalent to the equilibrium distribution, does strain lag behind stress appreciably, and hence is the internal friction large.

If the rate at which the distribution of pair axes tends to approach the equilibrium distribution is proportional to the difference between the instantaneous and equilibrium distribution, it may be shown[1] that the internal friction (Q^{-1}) varies with the angular frequency of measurement W as

$$Q^{-1} = \Delta_E \frac{\tau\omega}{1+\tau^2\omega^2}. \tag{2}$$

Here Δ_E is defined in terms of the unrelaxed and

relaxed Young's moduli, E_U and E_R, respectively, by

$$\Delta_E=(E_U-E_R)/E_R, \tag{3}$$

and is called the relaxation strength. The observations on the brass crystal were found to obey this formula provided τ was assumed to vary with temperature through a heat of activation type of relation, i.e.,

$$\tau=\tau_0 e^{H/RT}. \tag{4}$$

In Section I an analysis is given of the manner in which the relaxation strength varies with temperature and with the material constants of the metal. In Section II an analysis is given of the manner in which the relaxation strength varies with the crystallographic orientation, and a comparison is given of the relaxation strengths in the case of a pure tensile test, Δ_E, and in a pure torsion test, Δ_G.

The theory of the anelasticity arising from the preferential orientation of pair axes is formally very similar to that arising from the stress induced macroscopic diffusion of solute atoms studied by Gorsky,[3] and to the stress induced preferential distribution of the interstitial carbon and nitrogen atoms in alpha-iron studied by Snoek[4] and Polder.[5]

I. TEMPERATURE DEPENDENCE OF RELAXATION STRENGTH

In this section we shall compute the relaxation strength for a particular case where the crystal axes are so oriented as to simplify the computations. The influence of crystal orientation is reserved for the next section.

An f.c.c. lattice will be considered in which a tensile stress is applied along the [111] direction. The pair axes of the solute atoms may lie along any of the six ⟨110⟩ directions. Of these six directions three [011], [101], [110] have a direction cosine of $(2/3)^{\frac{1}{2}}$ with respect to the [111] axis, while three, $[0\bar{1}1]$, $[\bar{1}01]$, $[\bar{1}10]$, are normal to the [111] direction. If the solute atoms are larger than the solvent atoms, a tensile stress along the axis of the specimen will therefore tend to orient the pair axes from the second group, the n group, into the first, the p group, of the ⟨110⟩ directions.

The tensile strain ϵ will be regarded as a function of the tensile stress σ, the temperature T, and the number of pair axes in the p group per unit volume n_p. The tensile strain could also be regarded as a more complex function of atomic distribution, such as the relative orientation of next nearest neighbors. However, it is anticipated that only a small error will be introduced by neglecting the correlation in positions of pairs of solute atoms which are not nearest neighbors. According to the present assumption, a variation in the tensile strain is specified by

$$d\epsilon=E_U^{-1}d\sigma+\alpha dT+(\partial\epsilon/\partial n_p)dn_p. \tag{5}$$

Here E_U is the isothermal unrelaxed tensile elastic modulus, i.e., the tensile modulus when n_p remains unchanged, and α is the linear thermal expansion coefficient when n_p remains unchanged. We shall now compute the change in the elastic modulus occasioned by n_p changing in such a way as to maintain equilibrium. Under equilibrium conditions

$$n_p=ne^{-U/kT}/(1+e^{-U/kT}),$$

where n is the number of pairs per unit volume, and U is the work necessary to transfer a pair axis from an n to a p direction, the transfer being performed at constant strain and at constant temperature. If, as is normally the case, U/kT is small compared with unity, the above equation reduces to

$$n_p=n/2-nU/4kT. \tag{6}$$

It remains to obtain an estimate of U. It is anticipated that U will not depend appreciably upon temperature. It will therefore be estimated by considerations at the absolute zero temperature where thermal effects are absent. The change in energy per unit volume is then given by

$$dE=\sigma d\epsilon+Udn_p.$$

The differential of $E-\sigma\epsilon$ is therefore

$$-\epsilon d\sigma+Udn_p.$$

Since this is a perfect differential,

$$\partial U/\partial\sigma=-\partial\epsilon/\partial n_p.$$

We now introduce the assumption that U is a

[3] W. Gorsky, Physik. Zeits. Sowjetunion 8, 457 (1935).
[4] J. Snoek, Physica 6, 591 (1939); 8, 711 (1941); 9, 862 (1942); Chemisch Weekblad 39, 454 (1942).
[5] D. Polder, Phillips Res. Rep. 1, 1 (1945).

function only of σ, and is independent of n_p. We thereby exclude any effects arising from the mutual interaction of neighboring pairs of atoms, an interaction which may, in certain cases, be of importance, perhaps even leading to an ordered arrangement of the pairs at zero stress. This assumption leads to

$$U=-(\partial\epsilon/\partial n_p)\sigma. \tag{7}$$

When we now substitute Eqs. (6) and (7) into Eq. (5), we obtain

$$E_R^{-1}-E_U^{-1}=n(\partial\epsilon/\partial n_p)^2/4kT,$$

and therefore, from Eq. (3),

$$\Delta_E=nE_U(\partial\epsilon/\partial n_p)^2/4kT. \tag{8}$$

An estimate of the relaxation strength Δ_E will now be given for the case of alpha-brass with 30 percent zinc. In this solution[6]

$$\partial\epsilon/\partial C=0.071,$$

where C is the zinc concentration. Upon using this value, and upon taking n as identical with the number of zinc atoms per unit volume, and upon replacing $(\partial\epsilon/\partial n_p)$ by $r(\partial\epsilon/\partial n)$, we obtain for the relaxation strength at 400°C

$$\Delta_E=0.075r^2.$$

It is anticipated that the numerical coefficient r will be less than, but of the order of magnitude of, unity. In the crystal examined Δ_E was[2] 0.025, a value whose order of magnitude is in agreement with the above theoretical computation.

II. ORIENTATION DEPENDENCE OF RELAXATION STRENGTH

In an experimental study of the anelasticity arising from stress induced preferential orientation of pair axes it is highly desirable that single crystals be used in order to avoid the anelasticity associated with the viscous[7] grain boundaries. Since it is difficult to grow a set of single crystals all of the same orientation, it is desirable that a theoretical formula be at hand which gives the dependence of the relaxation strength upon crystal orientation.

In the type of relaxation we are here considering no relaxation will be induced in cubic crystals by pure hydrostatic pressures. The relaxation under an arbitrary stress system may therefore be represented in terms of the relaxation in the two shear moduli c_{44} and $(c_{11}-c_{12})/2$. The relaxation strengths of these two moduli will be denoted by δ and δ', respectively. Thus

$$\delta=\{(c_{44})_U-(c_{44})_R\}/(c_{44})_R. \tag{9}$$

In order to compute Δ_E and Δ_G in terms of δ and δ', use will be made of the following formulae for the tensile and shear moduli:[8]

$$E^{-1}=s_{11}-[2(s_{11}-s_{12})-s_{44}]\phi, \tag{10}$$

$$G^{-1}=s_{44}+2[2(s_{11}-s_{12})-s_{44}]\phi, \tag{11}$$

where

$$\phi=\gamma_1^2\gamma_2^2+\gamma_2^2\gamma_3^2+\gamma_3^2\gamma_1^2, \tag{12}$$

with γ_1, γ_2, γ_3 being the direction cosines of the specimen axis with respect to the principal axes of the specimen. We now subtract E_U^{-1} from E_R^{-1}, and divide by E_U^{-1}. The right-hand member will now be transformed from the s's to the c's. Towards this end we introduce the notation

$$s=s_{44}, \qquad c=c_{44},$$
$$s'=2(s_{11}-s_{12}), \quad c'=(c_{11}-c_{12})/2,$$

and observe that

$$s=1/c; \quad s'=1/c'; \quad s_{11}+2s_{12}=1/(c_{11}+2c_{12});$$
$$\delta\equiv(c_U-c_R)/c_R=(s_R-s_U)/s_U;$$
$$\delta'\equiv(c'_U-c'_R)/c'_R=(s'_R-s'_U)/s'_U.$$

Upon dividing the right-hand member by ss', and upon using these relations, we obtain

$$\Delta_E=\frac{c\delta'/3-(c\delta'-c'\delta)\phi}{\dfrac{c_{44}(c_{11}+c_{12})}{2(c_{11}+2c_{12})}-(c-c')\phi}. \tag{13}$$

In a similar manner one obtains

$$\Delta_G=\frac{c'\delta+2(c\delta'-c'\delta)\phi}{c'+2(c-c')\phi}. \tag{14}$$

It remains to determine which, if any, of the two unknown quantities δ and δ' are zero in cubic lattices. In b.c.c. lattices the axes passing through nearest neighbors lie along one of the

[6] E. A. Owen and L. Pickup, Proc. Roy. Soc. 140, 179 (1933).

[7] See the coming paper by T. S. Kê.

[8] E. Schmid and W. Boas, *Kristallplastizität* (Berlin, 1935), p. 23.

four ⟨111⟩ directions. Pairs of solute atoms lying along these four directions will be affected equally by a shear stress $\sigma_{xx}-\sigma_{yy}$ across the (110) planes, but unequally by a shear stress σ_{xy} across a (001) plane. The first type of shear stress will therefore not cause a preferred orientation of pair axes, i.e., δ' is identically zero, and therefore the Δ_E due to interaction of nearest neighbors is zero when a tensile stress is applied along one of the principal axes. On the other hand, the shear stress σ_{xy} will tend to cause a preferred orientation, and hence δ is not zero. These conclusions may be arrived at in a more elegant manner. Let $n_{111}, n_{\bar{1}11}\cdots$ be the number of pairs of solute atoms with axes lying along the directions [111], [$\bar{1}$11], $\cdots$. The potential energy of the lattice can then contain three interaction terms which are linear in the n's and in the strains. One interaction term will contain the product of the sum of the n's and of the sum $\epsilon_{xx}+\epsilon_{yy}+\epsilon_{zz}$. This term will cause no relaxation, and hence will not be further considered. The remaining two terms represent interaction of the orientation variables with shear strains. These terms must have the same symmetry as the lattice. One term is

$$\alpha\{n_{111}(\epsilon_{yz}+\epsilon_{zx}+\epsilon_{xy})+n_{\bar{1}11}(\epsilon_{yz}-\epsilon_{zx}-\epsilon_{xy})+n_{1\bar{1}1}(-\epsilon_{yz}+\epsilon_{zx}-\epsilon_{xy})+n_{11\bar{1}}(-\epsilon_{yz}-\epsilon_{zx}+\epsilon_{xy})\}.$$

No interaction term can be formed of the ϵ_{xx}, ϵ_{yy}, ϵ_{zz} strains, other than that representing a uniform dilation, which has the cubic symmetry of a cubic lattice.

In f.c.c. lattices the axes passing through nearest neighbors lie along one of the six ⟨110⟩ directions. These pairs are affected unequally by both types of shearing stress, and hence both δ and δ' are different from zero. This conclusion is vindicated by the existence of two shear interaction terms which satisfy the symmetry relations. These are

$$\beta\{(n_{011}+n_{0\bar{1}1})(2\epsilon_{zz}-\epsilon_{yy}-\epsilon_{zz})+(n_{101}+n_{\bar{1}01})(2\epsilon_{yy}-\epsilon_{zz}-\epsilon_{xx})+(n_{110}+n_{\bar{1}10})(2\epsilon_{zz}-\epsilon_{xx}-\epsilon_{yy})\}$$

and

$$\gamma\{(n_{011}-n_{0\bar{1}1})\epsilon_{yz}+(n_{101}-n_{\bar{1}01})\epsilon_{zx}+(n_{110}-n_{\bar{1}10})\epsilon_{xy}\}.$$

PHYSICAL REVIEW VOLUME 71, NUMBER 1 JANUARY 1, 1947

Quantized Space-Time

HARTLAND S. SNYDER
Department of Physics, Northwestern University, Evanston, Illinois
(Received May 13, 1946)

It is usually assumed that space-time is a continuum. This assumption is not required by Lorentz invariance. In this paper we give an example of a Lorentz invariant discrete space-time.

THE problem of the interaction of matter and fields has not been satisfactorily solved to this date. The root of the trouble in present field theories seems to lie in the assumption of point interactions between matter and fields. On the other hand, no relativistically invariant Hamiltonian theory is known for any form of interaction other than point interactions.

Even for the case of point interactions the relativistic invariance is of a formal nature only, as the equations for quantized interacting fields have no solutions. The uses of source functions, or of a cut-off in momentum space to replace infinity by a finite number are distasteful arbitrary procedures, and neither process has yet been formulated in a relativistically invariant manner. It may not be possible to do this.

It is possible that the usual four-dimensional continuous space-time does not provide a suitable framework within which interacting matter and fields can be described. I have chosen the idea that a modification of the ordinary concept of space-time may be necessary because the "elementary" particles have fixed masses and associated Compton wave-lengths.

The special theory of relativity may be based on the invariance of the indefinite quadratic form

$$S^2=c^2t^2-x^2-y^2-z^2, \qquad (1)$$

for transformations from one inertial frame to another. It is usually assumed that the variables x, y, z, and t take on a continuum of values and that they may take on these values simultaneously. This last assumption we change to the following:

x, y, z, and t are Hermitian operators for the space-time coordinates of a particular Lorentz frame; the spectrum of each of the operators x, y, z, and t is composed of the possible results of a measurement of the corresponding quantity; the operators x, y, z, and t shall be such that the spectra of the operators x', y', z', t' formed by taking linear combinations of x, y, z, and t, which leave the quadratic form (1) invariant, shall be the same as the spectra of x, y, z, and t.

In other words, we assume that the spectra of the space-time coordinate operators are invariant under Lorentz transformations. It is evident that the usual space-time continuum satisfies the above definition; it is, however, not the only solution. The principal result in this paper is that there exists a Lorentz invariant space-time in which there is a natural unit of length. We hope that the introduction of such a unit of length will remove many of the divergence troubles of present field theory.

It can be shown easily that the introduction of a smallest unit of length in space-time will force one to drop the usual assumptions of commutativity of x, y, z, and t, otherwise the assumption of Lorentz invariance of the spectra of the operators x, y, z, and t, if they commute, implies continuous spectra.

To find operators x, y, z, and t possessing Lorentz invariant spectra, we consider the homogeneous quadratic form[1]

$$-\eta^2=\eta_0^2-\eta_1^2-\eta_2^2-\eta_3^2-\eta_4^2, \tag{2}$$

in which the η's are assumed to be real variables. The variables η_0 to η_4 may be regarded as the homogeneous (projective) coordinates of a real four-dimensional space of constant curvature[2] (a De Sitter space). We now define x, y, z, and t by means of the infinitesimal elements of the group under which quadratic form (2) is invariant. We take

$$\begin{aligned} x&=ia(\eta_4\partial/\partial\eta_1-\eta_1\partial/\partial\eta_4),\\ y&=ia(\eta_4\partial/\partial\eta_2-\eta_2\partial/\partial\eta_4),\\ z&=ia(\eta_4\partial/\partial\eta_3-\eta_3\partial/\partial\eta_4),\\ t&=(ia/c)(\eta_4\partial/\partial\eta_0+\eta_0\partial/\partial\eta_4), \end{aligned} \tag{3}$$

in which a is the natural unit of length, c is the velocity of light. The operators x, y, z, and t are assumed to be Hermitian and may be regarded as operating on single valued functions of η_0, $\eta_1\cdots$. From the assumption that x, y, and z are Hermitian operators of the form (3), one can show that each of them has a spectrum consisting of the characteristic values, ma where m is an integer, positive, negative, or zero. The operator, t, has a continuous spectrum extending from minus infinity to plus infinity. The spectrum of each of the operators x, y, z, and t is infinitely degenerate.

Transformations which leave quadratic form (2) and η_4 invariant are covariant Lorentz transformations on the variables η_1, η_2, η_3, and η_0. When the transformed variables η_0', η_1', η_2', η_3', η_4 are substituted into Eqs. (3), it is found that x, y, z, and t undergo contravariant Lorentz transformation. It is evident that the new operators x', y', z', and t' which are formed by replacing η_0, η_1, η_2, η_3, η_4 in Eqs. (3) by η_0', η_1', η_2', η_3', η_4 are linear expressions with real constant coefficients in x, y, z, and t, and are consequently Hermitian operators if x, y, z, and t are Hermitian. The functions on which these operators operate are left invariant except for change in argument. Thus, we see that x', y', z', and t' which are Hermitian operators of the same form in the variables η_0', η_1', η_2', η_3', η_4 as x, y, z, and t were in the variables η_0, η_1, η_2, η_3, η_4 have the same spectra as do x, y, z, t.

We define six additional operators by the equations

$$\begin{aligned} L_x&=ih(\eta_3\partial/\partial\eta_2-\eta_2\partial/\partial\eta_3),\\ L_y&=ih(\eta_1\partial/\partial\eta_3-\eta_3\partial/\partial\eta_1),\\ L_z&=ih(\eta_2\partial/\partial\eta_1-\eta_1\partial/\partial\eta_2),\\ M_x&=ih(\eta_0\partial/\partial\eta_1+\eta_1\partial/\partial\eta_0),\\ M_y&=ih(\eta_0\partial/\partial\eta_2+\eta_2\partial/\partial\eta_0),\\ M_z&=ih(\eta_0\partial/\partial\eta_3+\eta_3\partial/\partial\eta_0), \end{aligned} \tag{4}$$

[1] We could also have taken the quadratic form
$$\eta^2=\eta_0^2-\eta_1^2-\eta_2^2-\eta_3^2+\eta_4^2.$$
This leads to another Lorentz invariant discrete space-time.

[2] I am indebted to W. Pauli in a private communication for this interpretation of the variables η_0, $\eta_1\cdots$.

in which $\hbar$ is Plank's constant divided by 2π. Now, L_x, L_y, L_z, M_x, M_y, M_z are, with the exception of the factor $i\hbar$, the infinitesimal elements of the four-dimensional Lorentz group. It may be shown that each of the above operators commutes with quadratic form (1) when the values of x, y, z, t given by (3) are used. This is another way of stating the Lorentz invariance of quadratic form (1). It will be observed that L_x, L_y, L_z, M_x, M_y, M_z do not involve η_4, and that as a consequence the Lorentz transformation which leaves form (2) and η_4 invariant leaves quadratic form (1) invariant, and as has already been shown, leaves the spectra of the operators x, y, z, and t invariant. We see from these facts that the usual assumptions concerning the continuous nature of space-time are not necessary for Lorentz invariance. This result is the minimum objective of this work.

The ten operators defined in (3) and (4) have a total of forty-five commutators. Only six of these commutators differ from the ordinary ones and these six are

$$\begin{aligned} &[x, y]=(ia^2/\hbar)L_z, \quad [t, x]=(ia^2/\hbar c)M_x, \\ &[y, z]=(ia^2/\hbar)L_x, \quad [t, y]=(ia^2/\hbar c)M_y, \\ &[z, x]=(ia^2/\hbar)L_y, \quad [t, z]=(ia^2/\hbar c)M_z. \end{aligned} \tag{5}$$

We see from these commutators that if we take the limit $a\rightarrow 0$ keeping $\hbar$ and c fixed, our quantized space-time changes to the ordinary continuous space-time.

The commutators for the quantities L_x, L_y, L_z, M_x, M_y, M_z are those of the infinitesimal elements of the Lorentz group, and for this reason we introduced the factor of $i\hbar$ in their definition. Thus, L_x, L_y, L_z have the usual properties of quantum angular momentum. The commutators which involve one of the operators x, y, z, or t, with one of the operators L_x, L_y, L_z, M_x, M_y, M_z are independent of a, the natural unit of length. Thus all of the commutators pass in the limit $a\rightarrow 0$ to their usual expressions.

In addition to the ten quantities defined in (3) and (4) we define four additional operators, having the transformation properties of space or time displacement operators, or the equivalent, of energy and momentum operators.[3]

$$\begin{aligned} &p_x=(\hbar/a)(\eta_1/\eta_4), \quad p_z=(\hbar/a)(\eta_3/\eta_4), \\ &p_y=(\hbar/a)(\eta_2/\eta_4), \quad p_t=(\hbar c/a)(\eta_0/\eta_4). \end{aligned} \tag{6}$$

By means of algebraic manipulations one can show that

$$L_x=yp_z-zp_y; \quad M_x=\frac{1}{c}{-xp_t+ctp_x}; \text{ etc.} \tag{7}$$

The angular momenta have their usual expression in terms of coordinate and momentum. One must exercise care as to the order in which the factors in (7) are written since they do not commute. The four quantities p_x, p_y, p_z, p_t commute with one another, and have the same commutators with L_x, L_y, L_z, M_x, M_y, M_z as do the usual expressions for the space or time displacement operators. In addition, each has a continuous spectrum running from minus infinity to plus infinity. Their commutators with the coordinates and time are not the same as usual and are given by

$$\begin{aligned} &[x, p_x]=i\hbar[1+(a/\hbar)^2px^2]; \\ &[t, p_t]=i\hbar[1-(a/\hbar c)^2p_t^2]; \\ &[x, p_y]=[y, p_x]=i\hbar(a/\hbar)^2p_xp_y; \\ &[x, p_t]=c^2[p_x, t]=i\hbar(a/\hbar)^2p_xp_t; \text{ etc.} \end{aligned} \tag{8}$$

Here we note that if all the components of the momentum are small compared to $\hbar/a$ and the energy is small compared to $\hbar c/a$ then these commutators approach those which are given in orinary quantum mechanics. Further, as we take the limit $a\rightarrow 0$ these commutators change to their standard values.

The fact that these new commutators between coordinate and momentum differ from the old ones appreciably only for large values of the momentum, and that they differ by large amounts when $|p|>\hbar/a$ implies that a field theory based on quantized space-time will give substantially the same results as the usual field

[3] The most general form for the energy momentum operators with the correct transformation properties is

$$p_x=\frac{\hbar}{a}\frac{\eta_1}{\eta_4}f\left(\frac{\eta_4}{\eta}\right), \cdots, p_t=\frac{\hbar c}{a}\frac{\eta_0}{\eta_4}f\left(\frac{\eta_4}{\eta}\right),$$

in which $f(\eta_4/\eta)$ is a dimensionless function of its argument. A choice of $f(\eta_4/\eta)$ other than the choice which gives Eqs. (6) may be more useful for physical problems.

theory for all processes which do not involve large components of the momenta, but will produce large effects for processes which do involve large components of the momenta. We might expect that the usual atomic and molecular formulas will suffer no appreciable change, while expressions for self-energy, polarization of the vacuum, and possibly nuclear forces will be considerably altered. Alterations in the last mentioned quantities are certainly necessary.

We note here that the commutator relations (7) have a solution for x, y, z, t.

$$x=ih\left[\frac{\partial}{\partial p_x}+(a/h)^2p_x\left(p_x\frac{\partial}{\partial p_x}+p_y\frac{\partial}{\partial p_y}+p_z\frac{\partial}{\partial p_z}+p_t\frac{\partial}{\partial p_t}\right)\right];$$
$$t=ih\left[\frac{\partial}{\partial p_t}-(a/hc)^2p_t\left(p_x\frac{\partial}{\partial p_x}+p_y\frac{\partial}{\partial p_y}+p_z\frac{\partial}{\partial p_z}+p_t\frac{\partial}{\partial p_t}\right)\right];\text{ etc.} \tag{9}$$

This solution of the commutator relations (8) is completely analogous to the solution of the conventional commutator relations between coordinate and momentum for the coordinates in terms of derivatives with respect to the momentum. It would not be surprising to find in our case that no corresponding solution for the momenta in terms of derivatives with respect to the coordinates exists since our coordinates and time do not have continuous spectra in general and do not commute.

It is not difficult to verify that if the expressions for x, y, z, and t given by (9) are substituted in the commutators (5) and the corresponding L_x, L_y, L_z, M_x, M_y, M_z computed, then these last mentioned quantities satisfy their usual commutation relations.

It might appear that x, y, z, and t as given by Eqs. (9) are not Hermitian operators. It may be shown, however, that they are Hermitian operators when the correct volume elements of group space are used. The group which concerns this is the transformation group which leaves quadratic form (2) invariant. An infinitesimal volume element, $d\tau$, of group space is given in terms of p_x, p_y, p_z and p_t by the formula

$$d\tau=\frac{h\,dp_x\,dp_y\,dp_z\,dp_t}{ac(p_x^2+p_y^2+p_z^2+(h/a)^2-(p_t/c)^2)^{5/2}}. \tag{10}$$

To this point the invariance properties of quantized space-time have been considered only with respect to rotations and Lorentz transformations which leave the origin fixed. A continuum of translations is not admissable in this space, indeed one can prove that if x, y, z, and t are such that quadratic form (1) is invariant under infinitesimal displacements, the space x, y, z, and t must be a continuum. Translations of the origin may be introduced as follows. Let $S(\eta_0, \eta_1, \eta_2, \eta_3, \eta_4)$ be an arbitrary unimodular single-valued homogeneous function of the degree zero in the variables, η_0, η_1, η_2, η_3, η_4. Let A be any one of the operators defined by Eqs. (3), (4), or (6). Form the new operators $A'=\bar{S}AS$ in which $\bar{S}$ means the complex conjugate of S. It may then be shown that the primed operators satisfy exactly the same commutation relations as did the original operators and that they are Hermitian. The primed operators thus have exactly the same transformation properties with respect to Lorentz transformations as did the original operators. In particular, the displacement operators p_x, p_y, p_z, p_t are not changed by this process. This is a result which we must demand for the space and time displacement operators. If we choose $S=\exp[im\arctan(\eta_1/\eta_4)]$, we find that this results in a translation of ma in the x direction. It should not be expected, nor is it possible in this space, to find a function S which corresponds to sharply defined translational values of x, y, z, and t simultaneously. The relation between two different frames of reference cannot be set up more precisely than the commutation relations between the coordinates permit.

We will not discuss in any detail in this paper the limitations placed upon the simultaneous measurability of x, y, z, and t due to the noncommutativity of these quantities. Some preliminary calculations which I have made indicate that these limitations are not serious enough to interfere with the ordinary description of atomic phenomena in terms of a continuous space-time nor with our usual macroscopic theory.

The Normal Reflection of Shock Waves

R. FINKELSTEIN*
Bureau of Ordnance, Navy Department, Washington, D. C.
(Received September 9, 1946)

The problem of the normal reflection of a shock wave is solved by an approximate analytical integration of the hydrodynamical equations. The solution given here leads to nearly the same numerical results as an exact method, based on a graphical integration of the hydrodynamical equations, which has been described by Chandrasekhar. A method of computing the complete pressure-time curve at the reflector is given and applied to reflection in a class of fluids obeying the Tait adiabatic equation of state. It is found that in compressible fluids (gases) the pressure on the reflector is prolonged and that the impulse delivered to it *exceeds* the value predicted by the acoustic theory. In slightly compressible media (liquids and solids), on the other hand, the blow is shorter and the impulse delivered to the reflector is *less* than one would expect from the acoustic approximation. The method given here is also applicable to the reflection of gravity waves on the surface of a liquid.

INTRODUCTION

WHEN a shock wave is reflected from a solid, the pressure on the reflector at first rises to a high peak and then decays to the value previously existing. For weak shocks, or sound waves, which strike a rigid reflector, this initial peak is of such a height that the pressure ratio (ζ_r) across the reflected shock front and the pressure ratio (ζ_i) across the incident shock front are equal,

$$\zeta_r=\zeta_i,$$

so that the overpressure at the reflector is twice the overpressure in the incident shock. In the limiting case of very strong and normally incident shocks, on the other hand,

$$\zeta_r=[(3\gamma-1)/(\gamma-1)]\zeta_i.$$

For a fluid whose adiabatic constant, γ, is 1.4, ζ_r/ζ_i is 8. The rise in pressure at the first moment of reflection and the flow patterns simultaneously present have been studied at all angles of incidence and the theory is able to describe in an approximate way both the regular and the irregular, or Mach, reflection. One is, however, rarely interested in the initial, or peak, pressure alone unless the period of the reflector is very short compared to the duration of the incident wave. Similarly in the collision of equal and opposite shocks, which is hydrodynamically equivalent to reflection from a rigid wall, it is not just the first instant of the collision but rather the subsequent history of the interaction which is interesting. It is the complete course of the reflection of one shock, or of the interaction of two shocks, which we wish to discuss here.

QUALITATIVE DESCRIPTION OF RESULTS

For the case of normal incidence alone has the problem been solved. The possibility of using a very simple numerical method based on the Riemann form of the equations of motion was indicated by Chandrasekhar[1] who considered reflection in air. Here we replace the numerical method by an analytical one and extend the work to other media besides air. All media covered by our calculations are subject to the Tait equation of state for isentropic changes.

$$(p+\pi)v^\gamma=k. \tag{1}$$

Here p is overpressure; v is specific volume; π, γ, and k, which are characteristic of the medium, are constants for isentropic processes but are functions of the entropy. When Eq. (1) is applied to ideal gases, γ is the adiabatic constant lying between 1 and 1.67. The same equation is also applicable to matter in the condensed state, if π is now interpreted as the internal pressure and γ is an empirical constant, not simply related to the specific heats: e.g., for water, $\pi=3000$ atmos., $\gamma=7.15$; for freshly detonated explosives which

* Now at Argonne National Laboratory, Chicago, Illinois.

[1] S. Chandrasekhar, a report of limited circulation issued by the Ballistics Research Laboratory, Aberdeen, Maryland.

have not yet expanded, $\gamma=3$. It has also been pointed out that an analogy may be set up between the equations of gas dynamics and of gravity waves on the surface of a fluid and this analogy corresponds to the case of $\gamma=2$; our results are in fact applicable to gravity waves if pressure is interpreted as h^2, where h is the height of the gravity wave.[2]

Although the numerical method used by Chandrasekhar is rigorous, the analytical method employed here contains certain approximations and the two methods were, therefore, compared for an incident linear shock (i.e., the pressure falls linearly with time behind the peak) of 1.5 atmos. in air (the particular example computed by him) and an incident linear shock of 1800 atmos. in water. The pressure time curves at the wall are shown in Fig. 1. The two methods agree well and differ considerably from the acoustic approximation.

The results of our calculations can be most conveniently expressed in terms of $\int_0^T p dt$, the time integral of the pressure at the wall, where T is the total time required for reflection. This integral is the momentum delivered to the wall or the difference in momenta between the incident and reflected pulses, i.e.,

$$\int \rho_r u_r dx = \int \rho_i u_i dx + \int_0^T p dt, \qquad (2)$$

where ρ and u are density and material velocity, respectively, and where the subscripts i and r refer to incident and reflected pulses. The space integration is extended over the whole lengths of the incident and reflected shocks. In Fig. 2 the impulse $\int_0^T p dt$ is normalized by dividing by the acoustic impulse, i.e., $2\int p_i dt$, where p_i is the value the over-pressure would have at the position of the wall if the incident wave moved forward without change of shape and with the velocity of sound corresponding to zero over-pressure. The intensity of the incident shock is also normalized in Fig. 2: it is specified by $\zeta=(p+\pi)/\pi$. In Fig. 2 the normalized impulse is plotted as a function of γ; the most interesting physical result of our calculation—the difference of behavior shown by compressible and incompressible media—is then brought out: in the case of gases ($1\leqslant\gamma\leqslant 1.67$) the impulse is *greater* than the prediction of acoustic theory; but in the case of liquids and solids the impulse is *less* than the acoustic approximation. Non-linear theory happens to agree with the acoustic estimate in the neighborhood of $\gamma=2$; $\gamma=2$ also corresponds to the analogy between gravity waves and gas flow. The reason for this difference between gaseous and condensed matter is that the *duration* of the blow exceeds the acoustic approximation in the gaseous case, whereas the situation is reversed for solids and liquids, as one can see by the following qualitative consideration of the reflection process.

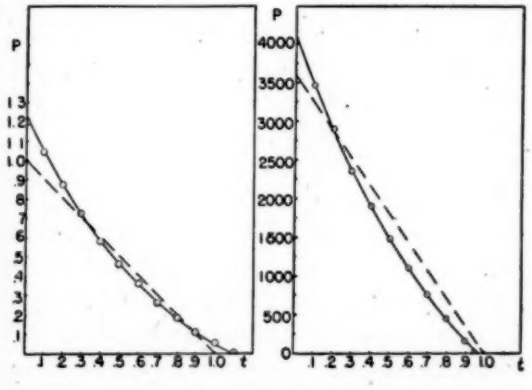

FIG. 1. Pressure-time curves at reflector. The curve at the left corresponds to reflection in air of an incident pulse whose peak overpressure is 0.5 atmos. The other curve describes reflection in water of an incident pulse whose peak overpressure is 1800 atmos. The ordinate is overpressure in atmos. and the unit of time is the duration of the incident pulse. ⊙ Computed by Chandrasekhar's method; — analytic approximation; – – acoustic approximation.

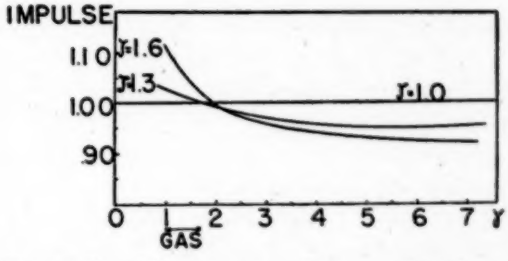

FIG. 2. Impulse given to reflector as function of γ. Ordinate is actual impulse given to rigid wall divided by approximate acoustic impulse. Abscissa is constant (γ) appearing in the equation of state. ζ is shock intensity. $\zeta=1.0$ corresponds to limiting case of sound wave.

[2] T. von Karman, "Flow in Compressible Fluids," to be found in a collection of papers entitled *Fluid Mechanics and Statistical Methods in Engineering* (University of Pennsylvania Press, Philadelphia, 1941), page 25.

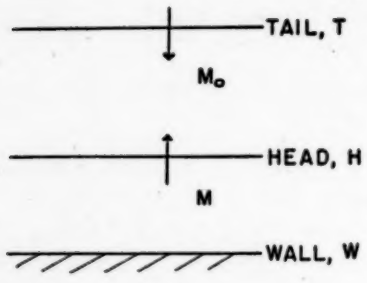

FIG. 3. Reflection in x space.

After the instant of impact the head, H, of the shock wave reverses direction and begins to travel toward its tail, T (Fig. 3). As soon as the direction of H has been reversed by the wall, the total disturbance may be regarded approximately as a (non-linear) composition of two waves of finite amplitude. One of these moves toward the wall and is bounded by T and W. The other moves away from the wall and is bounded by W and H. These two waves penetrate each other until T reaches the wall and thereby marks the end of the reflection. It is clear that the tail T moves toward the wall at speed, a, the velocity of sound corresponding to $p=0$, until it meets H. It is not so easy to guess the speed of H with respect to the wall, but it also turns out to be nearly a for the shock strengths of interest here. The reason is, roughly speaking, that the high pressure behind H produces a supersonic velocity not with respect to the wall but with respect to fluid rapidly moving *toward the wall*. The net effect is that H and T approach each other approximately with velocity a. Hence if the initial thickness of the pulse is L, the time until H and T meet is $L/2a$. After passing through the head the tail then moves with the velocity $c-u$, where c is the local velocity of sound and u is the material velocity of the fluid in the region M. Hence the total time of reflection is $L/2a+L/2\langle c-u\rangle_M$ where $\langle c-u\rangle_M$ is the average velocity of the tail in M. On the other hand the duration according to the acoustic approximation is L/a. Hence if u/c is so large that $\langle c-u\rangle_M<a$, as in air, the pressure on the wall lasts for a longer time than acoustic theory indicates; but if u/c is so small that $\langle c-u\rangle_M>a$, as in water, then we have the opposite situation. These qualitative considerations are supported by the detailed calculations to which we now turn.

ANALYTICAL METHOD

Consider a plane shock, S, impinging on a rigid wall, W, at normal incidence. Let the plane of the wall be $x=0$ and let the x axis be directed toward the oncoming shock. The time, t, is measured from the moment at which S strikes W. Since the problem is one-dimensional, there are only two independent variables, x and t, and it is convenient to speak in terms of the x, t plane shown in Fig. 4. Here D is the world line of the reflected shock front, and the world line of a typical element, initially at x_0, is shown with a discontinuity where it crosses D. M_0 and M are the regions between D and the x axis and t axis, respectively. The following boundary conditions are given on the axes and on D:

1. Distribution of pressure, p_i, and velocity, u_i, on the x axis. This is the distribution of pressure and velocity in the incident wave.
2. $u=0$ on the t axis since the wall is rigid.
3. Shock equations across the discontinuity, D, expressing the conservation of (a) mass, (b) momentum, (c) energy.

Subject to these boundary conditions three differential equations which again express the conservation of mass, momentum, and energy must be satisfied in M_0 and M. In these differential equations appear three unknown functions, e.g., pressure, velocity, and entropy, and the problem is to find these functions in the regions M_0 and M and in addition to find the equation of the curve D. Employing the usual approximation, however, we assume that the flow in M_0 and M is isentropic. In addition the stronger approximation is made that the entropy change across D can be neglected. The entropy change across D is actually only third order in the volume change; but a stronger argument is that results of the calculation made under this assumption agree very well with the results of the rigorous numerical method in which the change of entropy is properly taken into account. Under these assumptions the entropy becomes a constant of the motion and may be ignored. There are then only two unknown functions, say, p and u, and the exact conservation of energy condition is replaced by the approximate conservation of entropy condition.

The three conservation conditions in M and M_0

may then be written

$$\frac{\partial}{\partial x}(\rho u)+\frac{\partial \rho}{\partial t}=0, \tag{3}$$

$$\frac{\partial p}{\partial x}=-\rho\left(\frac{\partial u}{\partial t}+u\frac{\partial u}{\partial x}\right), \tag{4}$$

$$p+\pi=k\rho^{\gamma} \text{ (an approximation)}, \tag{5}$$

where ρ is density. There are two unknown functions and two differential equations. On the other hand the three conservation conditions across the shock front are

$$s=u_0+v_0\left[\frac{p-p_0}{v_0-v}\right]^{\frac{1}{2}}, \tag{6}$$

$$u=u_0+[(p-p_0)(v_0-v)]^{\frac{1}{2}}, \tag{7}$$

$$(p_0+\pi)v_0^{\gamma}=(p+\pi)v^{\gamma} \text{ (an approximation)}, \tag{8}$$

where s is the shock velocity (or slope of D) and $v=1/\rho$ is the specific volume. The variables in these equations are of course to be evaluated on D; subscripts refer to the two sides (M and M_0) of D.

By Riemann's method[3] Eqs. (3)–(5) are rewritten

$$\frac{\partial P}{\partial t}=-(c+u)\frac{\partial P}{\partial x}, \tag{9}$$

$$\frac{\partial Q}{\partial t}=(c-u)\frac{\partial Q}{\partial x}, \tag{10}$$

where P and Q are the Riemann functions which are defined in this paper as

$$P=2c/(\gamma-1)+u, \tag{11}$$

$$Q=2c/(\gamma-1)-u, \tag{12}$$

where

$$c=(dp/d\rho)^{\frac{1}{2}}=\text{velocity of sound}. \tag{13}$$

It is convenient to rewrite the shock equations (6) and (7) with the aid of (8) and (13) in terms of these five variables: c, u, c_0, u_0, and s. They become to the first order in c/c_0-1

$$s=u_0+ec+e_0c_0, \tag{14}$$

$$Q=Q_0, \tag{15}$$

[3] See, for example, H. Lamb, *Hydrodynamics* (Cambridge University Press, 1932), sixth edition, page 481.

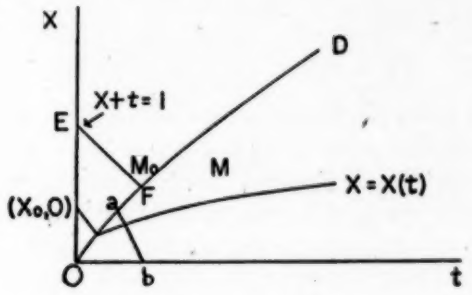

FIG. 4. Reflection in x, t space. OD and EF are world lines of reflected shock and tail of incident shock, respectively, and ab is a characteristic on which Q is constant.

where the following abbreviations have been introduced

$$e=(\gamma+1)/2(\gamma-1),$$
$$e_0=1-e.$$

It has been pointed out that Q is nearly constant[1] across a rather strong shock front in air, even without neglect of the entropy change.

INITIAL CONDITIONS

We come now to the formulation of the boundary conditions on the x axis or, in other words, to a description of the incident shock wave. For simplicity it is assumed that at $t=0$ the incident wave is progressive and that the velocity distribution in it is linear; the pressure distribution is then fixed. Equations (9) and (10) show how the progressive condition may be expressed. According to these equations a general one-dimensional hydrodynamical disturbance may be decomposed (non-linearly) into two waves, described by P and Q which travel in opposite directions with the velocities $c+u$ and $c-u$, respectively. The condition for a progressive wave is that either P or Q be constant; and in this case it must be P since the pulse is traveling toward $-\infty$. The required boundary conditions on the x axis are then

$$\begin{aligned} &u_0(x,0)=-B+Bx \qquad 0\leqslant x\leqslant 1,\\ &u_0(x,0)=0 \qquad\quad x>1,\ B>0, \end{aligned} \tag{16}$$

$$P_0(x,0)=2/(\gamma-1). \tag{17}$$

Here B is the peak velocity. The units of length and time are so chosen that the initial length of the incident pulse is unity and so that $c=1$ when $p=0$. Equation (17) together with (5) and (13) determine the pressure as the following function

of the velocity

$$p+\pi=\pi[1-(\gamma-1)u/2]^{2\gamma/(\gamma-1)}. \quad (18)$$

The pressure computed from (18) and (16) is very nearly linear for shocks in which $(p+\pi)/\pi<1.6$. In other words a pulse of the type considered here is essentially linear in both pressure and velocity.

A remark may be made about the progressive assumption at this point. Although a continuous wave of finite amplitude can propagate without increase of length, the same is no longer true as soon as it has evolved into a shock. After it has become a shock, reflection of the continuous portion of the pulse from the discontinuity begins; as a result the disturbance propagates backwards as well as forwards, and hence the progressive assumption cannot be rigorously satisfied by a shock any time after it is formed. Nevertheless it is often a good approximation, and as we have just seen, the pulse considered here is essentially linear in both pressure and velocity.

Although one could specify the pressure distribution in the incident pulse instead of the velocity distribution in it, we have not done so because it is analytically more convenient to regard the velocity as given. Since, however, experimental data generally concern pressure, it is necessary to have a way of determining the maximum velocity B from the measured peak pressure. B can be calculated from the following formula which follows from (7)

$$B=[(\zeta-1)(1-\zeta^{-1/\gamma})/\gamma]^{\frac{1}{2}}, \quad (19)$$

where $\zeta=(p_m+\pi)/\pi$ and p_m is measured peak pressure in the incident wave. This Eq. (19) is not consistent with (18) since (19) is a shock equation while (18) is based on the progressive assumption; and as we have just seen, they are not compatible. The procedure followed here is this: ζ is regarded as computed from the measured peak pressure. From (19) B is found. From (16) u is found. Equations (16) and (17) then completely determine the wave. The numerical discrepancy between (18) and (19) is actually insignificant for shocks of the intensity considered here ($\zeta\leqslant 1.6$).

SOLUTION IN M_0

The differential equations can be solved readily in M_0 if the disturbance in M_0 remains progressive. That it does remain nearly progressive may be verified by comparing the result of the rigorous Riemann numerical integration with the analytic progressive solution. Therefore we assume

$$P_0(x,t)=2/(\gamma-1). \quad (20)$$

Let

$$\Delta=c_0-u_0. \quad (21)$$

Then by (20), (21), (10)–(12) it follows that

$$\frac{\partial\Delta}{\partial t}=\Delta\frac{\partial\Delta}{\partial x}. \quad (22)$$

The solution of (22) is

$$t\Delta+x=w(\Delta), \quad (23)$$

where w is a function to be determined by the boundary conditions. When these conditions are (16) and (17) then

$$\Delta=[(\gamma+1)(-Bx+B)+2]/[B(\gamma+1)t+2] \qquad x<1-t, \quad (24)$$
$$=1 \qquad x>1-t.$$

The discontinuity in the derivatives of Δ along the line $x+t=1$ (Fig. 4) has its origin in the discontinuity at the tail of the incident pulse (Eq. (16)). The straight line EF is the world line of the tail of the incident shock and F represents its intersection with the head of the reflected shock. Here we are interested only in the part OEF of the region M: and so only the first representation of Δ in (24) will be carried. The quantities u_0, c_0, and Q_0 are now readily found.

$$u_0=2B(x+t-1)/(2+B(\gamma+1)t) \quad x<1-t, \quad (25)$$

$$c_0=1-(\gamma-1)u_0/2, \quad (26)$$

$$Q_0=2c_0/(\gamma-1)-u_0. \quad (27)$$

With these expressions the problem is solved in M_0.

SOLUTION IN M

To determine the solution in M one has to overcome a difficulty characteristic of shock problems; namely, although the boundary conditions on D are known, the equation of the line D is unknown and has to be determined simultaneously with the solution of the differential equations in M. The shock equations (14) and

(15) contain five variables: u_0, c_0, u, c, and s, of which u_0 and c_0 are known from (25) and (26). Still one more condition is necessary to fix u, c, and s, and this additional information is bound up in the solution of the differential equations. In order to separate the determination of the shock line from the solution of the differential equations we make the following approximation

$$P(g(t), t) = P(0, 0), \tag{28}$$

where

$$x = g(t) \tag{29}$$

is the equation of D. The best arguments for the condition (28) are that the decay of P along D, computed by the rigorous numerical method, is small and that the pressure-time curve, obtained on the basis of (28), agrees very closely with the corresponding curve computed according to the numerical method (as shown in Fig. 1). The function P actually decreases along D as t increases and this decrease causes the shock to decay. Therefore the physical meaning of the approximation (28) is that decay of the reflected shock is negligible during the period of reflection. Aside from its numerical success this assumption has in its favor two facts which make it plausible: first, the time of reflection is short; and second, since the shock travels faster with respect to M_0 than with respect to the wall, the wall behaves as a sustaining piston behind the shock.

The equations (14), (15), (25), (26), and (28) lead to the following differential equation for the shock line D

$$\frac{dx}{dt} = \frac{f + hx + jt}{1/B + (\gamma+1)t/2}, \tag{30}$$

$$f = 1/B + (3\gamma - 5)/4,$$

$$h = (3-\gamma)/2,$$

$$j = 2 + B(\gamma+1)^2/8.$$

The solution of this equation is

$$x = [2/(\gamma-1)B + (5\gamma-3)/4(\gamma-1)] \times [1 - (1+(\gamma+1)Bt/2)^{(3-\gamma)/(1+\gamma)}] + (2/(\gamma-1))[1 + B(\gamma+1)^2/16]t. \tag{31}$$

It is more convenient and numerical comparison with the complete equation again shows that it is little less accurate to use only the first two terms of the expansion of (31) in powers of t, i.e.,

$$x = \alpha t + \beta t^2, \tag{32}$$

where

$$\alpha = (3\gamma - 5)B/4 + 1, \tag{33}$$

$$\beta = [(5\gamma-3)B^2/4 + 2B](3-\gamma)/4. \tag{34}$$

Equation (32) fixes the boundary line D. The boundary conditions on it are

$$P(x, t) = P(0, 0), \tag{35}$$

$$Q(x, t) = Q_0(x, t). \tag{36}$$

Q_0 is given by (27) and (32). If the value of Q_0 so obtained is put in (36) one gets

$$Q(x, t) = q_0 + q_1 t + q_2 t^2, \tag{37}$$

where

$$q_0 = 2(1/\gamma - 1 + B), \tag{38}$$

$$q_1 = -4B[1 + (5\gamma-3)B/8], \tag{39}$$

$$q_2 = -B(3\gamma-1)q_1/4. \tag{40}$$

In (37) higher order terms were again found small enough to neglect. Finally

$$P(x, t) = P(0, 0) = Q(0, 0) = q_0. \tag{41}$$

The boundary conditions are most convenient in the forms (41) and (37).

The boundary D and the boundary conditions on it have now been found so that the differential equations in M can be solved. Numerical integration shows that in M the characteristics of Q are almost straight. Now the actual slope of a Q characteristic is $c-u$. Let the slope be assumed constant and equal to $-\lambda$ which is defined as follows

$$2\lambda = (c-u)_a + (c-u)_b, \tag{42}$$

where the points a and b are shown in Fig. 4. One then finds

$$(c-u)_b = c_b = (\gamma-1)Q_b/2 = (\gamma-1)Q_a/2,$$

and by (41)

$$(c-u)_a = (\gamma-3)P_a/4 + (\gamma+1)Q_a/4 = (\gamma-3)q_0/4 + (\gamma+1)Q_a/4.$$

Hence

$$\lambda = (\gamma-3)q_0/8 + (3\gamma-1)Q_a/8. \tag{43}$$

Then the equation of the characteristic passing

through $(0, t_b)$ is

$$x=\lambda(t_b-t), \tag{44}$$

where λ is given by the preceding equation.

To find Q_b as a function of t_b it is convenient to regard t_a as the independent variable. The relation between Q_b and t_b is then given by the parametric equations:

$$Q_b=q_0+q_1t_a+q_2t_a^2, \tag{45}$$

$$t_b=t_a+x(t_a)/\lambda(t_a), \tag{46}$$

according to (37) and (44), where

$$x(t_a)\doteq\alpha t_a+\beta t_a^2,$$
$$\lambda(t_a)=(\gamma-3)q_0/8+(3\gamma-1)Q_a(t_a)/8,$$

according to (32) and (43). The time t_a is the retarded value of the time t_b in the sense that t_b-t_a is the time required for a given value of Q to propagate itself from the shock front to the wall. If the shock and Q both traveled with the velocity of sound (unity), then one would have exactly $t_a=0.5t_b$. This relation is nearly satisfied in any case.

CALCULATION OF PRESSURE ON REFLECTOR

In order to calculate $p(0, t_b)$ from t_b it is sufficient to find $Q(0, t_b)$; because at the wall, where $u=0$,

$$c=(\gamma-1)Q/2, \tag{47}$$

and from c the pressure follows according to the equation

$$p+\pi=\pi c^{2\gamma/(\gamma-1)}. \tag{48}$$

It is convenient to combine (47) and (48)

$$p+\pi=\pi[(\gamma-1)Q/2]^{2\gamma/(\gamma-1)}. \tag{49}$$

Since $Q(0, t_b)$ is already known by (45) and (46), this equation completes the determination of $p(0, t_b)$ as a function of t_b.

The complete method for computing the pressure-time curve at the wall then runs as follows. The incident shock is specified by its pressure-ratio, ζ. The maximum material velocity, B, is first found from Eq. (19). The following constants, q_0, q_1, q_2, α, and β, which are functions of B and γ only, are then found from (38)–(40), (33), and (34). These constants then determine the auxiliary functions $x(t_a)$, $Q(t_a)$, and $\lambda(t_a)$ which are defined in Eqs. (32), (37), and (43). In terms of these functions the parametric equations of the pressure-time curve are (46) and (49). The duration of the pressure on the wall is determined by putting $Q=2/(\gamma-1)$ in (37) and then using (46).

The Hydrogen Atom in a Generalized Classical Electrodynamics

C. JAYARATNAM ELIEZER
University of Ceylon, Colombo, Ceylon and Christ's College, Cambridge, England

(Received May 20, 1946)

The author recently proposed a generalized classical electrodynamics in which the usual assumption that the field of a moving electron is given by its retarded field is abandoned, and a combination of retarded and advanced fields is considered. This paper considers the application of the generalized equations of motion to investigate the motion of the electron in the hydrogen atom. It is shown that, unlike the Lorentz-Dirac equations, these generalized equations permit the electron to spiral round and fall into the nucleus.

I. INTRODUCTION

IN some recent papers I have considered the application of Dirac's classical theory of radiating electrons[1] to various familiar problems; and the evidence gathered from these applications is that the equations of motion do not always have physically understandable solutions. There are, for instance, the self-accelerating motions that were considered by Dirac. Again, if an electron is moving along the x axis in an electric field of potential $\mu|x|$, that is, in the field due to a thin infinite charged plate in the yz plane, then the only motion allowed by the equations of motion is one in which the electron ultimately accelerates away from the plate with rapidly increasing speed, despite the attraction of the plate.[2] Further, when one investigates the motion of the electron in the hydrogen atom, it is seen that the electron does not spiral round and fall into the nucleus owing to loss of energy by radiation, as one would expect, but spirals outwards and escapes to infinity with increasing speed. The attraction of the nucleus has the effect of accelerating the electron away from the nucleus.[3] All these results point to the suggestion that the signs of certain terms in the Lorentz-Dirac equations do not fit in appropriately.

With a view to bring about the necessary alterations in sign, I have developed a generalized form of classical electrodynamics,[4] by abandoning the usual assumption that the field of a moving electron is given by its retarded field, and considering, instead, a combination of retarded and advanced fields. If F_{el} denotes the field due to an electron, and F_{ret} and F_{adv} the retarded and advanced fields, respectively, then we take

$$F_{el}=F_{ret}+k(F_{ret}-F_{adv}), \tag{1}$$

where k is a constant, the value of which is left arbitrary for the present. The equations of motion corresponding to the assumption (1) are then obtained in the usual way from the principles of conservation of energy, momentum, and angular momentum.

Suppose there are a number of electrons interacting with each other and with a given external field that is described by the field quantities $F_{ext}^{\mu\nu}$. If $z_{\mu n}(s_n)$, $(\mu=0, 1, 2, 3)$, denote the time and space coordinates of the nth electron of charge e_n and rest mass m_n, and dots denote differentiation with respect to the proper time s_n, and the metric tensor $g^{\mu\nu}$ is such that $g^{00}=1$, $g^{11}=g^{22}=g^{33}=-1$ while all the other components vanish, then the equations of motion of this electron are

$$\left.\begin{aligned} &m_n\frac{dv_{\mu n}}{ds}-\tfrac{2}{3}e_n^2(2k+1)\left[\frac{d^2v_{\mu n}}{ds^2}+\left(\frac{dv}{ds}\right)^2 v_{\mu n}\right] \\ &\quad=e_nv_{\sigma n}\Big[F^{\sigma}{}_{\mu,\,ext} \\ &\quad+\sum_{m\neq n}\{F^{\sigma}{}_{\mu m,\,ret}+k(F^{\sigma}{}_{\mu m,\,ret}-F^{\sigma}{}_{\mu m,\,adv})\}\Big], \\ &v_{\mu n}{}^2=1. \end{aligned}\right\} \tag{2}$$

As mentioned earlier the constant k is arbitrary. When $k=0$, Eqs. (2) reduce to the Lorentz-Dirac equations. When $k=-\frac{1}{2}$, then

$$F_{el}=\tfrac{1}{2}(F_{ret}+F_{adv}), \tag{3}$$

[1] P. A. M. Dirac, Proc. Roy. Soc. (A) **167**, 148 (1938).
[2] C. J. Eliezer, Bull. Calcutta Math. Soc. **37**, 125 (1945).
[3] C. J. Eliezer, Proc. Camb. Phil. Soc. **39**, 173 (1943).
[4] C. J. Eliezer, Nat. Acad. Sci., India (1946).

and the equations of motion (2) become

$$\left.\begin{aligned} m dv_{\mu n}/ds &= e v_{\sigma n}\Big[F^{\sigma}{}_{\mu,\,\mathrm{ext}} \\ &\quad + \tfrac{1}{2}\sum_{m\neq n}(F^{\sigma}{}_{\mu m,\,\mathrm{ret}} + F^{\sigma}{}_{\mu m,\,\mathrm{adv}})\Big], \\ v_{\mu n}{}^2 &= 1. \end{aligned}\right\} \quad (4)$$

Equations (4) do not contain the usual damping terms. If $k<-\frac{1}{2}$, then the sign of the radiation damping term is opposite to that of the corresponding terms in the Lorentz-Dirac equations, and in the particular case when $k=-1$, the equations are the same, except for this difference of sign.

II. APPLICATION TO THE HYDROGEN ATOM

If we take the nucleus of the atom to be fixed (by considering its mass to be infinite), then with reference to axes whose origin is at the position of the nucleus, the equations of motion of the electron are

$$\begin{aligned} m\frac{d^2\mathbf{r}}{ds^2} - \tfrac{2}{3}e^2(2k+1)\left\{\frac{d^3\mathbf{r}}{ds^3} + \left[\left(\frac{d^2t}{ds^2}\right)^2 - \left(\frac{d^2\mathbf{r}}{ds^2}\right)^2\right]\frac{d\mathbf{r}}{ds}\right\} \\ = -e^2\frac{dt}{ds}\frac{\mathbf{r}}{r^3}, \\ \left(\frac{dt}{ds}\right)^2 - \left(\frac{d\mathbf{r}}{ds}\right)^2 = 1, \end{aligned} \quad (5)$$

where the (t, x, y, z) notation is now used. When $k>-\frac{1}{2}$, the behavior of the solution of Eqs. (5) will be similar to that of the solution of the Lorentz-Dirac equations, which have already been considered and which do not allow the electron to fall into the nucleus. When $k=-\frac{1}{2}$, Eqs. (5) reduce to the usual equations of motion without the radiation damping terms, and the solutions of these equations are well known.

In this paper we shall consider the behavior of the solution of Eqs. (5) when $k<-\frac{1}{2}$. It will be seen that the equations then allow the electron to spiral round and approach the nucleus closer and closer and ultimately fall into it.

III. RECTILINEAR MOTION

We shall first consider the simpler case of rectilinear motion of an electron moving along the x axis, the proton being situated at the origin of coordinates. The equations of motion (5) then give

$$\begin{aligned} a\frac{d^2x}{ds^2} - (2k+1) \\ \times\left\{\frac{d^3x}{ds^3} - \frac{dx}{ds}\left(\frac{d^2x}{ds^2}\right)^2\left[1+\left(\frac{dx}{ds}\right)^2\right]^{-1}\right\} \\ = -3\left[1+\left(\frac{dx}{ds}\right)^2\right]^{\frac{1}{2}}\Big/2x^2, \end{aligned} \quad (6)$$

where $a=3m/2e^2$. It is unfortunately not possible to obtain an explicit solution of this equation. But our purpose here is to know roughly the nature of the motion, and this can be done without solving the equation. We write $dx/ds=u$ and transform the independent variable from s to x. Then $d^2x/ds^2=uu'$, $d^3x/ds^3=u(uu''+u'^2)$, where dashes denote differentiation with respect to x, and Eq. (6) becomes

$$(2k+1)\left\{u''+\frac{u'^2}{u(1+u^2)}\right\} - \frac{au'}{u} = \frac{3}{2}\frac{(1+u^2)^{\frac{1}{2}}}{u^2x^2}. \quad (7)$$

To discuss the behavior of the solution of Eq. (7) it is convenient to transform from u to y, where

$$y=(1+u^2)^{\frac{1}{2}}, \quad (8)$$

and y is taken to have positive values only. The cases u positive and u negative lead to different differential equations. For $u>0$, we have

$$(y^2-1)^{\frac{1}{2}}y''+\lambda y'+\mu x^{-2}=0, \quad (9)$$

where $\lambda=-a/(2k+1)>0$, $\mu=-3/2(2k+1)>0$; and for $u<0$, we have

$$(y^2-1)^{\frac{1}{2}}y''-\lambda y'-\mu x^{-2}=0, \quad (10)$$

where λ and μ are as before.

Suppose initially the electron is projected towards the proton from the point $x=x_0$. Its motion immediately afterwards is given by Eq. (10). The electron may be brought to rest at some point $x=\beta$ before it reaches the proton, or it may collide with the proton. In the former case the solution will be defined only in $\beta\leqslant x\leqslant x_0$, and in the latter case in $0\leqslant x\leqslant x_0$. Equation (10) is such that if $y'=0$ at any point where the solution is defined, then $y''>0$; and therefore y has no maxima and therefore at most one minimum. Also, if $y''=0$, then $(y^2-1)^{\frac{1}{2}}y'''$

$+2\mu x^{-3}=0$, and hence $y'''<0$. Therefore $y''=0$ at most once in $0\leqslant x<x_0$. We may therefore choose an interval $0\leqslant x\leqslant\gamma$ so that y' and y'' are of fixed signs in the portion of the interval in which the solution is defined.

Suppose $y'<0$. Then y increases as x decreases. Hence, as $x\to 0$, y tends to a finite limit $l(>1)$ or to infinity. It is easy to see that y cannot tend to a finite value l, because if it does, the equation obtained by integrating Eq. (10) with respect to x gives

$$y'-\lambda\cosh^{-1}y=\mu\int\frac{dx}{x^2(y^2-1)^{\frac{1}{2}}}+\text{constant} \tag{11}$$
$$=-\frac{\mu}{x}(1+\xi)(l^2-1)^{-\frac{1}{2}}+\text{constant},$$

where $\xi\to 0$ as $x\to 0$. Integrating again with respect to x we see that the left-hand side remains finite as $x\to 0$, but the right-hand side becomes infinite, being approximately of the order $\mu(l^2-1)^{-\frac{1}{2}}\log(1/x)$, for small x. We thus obtain a contradiction. Hence, if $y'<0$, the solution is such that $y\to\infty$ as $x\to 0$.

We have already seen that if initially y' is negative, then as x decreases, y' will continue to be negative, since y has no maximum. The condition that y' is negative is equivalent to the condition that the acceleration is towards the proton, since $d^2x/ds^2=uu'=yy'$. We thus have the result that if the electron is projected with initial velocity and acceleration which are both towards the proton, then the electron continues to approach the proton with steadily increasing velocity and ultimately collides with the proton, with velocity tending to that of light.

It is of interest to obtain an approximate solution valid for small values of x. To do this, we transform from x to τ where $x=e^{-\tau}$. We then have

$$(y^2-1)^{\frac{1}{2}}\frac{d^2y}{d\tau^2}+\{(y^2-1)^{\frac{1}{2}}+\lambda e^{-\tau}\}\frac{dy}{d\tau}-\mu=0. \tag{12}$$

To obtain a solution which is valid for large values of τ, we note that $y\to\infty$ and $dy/d\tau>0$ as $\tau\to\infty$. It is seen that $dy/d\tau$ cannot tend to infinity, because if it did, then from Eq. (12), $d^2y/d\tau^2$ must tend to minus infinity; hence $dy/d\tau$ must be decreasing with increasing τ, which gives a contradiction. Hence $dy/d\tau\to k\geqslant 0$ as $\tau\to\infty$, and therefore $d^2y/d\tau^2\to -k$.

But according to a theorem on limits, if a function $f(x)$ tends to a finite limit as x tends to infinity, and $f'(x)$ is known to tend to a limit, then this limit must be zero. Hence $k=0$. Thus $dy/d\tau\to 0$ and $d^2y/d\tau^2\to 0$ as $\tau\to\infty$.

For large values of τ, Eq. (12) is approximately

$$\frac{d^2y}{d\tau^2}+\frac{dy}{d\tau}-\frac{\mu}{y}=0. \tag{13}$$

Writing $dy/d\tau=p$ and changing the independent variable to p and the dependent variable to y we have

$$p\frac{dp}{dy}+p-\frac{\mu}{y}=0,$$

which is easily seen to have approximate solution $p=\mu/y$, and hence $y^2=2\mu\tau+\text{constant}$. Hence

$$\frac{dx}{ds}\sim-\left(2\mu\log\frac{1}{x}\right)^{\frac{1}{2}},\ \text{for small } x, \tag{14}$$

where $\mu=-3/2(2k+1)$.

If initially $y'>0$, that is, if the initial acceleration is directed away from the proton, then in the subsequent motion, y' may change sign soon afterwards or may continue to remain positive until the electron is brought to rest at $x=\beta$. If y' changes sign and thus becomes negative, the subsequent motion will then be as discussed above, namely a motion in which the electron continues to approach the proton with steadily increasing velocity and ultimately collides with it. If, however, y' remains positive until y reaches the value 1, then the electron is brought to rest at $x=\beta$ before it reaches the proton. The approximate solution near $x=\beta$ is of the form

$$y=1+l(x-\beta)+\frac{2\sqrt{2}}{3l^{\frac{1}{2}}}\left(\lambda l+\frac{\mu}{\beta^2}\right)(x-\beta)^2, \tag{15}$$

where $y\to 1$ and $y'\to l(>0)$ as $x\to\beta$. If, however, $y'\to 0$ as $x\to\beta$ then the approximate solution near $x=\beta$ is given by

$$(y-1)^{\frac{1}{2}}=\frac{9}{4}\frac{\mu}{\beta^2}(x-\beta)^2. \tag{16}$$

The electron being thus brought to rest before it reaches the proton, it would then turn back and move away from the proton. The subsequent motion is then described by Eq. (9). We do not discuss here the motion in detail, but merely give a summary of the results. It is easy to show that there is no solution with $y\to\infty$, $x\to\infty$. The only possible types of solution are those in which either the electron is brought to rest while moving away from the proton, or in which the electron escapes to infinity while the velocity ultimately decreases and tends to a finite value. In the first case, the approximate solution near the point where the electron is brought to rest is similar in form to (15). The subsequent motion is such that the electron steadily approaches the proton with increasing velocity. In the second case, the solution for large x is given approximately by

$$y=C+\frac{\mu}{\lambda}\frac{1}{x}(1+\theta), \tag{17}$$

where $C\geqslant 1$ and $\theta\to 0$ as $x\to\infty$.

Under given initial conditions the final motion consists of either:—(i) the electron moves towards the proton with increasing velocity and collides with it, the approximate solution being (14); or (ii) the electron recedes away from the proton with steadily diminishing velocity, the approximate solution being of the form (17). An interesting feature in this result is that in both motions the final acceleration is directed towards the proton, which is in accord with the ideas of Newtonian mechanics where the acceleration is always in the direction of the force, which, in the problem under investigation, is towards the proton.

IV. TWO-DIMENSIONAL MOTION

Now we shall consider the more general motion of an electron which is spiralling round a fixed proton. The general motion will be three-dimensional, since the initial position, velocity and acceleration can all be arbitrary. Under certain initial conditions, however, the motion will be two-dimensional, and it is these motions that we shall consider here, as these are the only ones which are likely to be physically permissible. We shall chiefly be concerned here with the existence of solutions in which the electron spirals round and falls into the nucleus. Such motions were found to be not allowable by the Lorentz-Dirac equations[3] and it is of interest to determine whether the modified Eqs. (2) lead to different results. Taking axes in the plane of motion and the origin at the position of the proton, the equations of motion are

$$\left.\begin{aligned} a\frac{d^2x}{ds^2}-(2k+1)\left\{\frac{d^3x}{ds^3}+\frac{dx}{ds}\left(\frac{d^2t^2}{ds^2}-\frac{d^2x^2}{ds^2}-\frac{d^2y^2}{ds^2}\right)\right\}&=-\frac{3}{2}\frac{dt}{ds}xr^{-3},\\ a\frac{d^2y}{ds^2}-(2k+1)\left\{\frac{d^3y}{ds^3}+\frac{dy}{ds}\left(\frac{d^2t}{ds^2}-\frac{d^2x^2}{ds^2}-\frac{d^2y^2}{ds^2}\right)\right\}&=-\frac{3}{2}\frac{dt}{ds}yr^{-3}\end{aligned}\right\} \tag{18}$$

where

$$\frac{dt^2}{ds}=1+\frac{dx^2}{ds}+\frac{dy^2}{ds}.$$

We transform to V and ψ, where

$$V=\left(\frac{dx^2}{ds}+\frac{dy^2}{ds}\right)^{\frac{1}{2}}$$

is the velocity, and $\pi-\psi$ is the angle between the radius vector and the velocity, so that

$$\frac{dx}{ds}=V\cos(\pi+\theta-\psi),\quad \frac{dy}{dt}=V\sin(\pi+\theta-\psi).$$

We change the independent variable from s to τ where $r=e^{-\tau}$ and let dashes now denote differentiation

with respect to τ. The equations of motion then give

$$(2k+1)\left\{V''+V'+\frac{V'^2}{V(1+V^2)}-V'\psi'\tan\psi-V(1+V^2)(\psi'-\tan\psi)^2\right\}-\frac{ae^{-\tau}V'}{V\cos\psi}=-\frac{3}{2}\frac{(1+V^2)^{\frac{1}{2}}}{V^2\cos\psi}, \tag{19}$$

$$(2k+1)\left\{\frac{d}{d\tau}(\psi'\cos\psi-\sin\psi)+\left(1+\frac{3V'}{V}\right)(\psi'\cos\psi-\sin\psi)\right\}$$

$$-\frac{ae^{-\tau}}{V\cos\psi}(\psi'\cos\psi-\sin\psi)=\frac{3}{2}\frac{(1+V^2)^{\frac{1}{2}}}{V^3}\tan\psi. \tag{20}$$

We seek those solutions according to which the electron spirals round and ultimately falls into the nucleus. Assuming that this happens, let us consider the behavior of the solution as $r\to 0$, that is, as $\tau\to\infty$.

We follow the method used in an earlier paper and easily see that except possibly for the case when $V\to\infty$ and $\psi\to 0$ as $\tau\to\infty$, there is no solution in which the electron falls into the nucleus. We shall therefore concentrate our attention on the possible solution in which $V\to\infty$ and $\psi\to 0$. For large τ, Eq. (20) is approximately

$$\psi''-\psi'+(1+3V'/V)(\psi'-\psi)=0,$$

which has solution

$$\psi'-\psi=Ce^{-\tau}/V^3, \tag{21}$$

where C is an arbitrary constant of integration. Substituting in (19) and approximating we obtain

$$(2k+1)\{V''+V'+V'^2/V^3\}=-3/2V. \tag{22}$$

This equation can be shown to be equivalent to Eq. (10) which has already been considered above. Hence we have as an approximate solution of (22) $V=(2\mu\tau)^{\frac{1}{2}}$. Substituting in (21), we obtain

$$\psi'-\psi=Ce^{-\tau}/(2\mu\tau)^{\frac{1}{2}}.$$

Hence

$$\psi e^{-\tau}=C\int_{\infty}^{\tau}\frac{e^{-2\tau}}{(\mu\tau)^{\frac{1}{2}}}d\tau \tag{23}$$

$$=\frac{Ce^{-2\tau}}{\mu^{3/2}}\left[-\frac{1}{2\tau^{3/2}}+\frac{3}{2^2}\cdot\frac{1}{\tau^{5/2}}-\frac{3\cdot 5}{2^3}\cdot\frac{1}{\tau^{7/2}}+\cdots\right]. \tag{24}$$

Hence for a first approximation we take

$$\psi=Ae^{-\tau}\tau^{-\frac{1}{2}}, \tag{25}$$

where A is a positive constant of integration. Therefore

$$rd\theta/dr=-\tan\psi=-Ae^{-\tau}\tau^{-\frac{1}{2}}, \text{ for large } \tau;$$

and hence

$$d\theta/d\tau=Ae^{-\tau}\tau^{-\frac{1}{2}}.$$

Therefore

$$\theta=A\int e^{-\tau}\tau^{-\frac{1}{2}}d\tau=Ae^{-\tau}\left\{-\frac{1}{\tau^{3/2}}+\frac{3}{2}\cdot\frac{1}{\tau^{5/2}}-\frac{3\cdot 5}{2^2}\cdot\frac{1}{\tau^{7/2}}+\cdots\right\}.$$

Hence the equation of the curve is given approximately, for small r, by

$$\theta=Ar\,(\log 1/r)^{-\frac{1}{2}}. \tag{26}$$

Thus, the equations of motion (2) allow the electron to spiral round and fall into the nucleus, whereas the Lorentz-Dirac equations do not permit such a collision.

Notes on Rotation and Rigid Bodies in Relativity Theory

NATHAN ROSEN
University of North Carolina, Chapel Hill, North Carolina
(Received October 15, 1946)

Covariant conditions for rigid-body motion are set up. They are equivalent to those proposed by Born and lead to the linear speed-distance law for the case of rotation about an axis. This result and also a discussion of the transformation equations in going over to a rotating frame of reference are used as arguments for the desirability of retaining the concept of rigid rotation with the linear speed-distance law, contrary to the opinion expressed by Hill. The rotation question is also considered from the standpoint of angular velocity, and one is lead rather naturally to two fluid velocity distributions, one of which was found by Hill. The expression for the spatial distance between two points on a rotating disk obtained by Berenda is derived without the use of the assumption introduced by the latter.

THE question of whether the geometry on a rotating disk is Euclidean or not has interested many writers. Berenda[1] has subjected the problem to a careful analysis. However, there are still a number of questions connected with the problem of rotation in relativity theory that require further investigation, and some of them will be considered in the present work.

1. MOTION OF A RIGID BODY

In discussing the rotating disk, one frequently begins with an inertial frame of reference described by a cylindrical polar coordinate system with coordinates r_0, θ_0, z_0, t_0, and one then goes over to a rotating frame of reference attached to the rotating body, with coordinates r, θ, z, t, given by

$$r_0=r, \quad \theta_0=\theta+\omega t, \quad z_0=z, \quad t_0=t, \qquad (1)$$

where ω, the angular velocity about the z axis, is constant. Starting with the usual expression for the line element in the non-rotating coordinate system, one gets in the rotating system:

$$ds^2=-(dr^2+r^2d\theta^2+dz^2+2\omega r^2 d\theta dt) +(1-\omega^2r^2)dt^2, \qquad (2)$$

with units in which the velocity of light in empty space is unity.

Hill[2] pointed out (as von Laue[3] had done earlier) that a body rotating in this way would have a limit to the radius it could have, for the velocity would vary linearly with the radius and would exceed that of light for $r>1/\omega$. For this reason, Hill was led to conclude that the speed-distance law must be non-linear.

While one can conceive of a fluid rotating with an arbitrary speed-distance law, the case of greatest interest is that of the speed-distance law for a rigid body. To investigate this, one must first have some criterion for rigid-body motion. Such a criterion was first given in relativity theory by Born.[4]

In classical physics one can characterize the motion of a rigid body by the fact that the rate of strain vanishes. In a Cartesian coordinate system, the velocity components satisfy the relation

$$\partial v_i/\partial x_k+\partial v_k/\partial x_i=0 \quad (i, k=1, 2, 3). \qquad (3)$$

In a relativistic treatment one looks for a covariant equation which reduces to (3) in a Galilean system if the velocity is small (compared to that of light). The obvious generalization is to introduce, in an arbitrary coordinate system, the symmetrical tensor

$$P_{\mu\nu}=\tfrac{1}{2}(u_{\mu;\nu}+u_{\nu;\mu}), \qquad (4)$$

where the velocity 4-vector u^λ is given by

$$u^\lambda=dx^\lambda/ds \qquad (5)$$

and a semi-colon denotes covariant differentiation, and to take as the condition for rigid-body

[1] C. W. Berenda, Phys. Rev. 62, 280 (1942). Other references will be found in this paper.
[2] E. L. Hill, Phys. Rev. 69, 488 (1946).
[3] M. von Laue, *Relativitätstheorie* (Vieweg, Braunschweig, 1921), Vol. 2, p. 24.
[4] M. Born, Ann. d. Physik 30, 1 (1909). See also W. Pauli, Jr., *Encyklopädie der math. Wissenschaften*, Vol. 5, Part 2, pp. 689–691.

motion

$$P_{\mu\nu}=0. \tag{6}$$

However, this condition represents too severe a restriction. In view of the fact that the vector u^λ satisfies the identity

$$u^\lambda u_\lambda=1, \tag{7}$$

it follows from (6) on multiplication by u^ν that

$$u_{\mu;\nu}u^\nu=0. \tag{8}$$

This expression is just the covariant form of the acceleration vector

$$\delta u^\lambda/ds=du^\lambda/ds+\{_\alpha{}^\lambda{}_\beta\}u^\alpha u^\beta, \tag{9}$$

so that every particle of the body moves along a geodesic, or in gravitation-free space, along a straight line.

It is therefore necessary to weaken the condition imposed on the motion. For this purpose we replace $p_{\mu\nu}$ by

$$p_{\mu\nu}=\tfrac{1}{2}(u_{\mu;\nu}+u_{\nu;\mu}-u_{\mu;\alpha}u^\alpha u_\nu-u_{\nu;\alpha}u^\alpha u_\mu), \tag{10}$$

since we then have the identity

$$p_{\mu\nu}u^\nu\equiv 0. \tag{11}$$

Let us now take as the condition for rigid-body motion

$$p_{\mu\nu}=0. \tag{12}$$

In a Galilean coordinate system, at a point where the velocity 3-vector vanishes, this reduces to the classical condition (3). Therefore it is equivalent to the condition proposed by Born.[4]

Since Eq. (12) is a tensor equation it can be applied in any frame of reference. If we take an inertial system with Cartesian coordinates then we can describe rotation about an axis by setting

$$u_1=-u^1=\sigma y,\quad u_2=-u^2=-\sigma x,$$
$$u_3=-u^3=0,\quad u_4=u^4=(1+\sigma^2r^2)^{\frac{1}{2}}, \tag{13}$$

with

$$\sigma=\sigma(r),\quad r^2=x^2+y^2. \tag{14}$$

From Eq. (12) one gets the single equation

$$d\sigma/dr=\sigma^2 r \tag{15}$$

which has for its solution

$$\sigma=\omega/(1-\omega^2r^2)^{\frac{1}{2}}, \tag{16}$$

where ω is a constant. Going over to the three-dimensional velocity v by the relations

$$u=(u_1^2+u_2^2)^{\frac{1}{2}}=\sigma r=v/(1-v^2)^{\frac{1}{2}}, \tag{17}$$

we get

$$v=\omega r. \tag{18}$$

This result was obtained by Herglotz[5] by means of a different procedure.

That it is possible to have a covariant law of rigid-body motion (even if it has only a small number of solutions) appears to be of importance in connection with the inner consistency of the theory of relativity. Since the fundamental concepts of the theory include those of the rigid frame of reference and the rigid measuring rod, it would be unsatisfactory if no rigid bodies or rigid-body motions existed in the theory.

In 1911, von Laue[6] presented an argument of a general nature against the existence of a rigid body in relativity theory. It is based on the fact that a rigid body is expected to have a finite number of degrees of freedom, while, on the other hand, one can set up N disturbances near N separated points of the body, and they will be non-interacting, i.e., independent, for a sufficiently short interval of time (because of the finite propagation time required by relativity theory) so that there are at least N degrees of freedom, where N can be increased indefinitely for a continuous medium. However, this argument assumes the possibility of setting up arbitrary deformations in the body initially. Since however the initial deformations can only be obtained by displacements with velocity components governed by Eq. (12) it follows that it is not possible to have arbitrary initial disturbances, but only those which can be arrived at by means of motions described by Eq. (12), i.e., displacements which can be obtained by integrating this equation, starting from an undeformed state.

It might be remarked here that the difficulty pointed out by Hill does not appear to provide a sufficiently strong argument for giving up the linear speed-distance law. It is true that no rigid body would have a radius equal to, or exceeding, $1/\omega$, but there seems to be no reason why an

[5] G. Herglotz, Ann. d. Physik **31**, 393 (1910).
[6] M. von Laue, *Relativitätstheorie* (1921), fourth edition, Vol. 1, pp. 203–204.

idealized rigid body with a smaller radius could not rotate according to the linear law. That it is desirable to retain the concept of the rigid rotation can be seen from the following considerations:

Let us go back to Eqs. (1) and (2), and let us look for the most general transformation that can be introduced in place of Eq. (1) which (a) will be linear in t and θ, (b) will have axial and cylindrical symmetry, (c) will be single-valued, and (d) will give a static line element. The conditions (a), (b), and (c) lead to the transformation equations

$$r_0=e(r)+f(r)t, \quad \theta_0=\theta+g(r)t+h(r), \quad z_0=z, \quad t_0=p(r)t+q(r). \tag{19}$$

Applying the condition (d), one finds that

$$f=g'=p'=0, \tag{20}$$

where a prime denotes a derivative with respect to r. What is of interest to us here is that unless $g'=0$ ($\theta-\theta_0$ a linear function of t with a constant coefficient), it will not be possible to have a static metric. This condition is, of course, just the linear relation between speed and distance from the axis.

2. ANGULAR VELOCITY IN RELATIVITY THEORY

Although it appears that the motion of a rigid body is best discussed by means of the criterion of the previous section, it is nevertheless interesting to examine the rotation problem by a consideration of the angular velocity distribution. This is the general method that was used by Hill.[2]

In classical physics the angular velocity is defined as the vector

$$\omega=\tfrac{1}{2}\nabla\times\mathbf{v}. \tag{21}$$

The obvious relativistic generalization consists in introducing an antisymmetric tensor

$$\Omega_{\mu\nu}=\tfrac{1}{2}(\partial u_\mu/\partial x^\nu-\partial u_\nu/\partial x^\mu) \tag{22}$$

in an arbitrary four-dimensional coordinate system.

In an inertial system with Cartesian coordinates, if we have rotation with the components u^λ given by Eqs. (13) and (14), the following components of $\Omega_{\mu\nu}$ are obtained:

$$\Omega_{12}=\sigma+\tfrac{1}{2}\sigma' r, \tag{23}$$

$$\Omega_{14}=-Fx, \quad \Omega_{24}=-Fy, \tag{24}$$

with

$$F=\tfrac{1}{2}(\sigma^2+\sigma\sigma' r)/(1+\sigma^2r^2)^{\frac{1}{2}}. \tag{25}$$

If we now set

$$\Omega_{12}=\omega=\text{constant}, \tag{26}$$

then from (23) we find for the singularity-free solution[7]

$$\sigma=\omega. \tag{27}$$

This gives

$$u=\omega r, \quad v=\omega r/(1+\omega^2r^2)^{\frac{1}{2}}. \tag{28}$$

The components ω_{14} and ω_{24} are given by Eq. (24), with

$$F=\tfrac{1}{2}\omega^2/(1+\omega^2r^2)^{\frac{1}{2}}, \tag{29}$$

so that, for small speeds, they are proportional to the centripetal acceleration components.

Now, it is not satisfactory for the fluid motion to be determined by Eq. (26) since the latter is a condition on only one component and is not covariant. One can improve matters by introducing

$$S^\lambda=\Omega^{\lambda\tau}u_\tau=u^\lambda{}_{;\tau}u^\tau=\delta u^\lambda/ds, \tag{30}$$

the acceleration vector. In the present case one finds

$$S^1=-\tfrac{1}{2}\sigma^2x, \quad S^2=-\tfrac{1}{2}\sigma^2y, \quad S^3=S^4=0, \tag{31}$$

so that the condition

$$S^\alpha{}_{;\alpha}=0 \tag{32}$$

would give the same solution as above. Another possibility, not as simple, is to take as the condition for the motion,

$$\Box S^\lambda=0. \tag{33}$$

If, instead of the above coordinate system, we follow Hill[2] in introducing a Galilean system (coordinates x', y', z', t') with a given point as origin and moving so that the fluid there is momentarily at rest with respect to it ($u_1'=u_2'=u_3'=0$, $u_4'=1$), we get for the angular velocity components

$$\Omega_{12}'=(\sigma+\tfrac{1}{2}\sigma' r+\tfrac{1}{2}\sigma^3r^2)/(1+\sigma^2r^2)^{\frac{1}{2}}, \tag{34}$$

$$\Omega_{14}'=\tfrac{1}{2}\sigma^2r, \tag{35}$$

[7] Nathan Rosen, Phys. Rev. 70, 93 (1946).

provided we take the X' axis in the radial direction and the Z' axis parallel to the Z axis. If one sets

$$\Omega_{12}' = \omega \tag{36}$$

and introduces a new variable

$$\xi = v/r, \tag{37}$$

so that

$$\sigma = \xi/(1-\xi^2 r^2)^{\frac{1}{2}}, \tag{38}$$

one gets

$$\xi' r + 2\xi = 2\omega(1-\xi^2 r^2), \tag{39}$$

which is essentially the equation obtained by Hill.

It is possible to put the condition expressed by Eq. (36) into covariant form. For this purpose let us introduce what might be called the "spatial angular velocity tensor"

$$\omega_{\mu\nu} = \Omega_{\mu\nu} - \Omega_{\mu\alpha}u^\alpha u_\nu + \Omega_{\nu\alpha}u^\alpha u_\mu, \tag{40}$$

which satisfies the identity

$$\omega_{\mu\nu}u^\nu \equiv 0. \tag{41}$$

It might be noted that the vanishing of $\Omega_{\mu\nu}$ leads to the absence of all acceleration; that is not the case with $\omega_{\mu\nu}$. Corresponding to Eqs. (34) and (35) one finds as the only non-vanishing components

$$\omega_{12}' = -\omega_{21}' = \Omega_{12}'. \tag{42}$$

Hence, an invariant condition corresponding to Eq. (36) can be written[8]

$$\omega_{\mu\nu}\omega^{\mu\nu} = 2\omega^2. \tag{43}$$

We see that, depending on whether one works in the fixed coordinate system or the system instantaneously moving with the fluid, one arrives naturally at one or the other of two velocity distributions, differing from that for the rigid body as discussed in the previous section. Other distributions are also possible, of course. However, at this time there does not appear to be any strong reason for giving up the linear speed-distance law in favor of any other distribution.

[8] In reference 7 the author questioned Hill's procedure because it made use of a uniformly moving coordinate system in describing the accelerated motion of the fluid, so that the acceleration components of the fluid were not taken into account. However, we see now that this is not an objection if the description is given in terms of $\omega_{\mu\nu}$, since the acceleration components in this case are not involved.

3. SPATIAL DISTANCE IN A ROTATING SYSTEM

Returning now to the rigid-body rotation as discussed in Section 1, let us consider a question treated by Berenda in his investigation of the nature of the geometry on the rotating disk. The question was this: given a frame of reference with the line element of Eq. (2), what is the correct expression for the distance dl between two neighboring points at rest in this reference frame? Berenda[1] obtained this distance as the length of a four-vector which had for its space components the three spatial coordinate differentials, but also had for its fourth component a value chosen to make this vector orthogonal to the world-lines of the two points. The identification of "rigid metric rod readings on the disk with spatial dimensions and geometry derived from such orthogonality" Berenda considered a matter of assumption. However since the expression for dl^2 derived from this assumption determines the spatial geometry of the disk, it seems desirable to derive it by another procedure free from such an assumption.

It is well known that in the general relativity theory the coordinates used in locating events in space-time need have no simple relations to the readings of measuring rods and clocks. What requires stressing here is the fact that even the value of the interval or line element need have no simple relation to the readings of scales and clocks in a given frame of reference. This is associated with the fact that the readings of scales and clocks will be influenced by gravitational and inertial forces. Only in a Galilean frame of reference can intervals be obtained simply from clock and scale readings, according to the ideas of special relativity. Hence, considering the two points of the body in the neighborhood of some particular values of r, θ, z, t, let us introduce a local Galilean coordinate system momentarily at rest relative to the rotating system by the relations

$$dx' = dr, \quad dy' = A\,d\theta, \quad dz' = dz, \quad dt' = B\,dt + C\,d\theta, \tag{44}$$

where A, B, and C are to be determined so as to make

$$ds^2 = -dx'^2 - dy'^2 - dz'^2 + dt'^2. \tag{45}$$

One readily finds that

$$A=r/(1-\omega^2r^2)^{\frac{1}{2}},\quad B=(1-\omega^2r^2)^{\frac{1}{2}},\quad C=-\omega r^2/(1-\omega^2r^2)^{\frac{1}{2}}. \tag{46}$$

This is essentially the same system as the one used by Hill.[2] From the form of Eq. (45) it follows that

$$dl^2=dx'^2+dy'^2+dz'^2, \tag{47}$$

or, on the basis of the transformation equations,

$$dl^2=dr^2+r^2(1-\omega^2r^2)^{-1}d\theta^2+dz^2, \tag{48}$$

which is the result obtained by Berenda and shows that the spatial geometry on the surface of a rotating disk (z=constant) is non-Euclidean.

It is also interesting to note that the time interval between two events dt' is given by

$$dt'=(1-\omega^2r^2)^{\frac{1}{2}}dt-\omega r^2(1-\omega^2r^2)^{-\frac{1}{2}}d\theta. \tag{49}$$

PHYSICAL REVIEW VOLUME 71, NUMBER 1 JANUARY 1, 1947

Note on Magnetic Energy

G. H. LIVENS
Department of Mathematics, University College of South Wales and Monmouthshire, Cathays Park, Cardiff, Wales
(Received April 8, 1946)

1.

IN a recent paper[1] under this same title E. A. Guggenheim discusses certain results from a paper[2] published by me recently and claims that they are special cases of more general ones obtained by him on a previous occasion.[3] As the results quoted from my paper are themselves special cases of quite general ones contained therein, and his note generally misrepresents the scope and purpose of my work, perhaps I may be permitted a reiteration of the main outlines of my arguments and the opportunity to discuss the relation they bear to the methods employed by him.

The following symbols are used:

B magnetic induction,
H magnetic force intensity,
I_i induced magnetization intensity,
I_p permanent magnetization intensity,
i_s linear electric current,
N_s magnetic flux through i_s,
μ permeability,
$\mathfrak{L}$ Lagrangian function,
$\mathfrak{H}$ Hamiltonian function.

Guggenheim bases his discussion not on Maxwell's theory in its original form but on the modification given to it by Cohn.[4] The essence of this form of the theory, like that proposed by Hertz which it follows closely, is that it incorporates the induced polarizations and the aether, whatever this may be, into a single transmitting medium whose elastic quality is summed up in the characteristic constant, the permeability μ. This hypothesis of a single medium, excluding as it does the possibility of a displacement of the polarized medium from one position of the field to another, proves however to be a fatal handicap in a theory which has eventually to be extended to cover electromagnetic phenomena in moving media. And it was precisely for this reason that Larmor and Lorentz were forced back to the views held by Kelvin and Maxwell that the only really satisfactory treatment of these affairs interprets them in terms of a separate universal transmitting medium with its own stress on which is superposed the polarized media with their reacting mechanical forces. This implies that it is absolutely essential to distinguish between the parts of the field vectors and energy which belong to the aether and remain with it and the parts which belong to the matter

[1] E. A. Guggenheim, Phys. Rev. **68**, 273 (1945).
[2] G. H. Livens, Phil. Mag. **36**, 1 (1945). Cf. also Proc. Roy. Soc. **A93**, 200 (1916), and Phil. Trans. Roy. Soc. **A220**, 207 (1919).
[3] E. A. Guggenheim, Proc. Roy. Soc. **A155**, 49 (1936).
[4] E. Cohn, *Das elektromagnetische Feld* (1900). My knowledge of this book is derived from this earlier edition.

and are carried along with it in its motion through the field.[5]

However, so far as the present discussion of the quasi-static energy relations of the field are concerned there is no essential difference between the different forms of the theory, except in the matter of interpretation. The differences, however, begin to appear when these energy formulae are applied to determine the forces on the magnetic media by applying the principle of virtual work, and it has long been known that the theory in the Helmholtz-Hertz-Cohn form leads, when properly interpreted, to quite untenable results.[6]

2.

My own discussions in this subject are based on the generalizations of Maxwell's theory formulated by Larmor and Lorentz, and so far as the mechanical relations of the magnetic field are concerned they start from an assumption which is really the basis of all electrodynamic theories from Maxwell onwards. This, in its most general form, asserts that the magnetic part $\mathfrak{L}_m$ of the Lagrangian function of a system consisting of a series of linear currents i_s enclosing fluxes N_s and a distribution of permanent polarity I_p in the presence of magnetizable media distributed over the field in any manner is such that

$$\begin{aligned}\delta\mathfrak{L}_m &= \textstyle\sum_s N_s\delta i_s + \int (F\delta I_p)dv \\ &= \frac{1}{4\pi}\int (B\delta H)dv + \int (F\delta I_p)dv \cdots .\end{aligned} \tag{1}$$

This formula is interpreted for the moment in terms of a theory which regards F as the intensity of the magnetic force acting on the polar elements. The usual assumption is that $F \equiv H$, but there are grounds for thinking that $F \equiv B$ is a better choice. The integrands of all space integrals are understood to relate simply to the local conditions at a point, and their variation produced in any process of building up the system from infinite dispersion of its elements.

Formula (1) is of the utmost possible generality, especially in this virtual differential form, and it defines the complete electrodynamic relations of the quasi-stationary system, and this includes not only the relations of the currents and permanent magnets, but also those of the induced magnets as well. There is no implied necessity for any relations between the vectors involved in it, anything in the nature of a law of induction, that would make it the complete differential of a unique function $\mathfrak{L}_m$, although naturally the greatest mathematical interest attaches to the cases when such relations exist.

Guggenheim starts not from the Lagrangian function, but from the associated Hamiltonian or available (conserved) energy function which he writes in the integrated form

$$\mathfrak{H}_m = \sum \int_0^{N_s} i_s dN_s,$$

and then, assuming with Maxwell, that the velocities in the electrical coordinates are i_s he derives the corresponding Lagrangian function $\mathfrak{L}_m$ in the form

$$\mathfrak{L}_m = \sum \int_{N_s=0}^{i_s} N_s di_s.$$

In both of these formulae the summations are taken not only over the ordinary currents of the system, but also over a whole series of other currents introduced to mask the effects of the permanent magnetism in the early stages of the build-up process represented in the integrals.

3.

The choice by Guggenheim of the Hamiltonian function as the more fundamental is based on the possibility of deducing it directly from Maxwell's equations. The argument used by him for this purpose depends however essentially on the concept of "zero states," and to define these he uses the following postulate, I quote his own words:[7]

"If, however, each permanent magnet is surrounded by suitable circuits it is theoretically possible for currents to flow in these circuits such

[5] This conclusion should be compared with Guggenheim's statement (in Proc. Roy. Soc. **A155**, 99 (1936)) that "as the ether and the matter occupy the same space, there is no means of distinguishing between the energy of the ether and the energy of the matter. We can therefore attach no physical meaning to this division of the energy into two parts."

[6] G. H. Livens, Phil. Mag. **32**, 162 (1916).

[7] E. A. Guggenheim, reference 3, page 55.

that magnetic induction due to them is everywhere equal and opposite to the magnetic induction due to the permanent magnetization."

This, of course, is true only when the permanent magnetism is distributed uniformly throughout the volume of each such magnet. If we try to solve Maxwell's equations for a steady magnetic system with currents *on the surfaces* of the permanent magnets and with $B=H+4\pi I=0$ everywhere, we soon realize that, in the general case, it is necessary to supplement the surface currents by a distribution of volume currents throughout each magnet with a density at each place proportional to curl I, and these volume currents vanish only when I is constant throughout each magnet. In the general case the two sets of currents, surface and volume, constitute a distribution which is then the exact opposite of that which is the effective equivalent of the electron current whirls ultimately constituting the magnetism. The two systems would thus cancel out completely in every detail except as regards their magnetic forces, the definition of which for a current distribution being somewhat different to that for the equivalent polarization.[8] Properly interpreted therefore Guggenheim's "zero states" are identical with the usual concept of the zero fields of the infinitely dispersed system in the more conventional building up procedure, except that there is in the interior of the magnets a residual magnetic force H_0' resulting from the different interpretations of this vector for the two cancelling systems.

The difficulty is, of course, the introduction of permanent magnetism and its associated energy into the simple form of the energy equation derived from Maxwell's theory. But if we are careful to interpret the energy equation properly this difficulty is soon overcome. The equation itself determines a formula for W_m, the part of the field energy associated with the magnetism, which is such that

$$\delta W_m=\frac{1}{4\pi}\int(H\delta B)dv.$$

But this formula represents the magnetic part of the corresponding Hamiltonian or conserved (available) energy only in so far as the magnetic connections of the system controlling the build-up of the polarizations and currents involve no dissipation other than that which occurs in the linear current circuits, and allowed for directly in the complete equation. But it is of the nature of a permanent magnet that any energy expended by the field in separating its poles in the general build-up of the field is immediately locked up in the rigid connections holding the magnetism permanent, so that it can no longer be reckoned as part of the available energy. In this case, therefore, the Hamiltonian or conserved energy function is diminished from the value W_m by the amount expended by the field in building up the permanent magnetism. We have therefore

$$\delta\mathcal{H}_m=\frac{1}{4\pi}\int(H\delta B)dv-\int(F\delta I_p)dv, \qquad (2)$$

and as we have assumed a kinetic origin for the linear currents only this corresponds to a Lagrangian function $\mathcal{L}_m$ which is such that

$$\delta\mathcal{L}_m=\frac{1}{4\pi}\int(B\delta H)dv+\int(F\delta I_p)dv,$$

the formula (1) above.

4.

Guggenheim also converts his general formulae for $\mathcal{L}_m$ and $\mathcal{H}_m$ into space integrals over the field obtaining results which are equivalent to

$$\begin{aligned}\mathcal{L}_m&=\frac{1}{4\pi}\int dv\int_{H_0'}^{H}(BdH'),\\ \mathcal{H}_m&=\frac{1}{4\pi}\int dv\int_{0}^{B}H'dB,\end{aligned} \qquad (3)$$

H_0' being the value of H', more clearly defined below, in the zero field when $H=B=0$ everywhere. These are apparently very different formulae from (1) and (2) above. But we must remember that in Guggenheim's treatment there are other currents involved in the build-up, so the

[8] Cf. Larmor, *Aether and Matter*, p. 106, "On the specification of a magnetic distribution in terms of a continuous distribution of currents." The same idea probably underlies Guggenheim's statement (Proc. Roy. Soc. **A88**, 100 (1936)) that "if we could imagine all matter removed leaving behind the molecular currents it is B, not H, which would remain unaltered." Actually, of course, it is the change in the specification of the magnetization as a distribution of poles to a distribution of currents which necessitates the change in H, and the presence, or otherwise, of the magnetically inert parts of the matter has nothing whatever to do with it.

magnetic field intensity which occurs in the integrands, and now called H', is a vector which is circuital with respect not only to the specified currents of the system, but also to all these additional currents as well. In other words it is a very different vector from the H employed in the usual treatment and used in our (1) and (2) above, although of course the upper limit of the two vectors, taken when the masking currents have disappeared, will be the same. The relation between the two vectors at any stage of the build-up is easily obtained if Guggenheim's method is properly interpreted to include the volume currents as well as the surface ones, and it shows that if H is the usual vector which is circuital with respect only to the original currents of the system at this stage then the H' of Guggenheim's formulae is

$$H' = H - 4\pi I_e$$

if the currents in this transition stage are just sufficient to cancel a distribution of magnetic polarity of intensity I_e. The formula for $\mathfrak{L}_m$ in (3) is therefore in the ordinary notation

$$\mathfrak{L}_m = \frac{1}{4\pi}\int dv \int_0^H (BdH) - \int dv \int_{I_{e0}}^0 (BdI_e), \quad (4)$$

where I_{e0} is the value of I_e which completely cancels I_p together with any induced magnetization I_{i0} in the zero state,

$$I_{e0} = I_p + I_{i0}.$$

Substituting then $I_q = I_p - I_e$, $dI_q = -dI_e$, in the second integral, it reduces to

$$\mathfrak{L}_m = \frac{1}{4\pi}\int dv \int_0^H BdH + \int dv \int_{-I_{i0}}^{I_p} (BdI_q)$$

which is the equivalent of our (1) with $F = B$ apart from a trivial constant which in fact measures the quasi-elastic energy associated with any induced magnetization which may be present in the zero field.

We have also

$$\mathfrak{K}_m = \frac{1}{4\pi}\int dv \int_0^B (H'dB)$$

$$= \frac{1}{4\pi}\int (HB)dv - \frac{1}{4\pi}\int dv \int_{H_0'}^H (BdH')$$

$$= \frac{1}{4\pi}\int dv \int_0^B (HdB) - \int dv \int_{-I_{i0}}^{I_p} (BdI_q)$$

which is the equivalent of formula (2).

Guggenheim considers two special cases of these formulae corresponding to two possible laws of induction. As H is zero in the initial field we have

$$H_0' = -4\pi I_{e0} = -4\pi(I_p + I_{i0}).$$

If then we write $I_{i0} = (\mu - 1)H_0'/4\pi$, we have

$$H_0' = -4\pi I_p/\mu, \quad I_{i0} = -[(\mu - 1)/\mu]I_p;$$

while if $I_{i0} = (\mu' - 1)B_0/4\pi = 0$, we have

$$H_0' = -4\pi I_p.$$

In this latter case the formulae (3) are actually identical with (1) and (2) interpreted of course with $F = B$, the lower limit of the second integral being zero.

5.

Guggenheim seems quite unaware of the difference between the H' of his formulae—he, of course, calls it H—and the more conventional H employed by Cohn and myself, for he criticizes Cohn's choice of a zero lower limit for his H, when this is precisely the value which corresponds to his own choice of $-4\pi I_p$ or $-4\pi I_p/\mu$ as the lower limit of H'.

The real difference between Cohn's formulae and those given by Guggenheim lies really in another direction altogether, and not, as surmised by Guggenheim, in the choice of a lower limit for the integrals involved. Cohn's whole treatment is in fact interpreted not in terms of the usual induction vector B, as implied by Guggenheim's quotations, but of another vector M, variously called by Hertz the polarization or magnetization of the field, and which is related to B by the equation

$$M = B - 4\pi I_p.$$

This makes Cohn's formula for $\mathfrak{K}_m$, *viz.*,

$$\mathfrak{K}_m = \frac{1}{4\pi}\int_0^M HdM$$

identical with our (2) with $F = H$. Guggenheim, thinking in terms of his own treatment seems inclined to write off the second integrals in dI_p in

all our formulae as having zero values when the configuration is kept constant. As he says in a letter to me "I need hardly point out that at constant configuration as I_p is constant

$$\int H dI_p = 0,"$$

and this generally speaking seems to form the basis of his claim to have generalized the results given by Cohn. But when properly interpreted by the conventional build-up process employed by Cohn and myself these integrals do not necessarily vanish. They will vanish in Guggenheim's treatment but only because an equivalent non-vanishing integral

$$\int H dI_e$$

is included with them.

It is this unwillingness to recognize the conventional build-up procedure used by all previous writers, as a legitimate method of evaluating, at constant configuration, integrals of the kind here under review which is the cause of Guggenheim's difficulties with previous treatments. And as he interprets "constant configuration" to include also a constant specification of the distribution of permanent magnetism he is obliged to employ the device of covering the magnetism with a current shield or mask, which has then to be removed gradually during the build-up of the finite currents which form the rest of the generating system. As we now see the two processes, removing the mask and building up the magnetism from zero are in effect almost the exact, equivalents of each other both mathematically and physically and they lead to identical formulae for the available energy in the field in every case. One method cannot therefore be described as any more general than the other.

6.

The rest of the argument of my paper was concerned with an attempt to derive the simplest and most natural form of the expression for the general Lagrangian function, or rather of its virtual variation, expressed as an integral over the field and in a form which exhibits its non-integrability when it occurs, as arising simply and solely in the hysteresis effects associated then with the induction of the polarization.

In the usual case when $F=H$ a familiar argument soon shows that

$$\delta \mathfrak{L}_m = \frac{1}{8\pi} \delta \int \{2(BH) - H^2\} dv - \int (H \delta I_i) dv;$$

while when $F=B$ the same argument gives

$$\delta \mathfrak{L}_m = \frac{1}{8\pi} \delta \int B^2 dv - \int (B \delta I_i) dv.$$

These expressions are independent of any particular law of induction, or even of whether a law exists at all, and they apply to every type of medium, isotropic or crystalline. In each of them the second integral measures the energy stored in the quasi-elastic connections holding the induced magnetism against the action of the field. The first integral, represented in both cases by a complete differential, thus represents the purely magnetic part of the function, the part not definitely located in the latter. And the fact that in the second case this purely magnetic part of the energy assumes a very simple natural form in terms of the single vector B provides one of the arguments in favor of the choice of this vector as the fundamental force vector of the theory.

This was the main conclusion of my paper, but being anxious naturally to show the relation between these general formulae and those given in the more familiar treatments, which invariably use linear laws of induction, a good deal of attention was devoted to the special form of the results when these linear laws are assumed. It was then shown that the formula for $\mathfrak{L}_m$ which, in the case when $F=H$, becomes

$$\mathfrak{L}_m = \frac{1}{8\pi} \int \{2(HB) - \mu H^2\} dv$$

is identical with that usually employed in the dynamical theory of currents, and that, while it apparently differs from the more familiar form when the field arises from permanent magnets it still, even in such cases, gives a total for the whole field which is identical with that given by the more usual formula.

When the law of induction is linear there is, of course, also an energy or Hamiltonian function, the special case of formula (2). This is shown to be represented in all cases by the familiar result

$$\mathcal{H}_m = \frac{1}{8\pi} \int \mu H^2 dv$$

so the theory provides a self-consistent set of simple formulae for determining all the details of the mechanical and electrical behavior of the system in all cases, whether the law of induction is linear or not.

Under the impression, as he says, that I have confined myself to what I call linear laws of induction, it is these special results from my paper which Guggenheim claims as particular examples of his own general formulae. The discovery as we now see is not a very surprising one, seeing that one form of the general formulae of my paper, to which, however, he makes no reference, is in fact identical with the general formulae given by him, when these are properly interpreted, however different they may be in appearance.

7.

There are other imperfections and misunderstandings involved in the rest of Guggenheim's work which will be dealt with in detail in a more comprehensive survey of the whole subject to be published elsewhere. Enough has now been said to justify the conclusion that his claim to have produced more general formulae which include those obtained by Cohn and myself as special cases is entirely without justification. His formulae when properly interpreted prove to be identical with formulae given by both of us many years previously so that they are certainly no more general than the results given by Cohn and, in so far as his discussion is framed on the restricted basis of Cohn's theory, his results have a far less degree of generality than the equivalent ones obtained by myself on the much wider basis of the Kelvin-Maxwell theory. The only advantage of Guggenheim's formulae is in their mathematical compactness, but, as his subsequent discussion shows, this may have its dangers when attempts are made to interpret the relevant parts of them for dynamical purposes.

There are two other small points raised in Guggenheim's note which can be disposed of quickly before closing this already over-long note.

The question of the compatibility of the two interpretations of the linear law of induction given in my paper, and discussed at some length by him, is entirely irrelevant. There is really no conceivable reason why two such alternative physical laws should be compatible among themselves, but it is hoped that eventually one of them will prove to be more consistent with experience than the other.

Then at the end of the note Guggenheim complains that I use the term "fundamental (aethereal) force vector" without explaining what I mean. In following, however, the example of Cohn and ignoring the physical processes involved in the induction of the polarizations, he thereby overlooks one of the most important functions of the magnetic force vector. The forces on the currents are determined in terms of the induction vector B and, as the same vector can also, without ambiguity, be used to determine the forces on the permanent magnets, it is the only field vector which functions as a force intensity in this restricted theory. In the more detailed theory, however, a choice has to be made for the force vector which is effective in the polarization process and tradition, following the electrostatic analogy, has chosen H for this purpose. My contention is that, if B is chosen for this purpose as well, so that it becomes the one and only fundamental vector which functions as a force intensity then the whole of the energy and mechanical relations of the field, in the only really consistent form so far framed, assume their simplest and most natural form.

Letters to the Editor

PUBLICATION of brief reports of important discoveries in physics may be secured by addressing them to this department. The closing date for this department is, for the issue of the 1st of the month, the 8th of the preceding month and for the issue of the 15th, the 23rd of the preceding month. No proof will be sent to the authors. The Board of Editors does not hold itself responsible for the opinions expressed by the correspondents. Communications should not exceed 600 words in length.

Rotational Spectra of Some Linear Molecules near 1-cm Wave-Length

C. H. TOWNES, A. N. HOLDEN, AND F. R. MERRITT
Bell Telephone Laboratories Inc., Murray Hill, New Jersey
November 20, 1946

ROTATIONAL spectra of several linear molecules have been found in the region near 1-cm wave-length. The lines are observed on an oscilloscope on which frequency is plotted against variation in absorption. Absorption takes place in a 4-meter length of wave guide containing a few tenths of one mm Hg pressure of the absorbing gas. The technique is similar to that already described.[1]

In some cases there are a number of weaker lines accompanying the main rotational line. The measured frequencies and relative intensities are given in Table I. For the stronger lines frequency measurements have a probable error of about two megacycles, although frequency differences are somewhat more accurate. Relative intensities are not highly accurate, particularly for the weakest lines. The ClCN lines at 23,885 and 23,389 mc appear to be caused by $Cl^{35}CN$ and $Cl^{37}CN$ molecules, respectively, which are in the ground vibrational state and undergo a transition from $J=1$ to $J=2$. Similarly the BrCN lines at 24,713 and 24,570 mc are attributed to molecules of $Br^{79}CN$ and $Br^{81}CN$, respectively, in the ground vibrational state which make a transition from $J=2$ to $J=3$. The single OCS line is caused by the rotational transition $J=1$ to $J=2$. With these lines and assignments, and with no corrections for vibrations in the ground state, the moments of inertia are as in Table II. Using the isotopic frequency shift in ClCN, the CN distance is calculated to be 1.15A. The isotopic shift in BrCN is also consistent with this value, but does not allow a very accurate determination of the CN distance. Assuming the CN distances in BrCN and ClCN are the same, we obtain the values for the internuclear distances given in Table III.

TABLE I. Measured frequencies and intensities of lines in rotational spectra near one cm wave-length.

	Frequency in megacycles	Intensity relative to strongest line
BrCN	24,468	.05
	24,506	.15
	24,570	1.00
	24,576	.1
	24,608	.4
	24,619	.1
	24,631	.1
	24,645	.1
	24,658	.1
	24,683	.1
	24,713	1.0
	24,754	.4
	24,759	.1
	24,780	.1
	24,799	.1
	24,824	.1
	24,884	.05
ClCN	23,373	.1
	23,389	.3
	23,401	.05
	23,862	.15
	23,864	.15
	23,885	1.00
	23,901	.15
OCS	24,325	

TABLE II. Computed moments of inertia.

Molecule	Moment of inertia ($g\ cm^2 \times 10^{-40}$)
$Br^{79}CN$	203.64
$Br^{81}CN$	204.83
$Cl^{35}CN$	140.47
$Cl^{37}CN$	143.45
OCS	137.93

TABLE III. Internuclear distances.

Bond	Bond distance	Bond distance from electron diffraction[2]
C−N	1.15A	1.13±0.04A
Br−C	1.79	1.79±0.02
Cl−C	1.64	1.67±0.02

The C−N distance determination is very sensitive to small changes in the isotopic shift. Until a satisfactory explanation of the subsidiary lines is obtained which will at the same time give assurance that no unknown effects are contributing to the isotopic shift, the internuclear distances given above must be regarded as tentative.

The data can be used to distinguish between different possible structures for these molecules. The moments of inertia determined here and the electron diffraction data are consistent with the structures Cl−C−N and Br−C−N, but not with Cl−N−C and Br−N−C which have sometimes been proposed.[3] If one assumes an arrangement Cl−N−C and takes 1.09A (the smallest reasonable value from electron diffraction data) as the N−C distance, the above value for the moment of inertia gives a total length for the molecule of 2.86A. This is in distinct disagreement with the electron diffraction value for the total length 2.80±0.02A. From the above table it may be seen that the spectroscopic data give, assuming the Cl−C−N arrangement, a total molecular length 2.79A which is in good agreement with electron diffraction results. Similarly Br−C−N gives a total length 2.94A as compared with the electron diffraction value 2.92±0.02A, but if the Br−N−C structure is assumed the total length of the molecule cannot be less than 3.01A.

The frequency of the OCS line is in agreement with that recently reported by Dakin, Good, and Coles.[4]

[1] C. H. Townes, Phys. Rev. **70**, 665 (1946).
[2] J. Y. Beach and A. Turkevich, J. Am. Chem. Soc. **61**, 299 (1939).
[3] For a discussion see Sidgwick, *Organic Chemistry of Nitrogen* (Oxford University Press, New York, 1937), p. 326.
[4] T. W. Dakin, W. E. Good, and D. K. Coles, Phys. Rev. **70**, 560 (1946).